UNIVERSITY OF OKLAHOMA

GRADUATE COLLEGE

MECHANISM OF SACCHAROPINE DEHYDROGENASE: THE LAST ENZYME IN THE LYSINE BIOSYNTHETIC PATHWAY IN *SACCHAROMYCES CEREVISIAE*

A DISSERTATION

SUBMITTED TO THE GRADUATE FACULTY

in partial fulfillment of the requirements for the

degree of

Doctor of Philosophy

By

HENGYU XU
Norman, Oklahoma
2007

Downloaded from SHAREOK. Persistent Handle URL: https://hdl.handle.net/11244/1151

UMI Number: 3249638



UMI Microform 3249638

Copyright 2007 by ProQuest Information and Learning Company.
All rights reserved. This microform edition is protected against unauthorized copying under Title 17, United States Code.

ProQuest Information and Learning Company
300 North Zeeb Road
P.O. Box 1346
Ann Arbor, MI 48106-1346

MECHANISM OF SACCHAROPINE DEHYDROGENASE:
THE LAST ENZYME IN THE LYSINE BIOSYNTHETIC PATHWAY IN
SACCHAROMYCES CEREVISIAE

A DISSERTATION APPROVED FOR THE
DEPARTMENT OF CHEMISTRY AND BIOCHEMISTRY

BY

_____

Paul F. Cook, Ph. D.

_____

Ann H. West, Ph. D.

_____

George B. Richter-Addo, Ph. D.

_____

Helen I. Zgurskaya, Ph. D.

_____

David P. Nagle, Ph. D.

© Copyright by Hengyu Xu 2007

All Rights Reserved

Seeking the Great White Bird of Absolute Truth

from Alan G. MacDiarmid
The Nobel Prize in Chemistry 2000

The dependency of any one person's research on the labors of scores of earlier scientific pioneers is illustrated very beautifully by a few sentences of this variation from a book by Olive Schreiner, written at the turn of the century, entitled, "The Story of an African Farm." I would like to share with you this adapted portion.

The story concerns a young hunter who, in his youth, heard about the great white bird of "absolute truth" which lived at the very top of a high mountain far in the east. He had spent all his life seeking it without success - and now he was growing old.

The old thin hands cut the stone ill and jaggedly, for the fingers were stiff and bent. The beauty and strength of the man were gone.

At last, an old, wizened, shrunken face looked out above the rocks. He saw the eternal mountains still rising to the white clouds high above him.

The old hunter folded his tired hands and lay down by the precipice where he had worked away his life.

"I have sought," he said, "for long years I have labored; but I have not found her. By the rough and twisted path hewn by countless others before me, I have slowly and laboriously climbed. I have not rested. I have not repined. And I have not seen her; now my strength is gone. Where I lie down, worn out, other men will stand, young and fresh. By the steps that I, and those before me, have cut, they will climb; by the stairs that we have built, they will mount. They will never know those who made them, their names are forgotten in the mists of time. At the clumsy work they will laugh; when the stones roll, they will curse us; but they will mount, and on our work they will climb, and by our stair! They will find her, and through us!"

The tears rolled from beneath the shriveled eyelids. If truth had appeared above him in the clouds now, he could not have seen her, the mist of death was in his eyes.

... Then slowly from the white sky above, through the still air, came something falling ... falling ... falling. Softly it fluttered down and dropped on to the breast of the dying man. He felt it with his hands –

- it was

a feather.

ACKNOWLEDGEMENTS

As I complete this dissertation, the great challenge of pursuing my doctoral degree, I find myself faced with the truly daunting task of expressing my gratitude to God and many people who have helped make a reality this experience. These are the people who have offered me their friendship, who have given me words of encouragement and strength when I was about to give up, who have shown me a smile at just the right moment, who have shared their expertise, their time, and their resources, selflessly, whenever and wherever I needed, and who have just simply shared with me in great and small ways, the highs and lows of my life, as a graduate student and as a brand-new mom.

I owe a debt of gratitude to my wonderful Ph.D. mentors Dr. Paul F. Cook and Dr. Ann H. West, who have supervised me for the past four years. They are the people who gave me wings and made me fly. They have always supported me in all projects that I was involved in and have been an invaluable resource. Almost all of my knowledge about enzymology is from Dr. Cook, and that of X-ray crystallography is from Dr. West. Without their guidance and help, none of the results presented in this dissertation would have existed. They are unusual mentors in that they give me extensive independence and opportunities, always encourage me to ask, think, and explore. Their enthusiasm and diligence lead me on a journey to *seek the great white bird of absolute truth*.

I am appreciative of the constructive criticism, continual encouragement, and sound advice from my graduate advisory committee members, Dr. George B. Richter-Addo, Dr. Helen I. Zgurskaya, and Dr. David P. Nagle over the years.

I am thankful for my past and present colleagues in the Cook and West research groups, particularly Dr. Fabiola Janiak-Spens, Dr. Stace Porter, Hui Tan, Dr. William Karsten, Dr. Lilian Chooback, Dr. Babak Andi, Dr. Ying Lin, Jinghua Qian, Rong Guan, Dr. Daniel Copeland, Dr. Xiaodong Zhao, Dr. Lei Li, Alla Kaserer, Deniz Aktas, Devi Ekanayake, Ashwani Vashishtha, and Francesca Speroni. It has been a genuine pleasure to work with each of them. I am also thankful for Jean Keil, Arlene C. Crawford, and Carol Jones for helping with all of the paperwork.

I appreciate all of the past and current students and faculty of the Biochemistry Division who have freely shared their knowledge and friendship with me, especially during Biochemistry seminars. I have learned a great deal and enjoyed knowing and interacting with each of them over the years.

I want to dedicate this dissertation to my lovely husband Biao Liu who has absolutely convinced me that no star is out of reach. I thank him for all of his love and trust, for standing behind me all the time, for lifting me up when I could not reach my dream, for making me who I really am. I also want to thank my parents Fu Xu and Qilin Wen and my sister Shuyi Xu for their life-love and never-ending support. Last but not least, I give special thanks to my baby daughter, Sarah Liu, who brings me so much happiness and inspiration, who always amazes me and gives me strength.

The research described in this dissertation is supported by a grant-in-aid from the Office of the Research and Administration at the University of Oklahoma (to P. F. C. and A. H. W.), the Grayce B. Kerr Endowment to the University of Oklahoma (to P. F. C.), and a grant (GM 071417) from the National Institutes of Health (to P. F. C. and A. H. W.).

TABLE OF CONTENTS

ACKNOWLEDGEMENTS **V**

LIST OF TABLES **XI**

LIST OF FIGURES **XII**

LIST OF SCHEMES **XIV**

LIST OF ABBREVIATIONS **XV**

ABSTRACT **XVIII**

CHAPTER 1 INTRODUCTION **1**

1.1 L-lysine Biosynthesis and Catabolism 1
1.1.1 Biosynthesis of L-lysine in bacteria and plants 1
1.1.2 Biosynthesis of L-lysine in fungi 2
1.1.3 L-Lysine Catabolism 3
1.2 The α-Aminoadipate Pathway 4
1.2.1 Significance of the α-Aminoadipate Pathway 8
1.2.2 Regulation of the α-Aminoadipate Pathway 8
1.2.2.1 Genetic Regulation 8
1.2.2.2 Regulation of Enzyme Activity 10
1.3 Enzymes of the α-Aminoadipate Pathway 12
1.3.1 Homocitrate Synthase 12
1.3.2 Homoaconitase 14
1.3.3 Homoisocitrate Dehydrogenase 14
1.3.4 α-Aminoadipate Aminotransferase 15
1.3.5 α-Aminoadipate Reductase 16
1.3.6 Saccharopine Reductase 18
1.3.7 Saccharopine Dehydrogenase 19
1.4 Saccharopine Dehydrogenase 20
1.4.1 Pyridine Nucleotide-Linked Oxidative Deamination 20
1.4.2 Expression and Purification of SDH 23
1.4.3 Kinetic Mechanism of SDH 23
1.4.4 Chemical Mechanism of SDH 24
1.4.5 Substrate Specificity of SDH 25
1.4.6 Structure and Sequence Allignment 26
1.5 Summary 27

CHAPTER 2 MATERIALS AND METHODS **29**

2.1 Chemicals 29
2.2 Molecular Cloning, Cell Growth, and Protein Expression 30
2.3 Enzyme Assays 31
2.4 Initial Velocity Studies 32

2.4.1 Systematic Analysis 32
2.4.2 Pairwise Analysis 33
2.5 Determination of K_{eq} and the Haldane Relationship 34
2.6 Inhibition Studies 34
2.6.1 Substrate Inhibition Studies 34
2.6.2 Product and Dead-End Inhibition Studies 35
2.6.3 Double Inhibition Studies 35
2.7 pH profiles and pK_i profiles 36
2.8 Isotope Effect Studies 37
2.8.1 Synthesis of A-side NADD 37
2.8.2 Primary Substrate Deuterium Kinetic Isotope Effects 37
2.8.3 Solvent Deuterium Isotope Effects and Proton Inventory Experiments 38
2.8.4 Multiple Solvent/Substrate Deuterium Isotope Effects 39
2.9 ^{1}H NMR Experiments 39
2.9.1 Measurement of the Saccharopine Secondary Amine pK_a by NMR 39
2.9.2 Product Identification by NMR 40
2.10 Data Analysis 41

CHAPTER 3 EXPERIMENTAL RESULTS 45

3.1 Protein Expression and Purification 45
3.2 Kinetic Mechanism Determination of SDH 45
3.2.1 Initial Velocity Studies: Systematic Analysis 45
3.2.2 Initial Velocity Studies: Pairwise Analysis 48
3.2.3 Determination of K_{eq} 49
3.2.4 Inhibition Studies: Substrate Inhibition 50
3.2.5 Inhibition Studies: Product Inhibition 52
3.2.6 Inhibition Studies: Dead-End Inhibition 53
3.3 Chemical Mechanism Determination of SDH 56
3.3.1 pK_a of the Saccharopine Secondary Amine: Determination by NMR 56
3.3.2 pH Dependence of Kinetic Parameters 57
3.3.3 pH Dependence of the K_i for Oxalylglycine and Leucine 61
3.3.4. Isotope Effects 62
3.3.4.1 Primary Substrate Deuterium Kinetic Isotope Effects 62
3.3.4.2 Solvent Deuterium Isotope Effects and Proton Inventory Studies 63
3.3.4.3 Multiple Solvent/Substrate Deuterium Isotope Effects 64
3.4 Substrate Specificity of SDH 64
3.4.1 Initial Velocity Studies with NAD/NADH Analogues 64
3.4.2 Inhibition Studies to Determine the Kinetic Mechanism with NADP 66
3.4.3 Initial Velocity Studies with Keto Acid Substrate Analogues 66
3.4.4 Confirmation of Product of Reaction with Alternative α-Keto Acid Substrates by ^{1}H NMR 67
3.4.5 Deuterium Kinetic Isotope Effects 68
3.4.6 Dead-end Inhibition by NAD/NADH Analogues 68
3.4.7 pH Dependence of the K_i for AMP 68
3.4.8 Dead-end Inhibition by Keto Acid Analogues 71
3.4.9 Dead-end Inhibition by Amino Acid Analogues 71

3.4.10 Double Inhibition Studies 74

CHAPTER 4 DISCUSSION 75

4.1 Kinetic Mechanism Determination of SDH 75
4.1.1 Initial Velocity Studies 75
4.1.2 Substrate Inhibition Studies 76
4.1.3 Product Inhibition Studies 78
4.1.4 Dead-end Inhibition Studies 80
4.1.5 Quantitative Analysis of Dead-end Inhibition Data 84
4.1.6 Previously Published Data 86
4.2 Chemical Mechanism Determination of SDH 88
4.2.1 Isotope Effects 88
4.2.1.1 Primary Substrate Deuterium Kinetic Isotope Effects 88
4.2.1.1.1 Substrate Dependence of Primary Deuterium Isotope Effects 90
4.2.1.1.2 pH Dependence of Primary Deuterium Isotope Effects 91
4.2.1.2 Solvent Deuterium Isotope Effects and Proton Inventory Studies 92
4.2.1.3. Multiple Solvent/Substrate Deuterium Isotope Effects 93
4.2.1.4. Proton Inventory Studies 94
4.2.2 Interpretation of the pH Dependence of Kinetic Parameters 95
4.2.3 Interpretation of pK_i profiles 99
4.2.4 Proposed Chemical Mechanism 100
4.3 Substrate Specificity of SDH 103
4.3.1. NAD/NADH Analogues 104
4.3.1.1 Kinetic Mechanism with NADP/NADPH 104
4.3.1.2 Substrate Analogues of NAD 106
4.3.1.3 Inhibitory Nucleotide Analogues 106
4.3.1.4 pH Dependence of the K_i for AMP 107
4.3.2 Keto Acid Analogues 108
4.3.2.1 Kinetic Mechanism with Pyruvate 108
4.3.2.2 Substrate Analogues of Keto Acid 109
4.3.2.3 Inhibitory Keto Acid Analogues 109
4.3.3 Amino Acid Analogues 113
4.3.3.1 Inhibitory Amino Acid Analogues 113
4.3.4 Double Inhibition Studies 114
4.4 Conclusion 115
4.4.1 Kinetic Mechanism 115
4.4.2 Chemical Mechanism 116
4.4.3 Substrate Specificity and Binding Pockets 117

APPENDIX I MULTIPLE SEQUENCE ALIGNMENTS 120

APPENDIX II PRE-STEADY-STATE KINETIC, PHYSICAL, AND SPECTRAL PROPERTIES OF SDH 126

II.1 INTRODUCTION 126
II.2 MATERIALS AND METHODS 126

II.2.1 Pre-Steady-State Study of SDH by Stopped-Flow Kinetic Experiment 126
II.2.2 Determination of the Oligomerization State of SDH by HPLC 127
II.2.3 Substrate Binding Study of SDH by Isothermal Titration Calorimetry 128
II.2.4 Substrate Binding by Fluorescence Titration 128
II.2.5 Secondary Structure Determination of SDH by Circular Dichroism 129
II.3 RESULTS AND DISCUSSIONS 129
II.3.1 Pre-Steady-State Study of SDH 129
II.3.2 Size Exclusion Chromatography HPLC 131
II.3.3 Substrate Binding by Isothermal Titration Calorimetry 132
II.3.4 Substrate Binding by Fluorescence Titration 134
II.3.5 Secondary Structure Determination of SDH by Circular Dichroism 135

APPENDIX III CRYSTALLIZATION OF SDH 138

III.1 INTRODUCTION 138
III.2 MATERIALS AND METHODS 139
III.2.1 Protein Sample Preparation 139
III.2.2 Protein Crystallization 139
III.2.3 Characterization of Crystals 139
III.2.4 Ellman (DTNB) Assay 140
III.3 RESULTS AND DISCUSSION 140
III.3.1 Ellman (DTNB) Assay 140
III.3.2 Protein Crystallization 141

APPENDIX IV CLONING AND EXPRESSION OF PIPOX 145

IV. 1 INTRODUCTION 145
IV. 2 MATERIALS AND METHODS 146
IV.2.1 Molecular Cloning of PIPOX 146
IV.2.2 PIPOX Reaction Monitored by NMR 147
IV. 3 RESULTS AND DISCUSSION 148

REFERENCES 150

LIST OF TABLES

Table 1.1: Genes and Enzymes Involved in the α-Aminoadipate Pathway in *S. cerevisiae*.

Table 3.1: Kinetic Parameters of Saccharopine Dehydrogenase at pH 7.0.

Table 3.2: Inhibition Kinetic Constants for Product Inhibitors of SDH.

Table 3.3: Inhibition Kinetic Constants for Dead-end Inhibitors of SDH.

Table 3.4: Results of Saccharopine gCOSY Experiments.

Table 3.5: pH Dependence of Kinetic Parameters for SDH from *S. cerevisiae*.

Table 3.6: pH Dependence of Primary Deuterium Kinetic Isotope Effect for SDH.

Table 3.7: Kinetic Parameters for Alternative Coenzyme Substrates of SDH.

Table 3.8: Kinetic Parameters of SDH in the Saccharopine Formation Reaction Direction at pH 7.0.

Table 3.9: Kinetic Parameters of SDH using Keto Acid Substrates at pH 7.0.

Table 3.10: Isotope Effects for SDH at pH 7.0.

Table 3.11: Inhibition Constants of NAD analogue inhibitors at pH 6.9.

Table 3.12: Inhibition Constants of α-Kg Substrate Analogue Inhibitors at pH 7.0.

Table 3.13: Inhibition Constants of Lysine Substrate Analogue Inhibitors.

Table II.1: Estimated Physical Properties of SDHs by ProtParam Tool.

Table III.1: Summary of Crystallization Conditions.

Table III.2: Data-collection and Processing Statistics for SDH Crystals.

LIST OF FIGURES

Figure 3.1.1: Systematic initial velocity studies of SDH in the saccharopine formation reaction direction at pH 7.0 – primary plots.

Figure 3.1.2: Systematic initial velocity studies of SDH in the saccharopine formation reaction direction at pH 7.0 – secondary replots of double-reciprocal plots vs α-Kg concentration.

Figure 3.1.3: Systematic initial velocity studies of SDH in the saccharopine formation reaction direction at pH 7.0 – tertiary replots of double-reciprocal plots vs lysine concentration.

Figure 3.2: Pairwise analysis of the SDH oxidative deamination reaction.

Figure 3.3: Determination of K_{eq} of SDH reaction at pH 7.0.

Figure 3.4: Competitive substrate inhibition by lysine against NADH.

Figure 3.5: Substrate inhibition by α-Kg against NADH.

Figure 3.6: S-parabolic noncompetitive inhibition by glutarate against NADH.

Figure 3.7: pH dependence of the ^{1}H NMR spectrum of saccharopine.

Figure 3.8: pH dependence of kinetic parameters for the SDH reaction from *S. cerevisiae* in the direction of saccharopine formation.

Figure 3.9: pH dependence of kinetic parameters for the SDH reaction from *S. cerevisiae* in the direction of lysine formation.

Figure 3.10: pH dependence of the reciprocal of the inhibition constant for oxalylglycine (A) and leucine (B).

Figure 3.11: pH dependence of primary substrate deuterium kinetic isotope effects of SDH.

Figure 3.12: pH(D) profile of SDH.

Figure 3.13: Proton Inventories for SDH.

Figure 3.14: Structures of coenzyme analogues.

Figure 3.15: pH dependence of the reciprocal of the inhibition constant for AMP.

Figure 3.16: Structures of α-Kg and L-lysine analogues.

Figure 3.17: Double inhibition by oxalylglycine and ornithine.

Figure 4.1: Binding affinity of keto acid substrates against chain length from C3 and including the side chain carboxylate.

Figure II.1: Spectra from rapid-scanning-stopped-flow kinetic experiments.

Figure II.2: HPLC elution profile.

Figure II.3: Titrations of SDH with substrates.

Figure II.4: Fluorescence emission spectra of SDH.

Figure II.5: Far-UV circular dichroism spectrum of SDH.

Figure III.1: Four crystal forms of SDH.

Figure IV.1: Enzymatic synthesis of saccharopine.

Figure IV.2: ^{1}H NMR spectra of PIPOX reaction.

LIST OF SCHEMES

Scheme 1.1: The enzymes of the lysine DAP biosynthetic pathway.

Scheme 1.2: The enzymes of the lysine AAA biosynthetic pathway.

Scheme 1.3: Proposed general chemical mechanism for amino acid dehydrogenases.

Scheme 4.1: Schematic of the saccharopine-binding pocket to illustrate possible inhibition binding modes.

Scheme 4.2: Proposed kinetic mechanism for SDH.

Scheme 4.3: Proposed chemical mechanism for SDH.

LIST OF ABBREVIATIONS

AAA α-aminoadipate acid

AAS α-aminoadipate semialdehyde

AcCoA acetyl CoA

Amp amplicillin

AMP adenosine 5'-monophosphate

ADP adenosine 5'-diphosphate

3-APAD 3-acetylpyridine adenine dinucleotide (the + charge is omitted for convenience)

ATP adenosine triphosphate

C competitive

CD circular dichroism

Ches 2-(*N*-cyclohexylamino)ethanesulfonic acid

2',3'-cyclic NADP β-nicotinamide adenine dinucleotide 2',3'-cyclic monophosphate (the + charge is omitted for convenience)

DAP diaminopimelate

DCl deuterium chloride

D_2O deuterium oxide

DTNB 5,5'-dithiobis (2-nitrobenzoate)

HCS homocitrate synthase

Hepes *N*-(2-hydroxyethyl)piperazine-*N*'-(2-ethanesulfonic acid)

IPTG isopropyl-β-D-1-thiogalactopyranoside

ITC isothermal titration calorimetry

kDa	kilodaltons
α-Kg	α-ketoglutarate
LB	Luria-Bertani
Mes	2-(*N*-morpholino)ethanesulfonic acid, monohydrate
NaOD	sodium deuteroxide
NAD(P)	β-nicotinamide adenine dinucleotide (phosphate) (the + charge is omitted for convenience)
NADD	reduced nicotinamide adenine dinucleotide with deuterium in the 4-A position
NAD(P)H	reduced β-nicotinamide adenine dinucleotide (phosphate)
NC	noncompetitive
NMN	nicotinamide mononucleotide
Ni-NTA	nickel-nitrilotriacetic acid
NTB	nitrothiobenzoate
Mes	2-(*N*-morpholino)ethane-sulfonic acid, monohydrate
OAA	oxaloacetate
OG	oxalylglycine
3-PAAD	3-pyridinealdehyde adenine dinucleotide (the + charge is omitted for convenience)
PCR	polymerase chain reaction
PDB	protein data bank
PEG	polyethylene glycol
PEGMME	polyethylene glycol monomethyl ether

Sacc	saccharopine
SDH	saccharopine dehydrogenase (L-Lys forming)
SDS-PAGE	sodium dodecyl sulfate- polyacrylamide gel electrophoresis
SOI	slope of intercept
SOS	slope of slope
SR	saccharopine reductase
Taps	*N*-[tris(hydroxymethyl)methyl]-3-aminopropanesulfonic acid
thio-NAD	thio-nicotinamide adenine dinucleotide (the + charge is omitted for convenience)
UC	uncompetitive

ABSTRACT

The uniqueness of the α-aminoadipate (AAA) pathway for lysine biosynthesis in fungi makes it a target for the rapid detection and growth control of pathogenic yeasts and molds. Selective inhibition of the enzyme(s) of this pathway by (an) appropriate substrate analog(s) may control or eradicate the growth of fungal pathogens *in vivo*. Saccharopine dehydrogenase (SDH) catalyzes the reversible pyridine nucleotide-dependent oxidative deamination of saccharopine to generate α-ketoglutarate (α-Kg) and lysine using NAD^+ as an oxidizing agent, the final step in the AAA pathway.

Kinetic data have been measured for SDH from *Saccharomyces cerevisiae*, suggesting the ordered addition of NAD^+ followed by saccharopine in the physiologic reaction direction. In the opposite direction, NADH adds to the enzyme first, followed by random addition of α-Kg and lysine. Lysine inhibits the reaction at high concentrations by binding to free enzyme. The α-Kg substrate inhibition and double inhibition by NAD^+ and α-Kg suggest the existence of an abortive E:NAD^+:α-Kg complex. Saccharopine product inhibition suggests a practical irreversibility of the reaction at pH 7.0, in agreement with the overall K_{eq}, and the existences of E:NADH:saccharopine and E:NAD^+:saccharopine complexes. Dead-end inhibition studies are consistent with the steady-state random mechanism, and also suggest that the lysine-binding site has a higher affinity for keto acid analogues than does the α-Kg site or that dicarboxylic acids have more than one binding mode on the enzyme. S-parabolic noncompetitive inhibition of glutarate indicates the formation of a E:$(\text{glutarate})_2$ complex as a result of occupying both the lysine- and α-Kg-binding sites. The equilibrium constant for the reaction has been

measured at pH 7.0 as 3.9 x 10^{-7} M, in very good agreement with the Haldane relationship.

A proton shuttle chemical mechanism is proposed on the basis of the pH dependence of kinetic parameters, dissociation constants for competitive inhibitors, and isotope effects. In the direction of lysine formation, once NAD^+ and saccharopine bind, a group with a pK_a of 6.2 accepts a proton from the secondary amine of saccharopine as it is oxidized, and then does not get involved until lysine is formed at end of the reaction. A general base with a pK_a of 7.2 accepts a proton from H_2O as it attacks the Schiff base carbon of saccharopine to form the carbinolamine intermediate. The same residue then serves as a general acid and donates a proton to the carbinolamine nitrogen. Collapse of protonated carbinolamine is then facilitated by the same group accepting a proton from the carbinolamine hydroxyl to generate α-Kg and lysine. The amine nitrogen is then protonated by the group that originally accepted a proton from the secondary amine of saccharopine, and products are released. In the saccharopine formation direction, finite primary deuterium isotope effects were observed for all parameters with the exception of V_2/K_{NADH}, consistent with a steady-state random mechanism and indicative of a contribution from hydride transfer to rate limitation. The observed solvent isotope effect indicates that proton transfer also contributes to rate limitation. A concerted proton and hydride transfer is suggested by multiple isotope effect, as well as a proton transfer in another step, likely hydrolysis of the carbinolamine. In agreement, dome-shaped proton inventories suggest that proton transfer exists in at least two sequential transition states.

A number of NAD^+ analogues, including $NADP^+$, 3-acetylpyridine adenine dinucleotide (3-$APAD^+$), 3-pyridinealdehyde adenine dinucleotide (3-$PAAD^+$), and thio-

nicotinamide adenine dinucleotide (thio-NAD^+), can serve as a substrate in the oxidative deamination reaction, as can a number of α-keto analogues, glyoxylate, pyruvate, α-ketobutyrate, α-ketovalerate, α-ketomalonate, and α-ketoadipate in the opposite direction. Inhibition studies using nucleotide analogues suggest that the majority of the binding energy of the dinucleotides comes from the AMP portion, and that distinctly different conformations are generated upon binding of the oxidized and reduced dinucleotides. Addition of the 2'-phosphate as in NADPH causes poor binding of subsequent substrates, but has little effect on coenzyme binding and catalysis. In addition, the 10-fold decrease in affinity of 3-APAD in comparison to NAD^+ suggests that the nicotinamide ring binding pocket is hydrophilic. Extensive inhibition studies using aliphatic and aromatic keto acid analogues have been carried out to gain insight into the keto acid binding pocket. Data suggest that a side chain with 3 carbons (from the α-keto group up to and including the side chain carboxylate) is optimal. In addition, the distance between the C1-C2 unit and the C5 carboxylate of the α-keto acid is also important for binding; the α-oxo group contributes a factor of 10 in affinity. The keto acid binding pocket is relatively large and flexible, can accommodate the bulky aromatic ring of a pyridine dicarboxylic acid, and a negative charge at the C3 but not the C4 position. However, the amino acid binding site is hydrophobic and the optimal length of the hydrophobic portion of amino acid carbon side chain is 3 or 4 carbons. In addition, the amino acid binding pocket can accommodate a branch at the γ-carbon, but not at the β-carbon.

CHAPTER 1

INTRODUCTION

1.1 L-lysine Biosynthesis and Catabolism

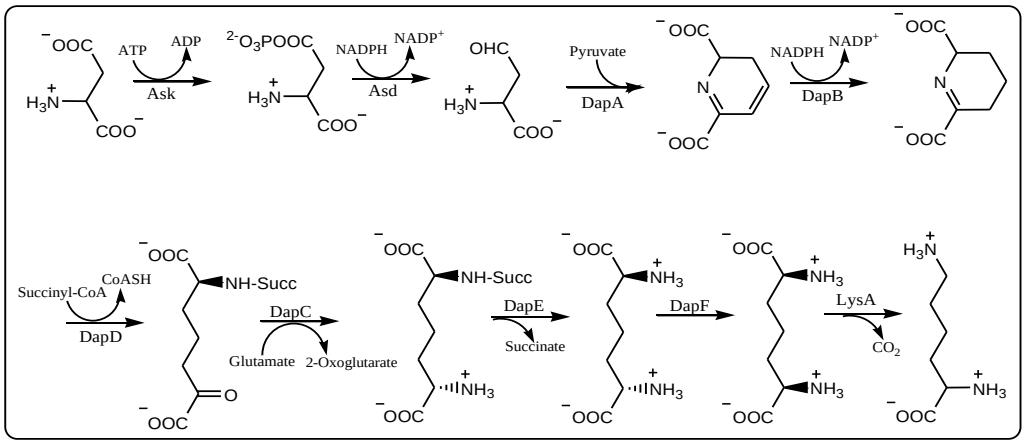
L-lysine is an essential amino acid for humans and animals and can only be obtained from protein in the diet. It can be synthesized *de novo* in bacteria, lower eukaryotes, and some plants. Among the 20 common proteinogenic amino acids, L-lysine is the only one known to have two distinct biosynthetic pathways: the diaminopimelate (DAP) pathway in plants, bacteria and lower fungi, and the α-aminoadipate (AAA) pathway in euglenoids and higher fungi (*1*). Unlike the pathways for lysine synthesis, pathways for other amino acid synthesis are similar in bacteria and fungi (*2, 3*).

1.1.1 Biosynthesis of L-lysine in bacteria and plants

The DAP pathway is found in most plants, bacteria, and lower fungi, and consists of seven enzyme-catalyzed reactions (Scheme 1.1) (*2, 4*). It belongs to the aspartate family of amino acid biosynthesis with aspartate as the common precursor. This pathway is the source of the DAP and lysine that are incorporated into bacterial cell wall peptidoglycan and transpeptidative cross-linking. Enzymes in the DAP pathway are therefore targets for developing new antibacterial agents (*5*).

The pathway begins with the phosphorylation of aspartate by aspartokinase to give aspartyl-β-phosphate followed by an NADPH-dependent reduction to give aspartate β-semialdehyde. Aldol condensation of aspartate semialdehyde with pyruvate yields, upon rearrangement, 2,3-dihydrodipicolinate, which is then reduced by NADPH to

Δ'piperideine-2,6-dicarboxylate. Succinylation (or acetylation) opens the ring to give N-succinyl (or acetyl) α-amino-ϵ-ketopimelate. After transamination, the acyl group is removed to yield L,L-DAP, which can be incorporated directly into the peptidoglycan, or racemized to the *meso* compound before incorporation. Racemization to the *meso* form is required, because this is the precursor to L-lysine, once it is decarboxylated.



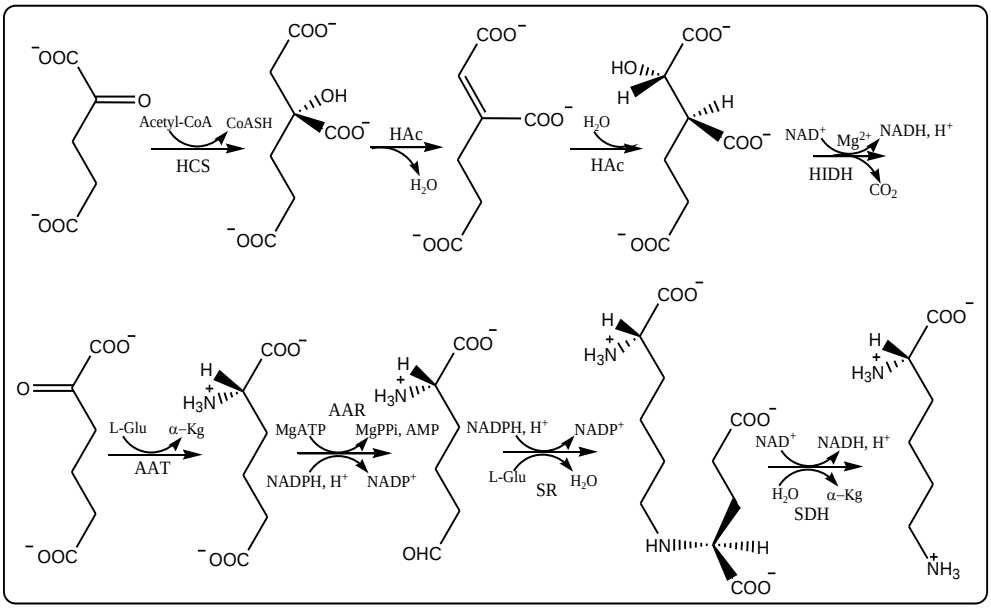
Scheme 1.1: The enzymes of the lysine DAP biosynthetic pathway are as follows: **(1)** Aspartate kinase (Ask, E.C.2.7.2.4), **(2)** Aspartate semialdehyde dehydrogenase (Asd, E.C.1.2.1.11), **(3)** Dihydrodipicolinate synthase (DapA, E.C.4.2.1.52), **(4)** Dihydrodipicolinate reductase (DapB, E.C.1.3.1.26), **(5)** Tetrahydrodipicolinate acyltransferase (DapD, E.C.2.3.1.117), **(6)** N-succinyl-α-amino-ε-ketopimelate-glutamate aminotransaminase (DapC, E.C.2.6.1.17), **(7)** N-acyldiaminopimelate deacylase (DapE, E.C.3.5.1.18, E. C. 3.5.1.47), **(8)** DAP epimerase (DapF, E.C. 5.1.1.7), **(9)** DAP decarboxylase (LysA, E. C. 4.1.1.20).

1.1.2 Biosynthesis of L-lysine in fungi

The presence of the α-aminoadipate (AAA) pathway for lysine biosynthesis has been demonstrated in several yeasts and molds, including *Saccharomyces cerevisiae* (*6, 7*), *Yarrowia lipolytica* (*8*), *Schizosaccharomyces pombe* (*9*), *Rhodotorula glutinis* (*10*), *Candida maltosa* (*11*), *Neurospora crassa* (*12*) and *Penicillium chrysogenum* (*13*); human pathogenic fungi, such as *Candida albicans* (*14*), *Cryptococcus neoformans* (*15*), and *Aspergillus fumigatus* (*15*); and plant pathogens, including *Magnaporthe grisea* (*2,*

15). The enzymes from *S. cerevisiae* are highly similar to their closest homologs from *C. albicans* and *A. fumigatus*. Multiple sequence alignment shows greater than 60% identity for all but one (aminotransferase) of the enzymes in the pathway from those organisms.

The AAA pathway is present only in euglenoids and higher fungi (*3, 6, 16, 17*), with α-ketoglutarate (α-Kg) serving as the precursor for L-lysine. The pathway is shown in Scheme 1.2. It is a member of the glutamate family of amino acid biosynthesis and resembles the pathway from glutamate to ornithine in bacterial arginine biosynthesis (*18, 19*). Enzymes involved in the fungal AAA pathway are unique to lysine synthesis (*2, 6*).



Scheme 1.2: The enzymes of the lysine AAA biosynthetic pathway are as follows: **(1)** Homocitrate synthase (HCS, E.C. 4.1.3.21), **(2)** Homoaconitase (HAc, E.C. 4.2.1.36), **(3)** Homoisocitrate dehydrogenase (HIDH, E.C. 1.1.1.87), **(4)** α-aminoadipate aminotransferase (AAT, E.C. 2.6.1.39), **(5)** α-aminoadipate reductase (AAR, E.C. 1.2.1.31), **(6)** Saccharopine reductase (SR, E.C. 1.5.1.10), **(7)** Saccharopine dehydrogenase (SDH, E.C. 1.2.1.31).

1.1.3 L-Lysine Catabolism

Lysine degradation is extremely varied in nature. In animals including humans, reversal of the yeast AAA pathway [lysine → saccharopine → α-aminoadipate-δ-

semialdehyde (AAS) → AAA → α-ketoadipate → glutarate] is used for the catabolism of lysine (*1, 3*). Interestingly, animals and plants have a single saccharopine dehydrogenase, a bi-functional enzyme, which catalyzes both the saccharopine dehydrogenase (SDH) and saccharopine reductase (SR) reactions with NADP as the cofactor (*20*). The enzyme may result from gene duplication and fusion of the two fungal genes. Considering that animals and plants do not synthesize lysine but can degrade it, it is possible that the bifunctional enzyme has been adapted to the degradation of lysine, whereas separation of the SR and the SDH in fungi may make them better suited for lysine synthesis, perhaps allowing differential regulation. Both yeast and mammalian SDHs exhibit strict substrate specificity and inhibition by ornithine and leucine; however, they differ in their coenzyme specificity and molecular weight (*3, 20*). The evolutionary origin of the lysine biosynthetic pathway in yeast and the catabolic pathway in animals still remains a subject of great interest.

The greatest diversity in the degradation of lysine is found in bacteria, yeasts, and molds (*3*). As an example, a survey of 28 yeast strains from several genera and species identified two lysine degradative pathways and resulted in separation of the organisms into three groups (*21*). The first of the pathways begins with formation of AAS by the action of either lysine 6-dehydrogenase or lysine 6-aminotransferase, whereas the second degradative pathway proceeds through a series of acetylated intermediates.

1.2 The α-Aminoadipate Pathway

The *S. cerevisiae* genome has been completely sequenced (*22-24*). Extensive genetic, enzymatic, and regulatory studies of the lysine biosynthetic pathway are being carried out in *S. cerevisiae* (*14*). Seven enzymes, eight steps and more than 12 nonlinked

genes are responsible for the biosynthesis of lysine in *S. cerevisiae* (*5, 25, 26*). Genes and their encoded enzymes involved in the AAA pathway are listed in Table 1.1, and the enzymatic steps are briefly described below.

Table 1.1: Genes and Enzymes Involved in the α-Aminoadipate Pathway in *S. cerevisiae.*

Enzyme	Gene
Homocitrate synthase	*LYS20* (cytosol) *LYS21* (mitochondria)
Homoaconitase	*LYS4 (LYS7)*
Homoisocitrate dehydrogenase	*LYS12*
α-Aminoadipate aminotransferase	--
α-Aminoadipate reductase (phosphopantetheinyl transferase)	*LYS2* (*LYS5*)
Saccharopine reductase	*LYS9* (regulated by *LYS14*)
Saccahropine dehydrogenase	*LYS1*

The first half of the pathway, formation of AAA from acetyl CoA (AcCoA) and α-Kg, takes place in the mitochondrion (*27*). The pathway is initiated by the homocitrate synthase (HCS)-catalyzed condensation of AcCoA and α-Kg to give the enzyme-bound intermediate homocitryl CoA, which is hydrolyzed by the same enzyme to give homocitrate. HCS catalyzes the first and committed step in the pathway, is highly regulated to economize the use of resources, and its reaction is thought to be the rate-limiting step in the pathway.

Homoaconitase (HAc), likely an enzyme containing an FeS cluster, catalyzes the interconversion of homocitrate and homoisocitrate via the intermediate homoaconitate. The enzyme is a member of the aconitase superfamily, which includes isopropylmalate isomerase (a member of the leucine biosynthetic pathway in bacteria and fungi) and

aconitases. This is the first documented evolutionary link between the AAA pathway in fungi and nonfungal organisms (*28*).

The resulting homoisocitrate is then oxidatively decarboxylated by the pyridine nucleotide-linked homoisocitrate dehydrogenase (HIDH) to give α-ketoadipate. This enzyme belongs to the pyridine nucleotide-linked β-hydroxyacid oxidative decarboxylase family, which is a well-studied class of enzymes (*29*).

α-Aminoadipate is then formed via a pyridoxal 5'-phosphate (PLP)-dependent aminotransferase (AAT) by using L-glutamate as the amino donor. Although the first half of the pathway takes place in the mitochondrion, the aminotransferase is thought to be present in both mitochondrion and cytoplasm. The aminotransferase reaction is also a branch point to secondary metabolism, including the *de novo* synthesis of β-lactam antibiotics. In addition, the product AAA can serve as the sole nitrogen source for *Filobasidiella neoformans*, *S. pombe*, *C. albicans*, and *A. fumigatus* (*30*).

In the cytoplasm, the AAA reductase (AAR) then reduces AAA to AAS via an adenosylated derivative, a unique process involving both adenylation and reduction that is found only in fungi. However, this enzyme has to be activated by a phosphopantetheinyl transferase (PPT). This unique two component system represents a novel reaction in fungal amino acid metabolism. In addition, phylogenetic studies and BLAST results show that the AAR in fungal lysine synthesis is evolutionarily related to some bacterial antibiotic peptide synthetases (*20*). The reductase-catalyzed reaction is believed to be the key to evolution of fungal lysine synthesis (*20*).

Once the semialdehyde is formed, it is condensed with glutamate, and the imine is reduced by NADPH to L-saccharopine (Sacc) catalyzed by SR. Finally, SDH catalyzes

the oxidative deamination of saccharopine to give L-lysine. It is of interest that saccharopine is a stable intermediate and pyridine nucleotides, rather than a vitamin B_6-dependent transamination of the semialdehyde is used by fungi. The last two enzymes have very little sequence homology at the amino acid level, but both enzymes are fungi specific and catalyze very similar reactions. Since NADPH and NADH are used as coenzymes by these two enzymes, respectively, a high NADPH-to-NADH ratio may favor the synthesis of lysine from AAS, whereas a low ratio would discourage such synthesis and favor the reverse reactions.

The pathway occurs in two compartments. One of the reasons may be because of the availability of NAD(P)H and adenosine triphosphate (ATP), of allosteric regulators, or the proper environment to give the active site residues of the enzymes an optimum protonation state to catalyze the reactions involved along the pathway. The split between two compartments also may contribute to a better overall regulation of the whole pathway, or a secondary metabolic pathway.

An AAA-like pathway is also found in *Thermus thermophilus* and *Pyrococcus horikoshii* (*31, 32*). However, this pathway is not the same as that found in fungi. The first half of the pathway is similar to that found in fungi, but AAA is first converted to N-acetyl-α-aminoadipate, which is phosphorylated at the ε-carboxylate, and then reductively dephosphorylated to the ε-aldehyde. The aldehyde is then transaminated to N-acetyl-L-lysine, which is deacetylated to give L-lysine (*18, 20*). In *T. thermophilus*, it has been recently reported that HAc catalyzes the reversible hydration of *cis*-homoaconitate to (2*R*, 3*S*)-homoisocitrate (*135*). However, no apparent "homocitrate dehydratase"

activity was observed for HAc, and the identity of the catalyst for this reaction is unknown.

1.2.1 Significance of the α-Aminoadipate Pathway

Several fungal alkaloids or peptides have lysine as a structural element or biosynthetic precursor. In addition, several AAA pathway intermediates are incorporated into secondary metabolites. The best example is AAA as an essential precursor for penicillins in the synthesis of ACV (L-δ-(α-aminoadipoyl)-L-cysteinyl-D-valine) tripeptide (*1*, *33*).

The uniqueness of the AAA pathway makes it a target for the rapid detection and control of pathogenic yeasts and molds. Selective inhibition of the enzyme(s) of this pathway by (an) appropriate substrate analog(s) may control or eradicate the growth of fungal pathogens *in vivo* (*9, 14*). To date, however, there are only a few novel compounds designed to target early steps in the pathway, specifically those steps involving the synthesis of (*R*)-homocitrate and (2*R*, 3*S*)-homoisocitrate (*34*).

1.2.2 Regulation of the α-Aminoadipate Pathway

The AAA pathway for the biosynthesis of lysine is highly regulated at the level of both enzyme synthesis and activity (*6*).

1.2.2.1 Genetic Regulation

The pathway is regulated by the general mechanism for the control of amino acid biosynthesis as well as a pathway-specific co-inducer-dependent transcriptional activation (*27, 35-37*). The co-inducer is AAS, which is an intermediate of the pathway (*35*). In *S. cerevisiae*, expression of the lysine genes can be stimulated by Lys14p in the

presence of its co-inducer AAS (*35*). Production of the co-inducer is also under the control of the metabolic flux mediated by feedback inhibition by lysine of the first enzyme in the pathway, HCS (*38, 39*). Thus, lysine can repress the expression of its biosynthetic genes. Excess lysine also acts as a repressor of six of the enzymes of the pathway (*27, 40*). Feller *et al*. (*41*) have proposed a mechanism to correlate these two types of regulation. Lysine inhibits its own biosynthesis by feedback inhibition of HCS, which decreases the concentration of AAS, and eliminates induction by Lys14p.

Two unlinked genes, *LYS9* (saccharopine reductase) and *LYS14* (transcriptional activator), are required for the production of saccharopine in *S. cerevisiae* (*25*). Strains mutated in these genes accumulate AAS and show a significant reduction in SR activity. Mutation of *LYS9* results in lysine auxotrophy and no reductase activity. Mutation of *LYS14* causes yeast to grow slowly in the absence of lysine with a low level of reductase activity. Lys14p is required for the expression of the *LYS9* gene, and it has a regulatory role with AAS as the co-inducer of transcriptional activation. Therefore, a low level of reductase activity in the *LYS14* mutants is because of the weak expression of the *LYS9* gene in the absence of the semialdehyde coinduction (*1, 35*).

Lys14p is a 90-kDa (790-amino acid) protein that participates in a complicated network of protein-protein interactions with 65 other proteins (Biomolecular Interaction Network Database; www.bind.ca). Lys14p contains a DNA binding domain similar to the Zn_2Cys_6 binuclear cluster of other fungal transcriptional activators such as Gal4p and Ppr1p (*42, 43*). Promoters of genes responding to this type of transcriptional activator usually contain an upstream activating sequence (UAS) that, in most instances, consists of two CGG triplets that are separated by a specific number of bases dependent on the

specific activator. In Gal4p and Ppr1p, the intervening sequence consists of 11 and 6 bp, respectively. These proteins bind as a dimer to the target sequence (UAS) with each of the zinc clusters binding to a CGG triplet (*44-46*).

Using a deletion and insertion approach, a UAS responsible for binding Lys14p has been identified in the promoter regions of the *LYS1* (SDH) and *LYS9* (SR) genes from *S. cerevisiae* that differs slightly from the aforementioned consensus sequence (*37*). The UAS for the transcriptional activation of the *LYS1* and *LYS9* genes consists of a TCC and GGA triplet separated by 3 bp. One or several copies of this 9-bp sequence has been found in the promoter of at least four other *LYS* genes, including *LYS20* (cytosolic HCS), *LYS21* (mitochondrial HCS), *LYS2* (AAR), and *LYS4* (HAc). *LYS5* (PPT), which does not respond to the Lys14p transcriptional activation, does not contain the UAS element (*37*).

In *S. cerevisiae*, one cannot exclude the possibility that some other enzyme-catalyzed step(s) may be rate-limiting step(s) and act in a manner similar to HCS in the regulation of lysine synthesis. For example, in *P. chrysogenum*, overexpression of HCS does not lead to an increase in AAA even in a strain in which the *LYS2* gene, which encodes AAR, is disrupted. These results suggest the presence of at least one additional rate-limiting step between the HCS and the AAR catalyzed reactions (*47*).

1.2.2.2 Regulation of Enzyme Activity

The activity of HCS is highly regulated. It can be feedback inhibited by lysine, the end product of the pathway. The K_i for lysine inhibition of HCS in *T. thermophilus* and *P. chrysogenum* is only approx 9 μM (*13*), whereas in *S. cerevisiae* it is approx 40 μM (*49*). A K_i for lysine inhibition in *S. cerevisiae* from steady-state kinetic studies is 500 μM, which differs from its K_d value of 40 μM determined from fluorescence titration (*49*).

There are two conformers of HCS, one active, and the other less active, with lysine binding to the less-active conformer of the free enzyme. Although lysine behaves as a competitive inhibitor, it binds to an allosteric site as indicated by HCS mutants that are still very active, even though they have lost sensitivity to lysine inhibition.

The concentration of Na^+ also influences the activity of HCS, by binding to free enzyme (*49*). When the concentration of AcCoA is high and α-Kg is low, Na^+ gives a 4-fold activation of HCS. However, when the concentrations of AcCoA and α-Kg are low, Na^+ is an activator at a low concentration, but an inhibitor at high concentration. This phenomenon is also observed with other metal ions. The inhibition is due to Na^+ binding to the AcCoA site, whereas activation is because of Na^+ likely binding to an allosteric site on free enzyme (not the lysine site). On the basis of the effects of lysine and Na^+ and given their physiological concentrations, the authors proposed that the concentration of α-Kg would determine the flux through the lysine biosynthetic pathway.

In *P. chrysogenum*, the synthesis of penicillin is regulated by lysine through the inhibition of HCS (*50, 51*), which results in a decrease in the concentration of α-aminoadipic acid, the branch point for the biosynthesis of penicillin and lysine. The effect of lysine can be reversed by addition of aminoadipic acid and other intermediates of the pathway such as α-ketoadipate and homocitrate. The inhibition by lysine in *S. cerevisiae* is linear (*49*), whereas it is partial in *P. chrysogenum* (*13*). It's been suggested that the partial inhibition is essential for maintaining a steady-state level of AAA for penicillin production (*52*).

The inhibition of HCS by lysine is pH dependent in *P. chrysogenum* (*13*). Inhibition could not be detected at pH 6.6 to 7.0, but at pH 8.0. In *P. chrysogenum*, the

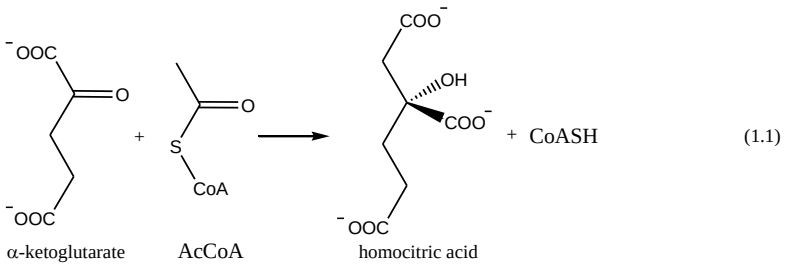
cytosolic pH is controlled by a proton gradient, generated by a cytoplasmic membrane ATPase. A decrease in the ATP concentration will result in a decreased cytosolic pH and an increase in HCS activity, allowing the fungus to use intermediates from the lysine biosynthetic pathway to produce secondary metabolites.

It's also been reported that CoA, the product of the HCS reaction, can inactivate the enzyme from *S. cerevisiae* and this could be prevented by lysine and α-Kg (*53-56*). The inactive enzyme could not be reactivated by addition of AcCoA.

1.3 Enzymes of the α-Aminoadipate Pathway

1.3.1 Homocitrate Synthase

HCS [3-hydroxy-3-carboxyadipate-2-oxoglutarate-lyase (CoA-acetylating); EC 2.3.3.14] catalyzes the condensation of AcCoA and α-Kg to give homocitrate and CoA (eq 1.1).



(1.1)

Recent studies of the HCS from *S. cerevisiae* indicate it self-associates, and its native molecular weight has not yet been determined, although the majority of the activity is associated with lower molecular weight forms (*15*). Two isoenzymes of HCS were identified in *S. cerevisiae*, both of which could be inhibited by lysine (*39*). HCS is a Zn^{2+}-metalloenzyme (*57*) and not stable as isolated. A solution containing 100 mM

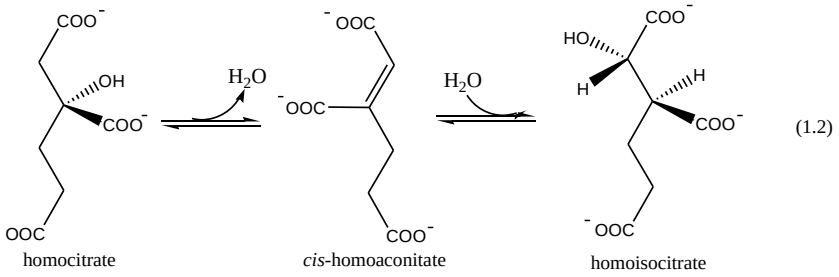
guanidine hydrochloride, 100 mM α-cyclodextrin, and 600 mM ammonium sulfate has been used to stabilize the HCS from *S. cerevisiae* (*15*).

An ordered Bi-Bi kinetic mechanism has been proposed for HSC with α-Kg binding to the enzyme first, followed by acetyl-CoA, and CoA released before homocitrate (*58*). A chemical mechanism of HCS has been proposed (*57*). α-Kg binds with its α-carboxylate and α-oxo groups coordinated to an active site Zn. AcCoA is then bound with its thioester oxygen hydrogen-bonded to an enzyme side chain and its methyl group in the vicinity of an enzyme residue that will function as a general base. The general base abstracts a proton from the methyl group of AcCoA, to generate the enol (or enolate). The C2 carbon will then carry out a nucleophilic attack on the carbonyl of α-Kg to give homocitryl-CoA likely facilitated by an enzyme general acid. It will attack the *re*-face, and the resulting homocitryl-CoA is then hydrolyzed.

Structure is currently not available for a HCS. However, HCS shares two conserved regions, signature patterns, with α-IPMS (*59*) for which a three-dimensional (3D) structure has been determined. The first of the conserved regions is ($TXLRDGXQX_{10}K$) (where X is any amino acid), located near the N-terminus, and the second is [L/I/V/M/E]X_2**H**X**H**[D/N]DXGX[G/A/S]X[G/A/S], located in the center of the HCS sequence. The two conserved histidines shown in bold are proposed to be involved in catalysis, and Copley *et al.* (*60*) propose that the HXH motif is involved in metal ion binding. Using the domain prediction program 3D-PSSM, circular dichroism spectra, and multiple sequence alignment, it is suggested that HCS has a $(\beta\alpha)_8$ TIM barrel domain at the N-terminal and a regulatory domain at its C-terminal (*15, 60*).

1.3.2 Homoaconitase

Homoaconitase (EC 4.2.1.36) also known as homoaconitate hydratase, encoded by the *LYS4* gene in *S. cerevisiae*, catalyzes the interconversion of homocitrate and homoisocitrate via the intermediacy of *cis*-homoaconitate (eq 1.2).

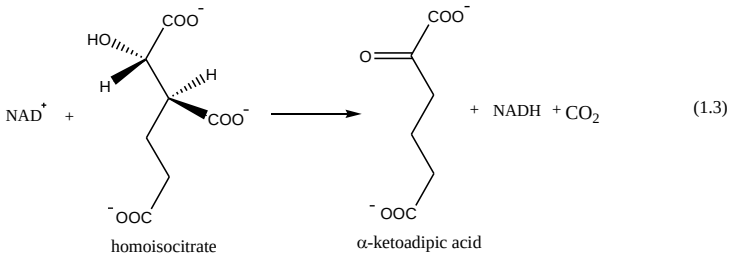


homocitrate *cis*-homoaconitate homoisocitrate (1.2)

The enzyme is a member of the aconitase superfamily. It is a mitochondrial enzyme that is repressed by both lysine and glucose. The enzyme from *Aspergillus nidulans* is 55% sequence identical to that from *S. cerevisiae*, with the greatest similarity in the region attributed to binding of an FeS cluster (*1*). However, little is known of the mechanism of the enzyme, but its mechanism may be similar to that of aconitase (*61*).

1.3.3 Homoisocitrate Dehydrogenase

Homoisocitrate dehydrogenase (3-carboxy-2-hydroxyadipate dehydrogenase; EC 1.1.1.87) catalyzes the NAD-dependent conversion of homoisocitrate to α-ketoadipate (eq 1.3).

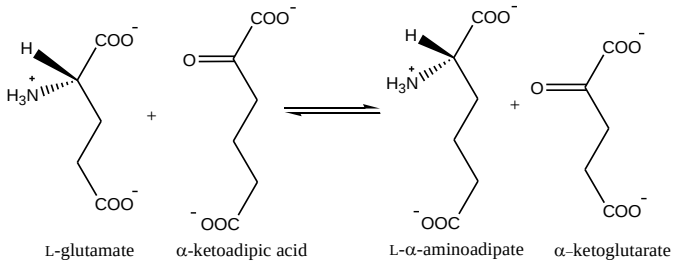


homoisocitrate α-ketoadipic acid (1.3)

Other than its sequence, almost nothing is known about the mechanism of this enzyme. Based on the general mechanism of the pyridine nucleotide-linked β-hydroxyacid oxidative decarboxylases (*29*), the mechanism may be similar to that of isocitrate dehydrogenase (IDH) (*62*). Whether the enzyme requires a divalent metal ion to catalyze its reaction as does IDH will have to be determined.

1.3.4 α-Aminoadipate Aminotransferase

α-Aminoadipate aminotransferase (EC 2.6.1.39) is a PLP-dependent enzyme responsible for the conversion of α-ketoadipate to AAA by using L-glutamate as the amino donor and generating α-Kg as the second product (eq 1.4). The aminotransferase reaction is also a branch point to secondary metabolism, including the *de novo* synthesis of β-lactam antibiotics.



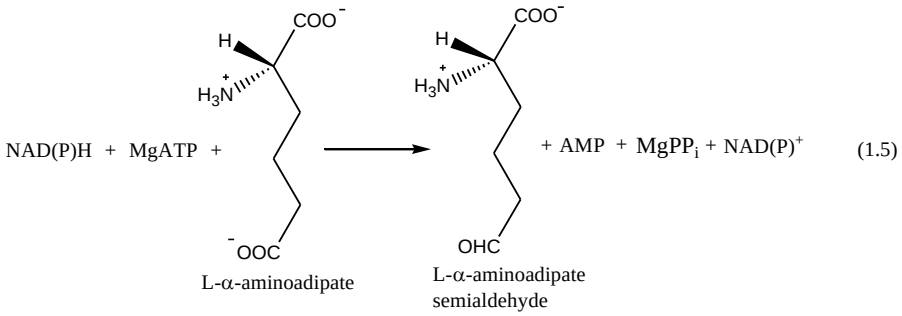
(1.4)

In *S. cerevisiae*, two isozymes of the aminotransferase have been isolated (*1, 63, 64*). Isozyme I is localized in the mitochondrion, is inhibited by α-Kg, and will utilize either L-glutamate or L-aspartate as the amino donor, but it exhibits only weak activity with AAA as the amino donor. Isozyme II is localized in the cytosol, has a strict requirement for L-glutamate as the amino donor, and is not inhibited by α-Kg. Neither isoform is inhibited by lysine, but the activity of isozyme II is repressed by AAA and slightly repressed by glucose. Only the cytosolic isoform seems to be specific for AAA

pathway. Its mechanism is expected to be ping pong on the basis of ample precedence from other aminotransferases, but its specific mechanism will have to await future studies.

1.3.5 α-Aminoadipate Reductase

α-Aminoadipate reductase (EC 1.2.1.31), also known as AAS dehydrogenase, catalyzes the reduction of AAA to AAS in the cytoplasm, a unique reaction involving both adenylation and reduction (eq 1.5).



On the basis of early investigations (*65, 66*), the AAR-catalyzed reaction is thought to be a three-step process, with the amino acid first reacting with ATP to form an adenylyl derivative, followed by the reduction of the adenylyl derivative of AAA by NADPH, followed by cleavage of the reduced adenylyl derivative of the amino acid to form AAS. The first and second steps require MgATP and NADPH, respectively, whereas the third step requires no co-factors. The product of the first step was successfully isolated and identified as a δ-5'-adenylyl-L-α-aminoadipate by Bhattacharjee's group, whereas the product of the second step was too unstable to be identified (*67*). Formation of the δ-5'-adenylyl-L-α-aminoadipate, rather than phosphorylation of the substrate by ATP, makes this reaction a unique process.

The enzymatic conversion of AAA to AAS requires expression of two genes in *S. cerevisiae*, *LYS2* and *LYS5*. The reductase, encoded by *LYS2*, contains domains for ATP

hydrolysis, thioester formation with a 4-phosphopantetheine-binding consensus sequence, and an active site serine residue. The reductase is feedback inhibited by lysine and thialysine (*1, 68*). The active form of the reductase requires an additional activity catalyzed by Lys5p, a member of the PPT family (*69*). It has recently been shown that Lys5p is a posttranslational modification catalyst, which uses coenzyme A (CoASH) as a cosubstrate to phosphopantetheinylate Ser880 of AAR, activating it for catalysis (*70*). Thus, the PPT and AAR (Lys2p/Lys5p heterodimer) represent a two-component system with the transferase covalently priming the reductase, a novel mechanism for fungal amino acid-metabolizing enzymes. A human homolog of the AAR-PPT gene has been identified (*71*). The posttranslational activation of the *LYS2* encoded AAR from *C. albicans* has also been investigated (*72*).

A mechanism for the reductase from *S. cerevisiae* has been proposed by Walsh's group (*70*). The reductase is first activated by phosphopantetheinylation using the transferase. The activated reductase then catalyzes the adenylation of the δ-carboxylate of AAA via the adenylation (A) domain, followed by acyl transfer of the aminoadipoyl moiety to the thiol of the phosphopantetheine to generate the thioester of the phosphopantetheinyl cleavage protein domain. Hydrolysis of the $MgPP_i$ product of the adenylation reaction is used to drive the reaction toward the adenylated intermediate. The covalent thioester intermediate is reduced by NADPH to regenerate reduced phosphopantetheine and the final semialdehyde product. The latter reaction is similar to the reverse of the glyceraldehyde 3-phosphate dehydrogenase reaction. Each of the partial reactions of the overall reaction can be studied independently, but mechanistic details will have to await future studies.

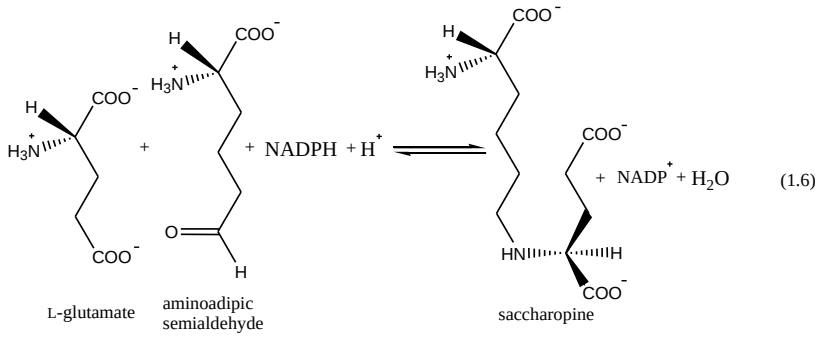
The *S. cerevisiae* AAR is evolutionarily related to some of the bacterial antibiotic peptide synthetases (*20*). Multienzyme complexes also exist for adenylation and partner-protein-specific posttranslational activation of nonribosomal peptide synthetases (NRPS) in the synthesis of antibiotics, *e.g.* bacitracin, cyclosporine, penicillin, and vancomycin (*69*). However, the yeast AAR has two unusual features as a nonribosomal peptide synthetase type catalyst, an unusual organization with a reductase domain fused down-stream of the prototypic adenylation/peptidyl carrier protein domains, and an unusual regiospecific activation of its amino acid substrate (*70*). Nonetheless, the homology of adenylation and posttranslational modification of AAR to those of NRPS suggests the reductase-catalyzed reaction is the key to the evolution of fungal lysine synthesis. The link between AAR and NRPS may be useful for the design of antifungal agents because Lys2p and Lys5p are essential for fungal growth.

1.3.6 Saccharopine Reductase

Saccharopine reductase (EC 1.5.1.10), also known as aminoadipate semialdehyde-glutamate reductase or saccharopine dehydrogenase [N^6-(L-1,3-dicarboxypropyl)-L-lysine:NADP oxidoreductase (L-glutamate-forming)], is the penultimate enzyme of the AAA pathway for lysine biosynthesis (*3, 12, 73*). The enzyme catalyzes the synthesis of saccharopine via the reversible condensation of AAS with L-glutamate by using NADPH as the reducing agent (eq 1.6).

The structure of SR in the apo form from *S. cerevisiae* has been solved (*74*). The polypeptide chain of the SR folds into three domains. The first domain is a variant of the dinucleotide-binding Rossmann fold (*75*) that binds to NADP or NADPH. The second domain is an α/β fold known as the SR fold. This domain consists of a central seven-

stranded mixed β-sheet. The third domain is an all-helical domain that moves upon binding of substrates. The active site is in a deep cleft that forms between domains 1 and 2 (*76*).



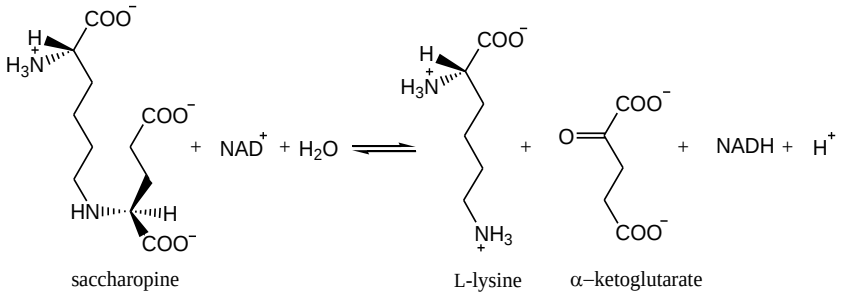
(1.6)

A chemical mechanism can be written using the general mechanism for amino acid dehydrogenases. An imine is formed by attack of the α-amine of glutamate on the δ-aldehyde of AAS, likely facilitated by a general acid-base catalyst. Reduction of the imine then gives the product saccharopine. A second possibility involves the cyclic imine formed by attack of the α-amine of AAS on its δ-aldehyde. In this case, the α-amine of glutamate attacks the imine carbon in a transimination reaction, generating the same imine intermediate. Similar acid-base chemistry is used, but the physical rearrangement to generate the common imine may not be accommodated in the SR active site. The conformation of saccharopine as bound in the E:NADPH:saccharopine structure from *M. grisea* favors the first possibility (*76*). In addition, the principle of microscopic reversibility requires the imine be formed as the product in the reverse reaction, which is unlikely. Nevertheless, this mechanism cannot be ruled out at present.

1.3.7 Saccharopine Dehydrogenase

Saccharopine dehydrogenase [N^6-(glutaryl-2)-L-lysine:NAD oxidoreductase (L-lysine forming); (EC 1.5.1.7)] is the last enzyme in the AAA pathway for lysine

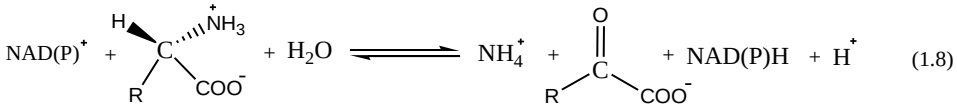
biosynthesis. It catalyzes the reversible pyridine nucleotide-dependent oxidative deamination of saccharopine to generate α-Kg and lysine using NAD as an oxidant, as shown in eq 1.7.



1.4 Saccharopine Dehydrogenase

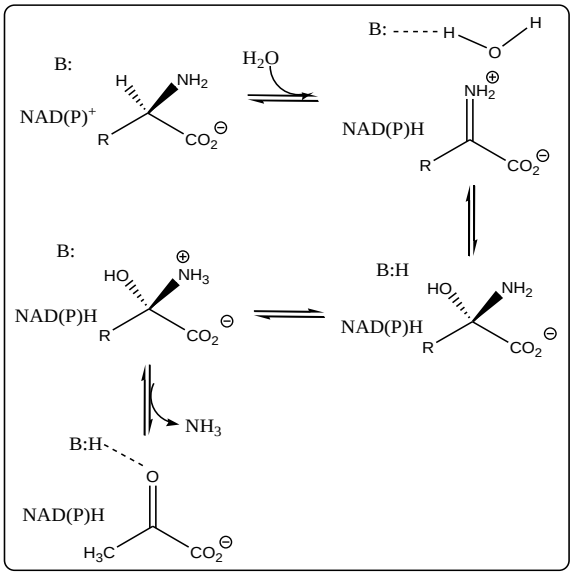
1.4.1 Pyridine Nucleotide-Linked Oxidative Deamination

The overall reaction catalyzed by SDH place it in the class of pyridine nucleotide-linked amino acid oxidoreductases. Enzymes in this class include amino acid dehydrogenases such as L-glutamate (GluDH), L-leucine (LeuDH), L-alanine (AlaDH), and L-phenylalanine (PheDH) dehydrogenases. They catalyze the reversible oxidative deamination of an amino acid to its keto acid and ammonia with the concomitant reduction of NAD(P), as shown in Eq 1.8 (*77*).



The kinetic mechanism reported for most amino acid dehydrogenases is ordered with coenzyme bound first and released last. Among amino acid dehydrogenases, AlaDH and GluDH are the two most extensively studied enzymes. A chemical mechanism consistent with data obtained for these two enzymes is shown in Scheme 1.3. The bound

amino acid is first oxidized by NAD(P) to an imine. A general base, usually an imidazole side chain, activates water to attack the imine to form a carbinolamine intermediate. The hydroxyl of the carbinolamine is deprotonated, resulting in the expulsion of ammonia, forming the keto product.



Scheme 1.3: Proposed general chemical mechanism for amino acid dehydrogenases.

For the AlaDH reaction, a combination of ^{15}N, solvent deuterium, and primary deuterium isotope effects suggested rate limitation at limiting substrate concentration is shared by all of the chemical-steps, oxidization of amino acid to imine, imine formation, and carbinolamine formation (*78*). The overall AlaDH reaction, i.e. at saturating reactant concentrations, is limited by the release of reduced nucleotide. In agreement with this suggestion, AlaDH and GluDH both exhibit substrate inhibition, resulting from formation of a dead-end ternary E:NAD(P)H:amino acid complex (*79, 80*). Only when alternative dinucleotides or substrates were used for AlaDH or GluDH did hydride transfer contribute to limitation under *V* conditions. The *pro*-S (B side) stereospecificity of

hydride transfer is highly conserved among amino acid dehydrogenases, with notable exceptions being L-alanine dehydrogenase (*81, 82*), L-lysine ε-dehydrogenase (*83*), and *meso*-DAP dehydrogenase (*84*), which are *pro*-R (A side) specific. In addition, SDH is *pro*-R specific (*85, 86*).

3-D structures are available for Glu (*87*), Leu (*88*), Ala (*89*), Phe (*90*), and *meso*-DAP dehydrogenases (*84*). Among them, *meso*-DAP dehydrogenase is unique in that it catalyzes the oxidative deamination of a D-amino acid. All structures share very high similarity in that they have the same quaternary structure, similar active sites, and identical residues involved in catalysis with one exception, i.e. AlaDH. A subunit is composed of large N- and C-terminal domains that are separated by a deep cleft containing the active site (*84, 87, 88*). One of the domains (usually C-terminal) contains the "Rossmann fold", providing binding interactions for the pyridine nucleotide, whereas the other domain binds the amino acid. In addition, a conformational transition exists from an "open" to a "closed" form upon binding of substrates or inhibitors in the amino acid binding site (*84, 87*). However, a combination of amino acid substitutions and subtle main chain movement in the substrate side-chain binding sites linked to the quaternary structure account for differences in substrate specificity seen within this family of enzymes (*91*). These changes are also expected in the SR and SDH structures.

In contrast, the structure of AlaDH, obtained from the *Phormidium lapideum* and *Bacillus stearothermophilus* (*89*) is structurally different, with a subunit structure, identity of residues in the dinucleotide binding fold, and active site location similar to the D-2-hydroxyacid dehydrogenases and component dI of transhydrogenase (*89*). In all of these enzymes, a histidine residue acts as the acid-base catalyst activated by an adjacent

glutamate or aspartate carboxyl group, whereas the substrate carbonyl group is polarized by hydrogen bonding to the guanidinium group of an arginine or the amino group of a lysine residue. The substrate carboxyl group is anchored by interactions with either the guanidinium group of a second arginine or with two main chain NH groups (*89*).

1.4.2 Expression and Purification of SDH

A monomeric subunit structure was reported for the enzyme from *S. cerevisiae* with a molecular weight of 39,000 Da (*92*). It is a basic protein with a pI of 10.1, and is stable for months at -20 °C at concentrations greater than or equal to 0.1 mg/ml and a pH of 5.0-8.0 (*92*). It contains four cysteine residues but no disulfide bonds, and one binding site for reactants per molecule of enzyme (*93*). The *LYS1* gene has been cloned from *C. albicans* (*14*) and *S. pombe* (*94*).

1.4.3 Kinetic Mechanism of SDH

The overall reaction catalyzed by SDH is reversible. The *S. cerevisiae* enzyme has pH optimum of 10.0 in the direction of lysine formation and 7.0 in the direction of saccharopine formation (*1, 95*). The K_m values for NAD, saccharopine, lysine, α-Kg, and NADH were estimated as 0.1, 1.7, 2, 0.55, and 0.089 mM, respectively (*1*). An ordered Bi-Ter kinetic mechanism was proposed for the SDH with NAD binding first, followed by saccharopine, and products released in the order of lysine, α-Kg, and NADH (*1, 96, 97*). Because all substrates must add to the enzyme before any product is released, the enzyme may be considered to have separate binding sites for the coenzyme, keto and amino substrates. With pyruvate as a substrate, data also suggest an ordered Ter-reactant mechanism in the direction of ε-N-(L-propionyl-2)-L-lysine formation, but with the order

NAD, ε-N-(L-propionyl-2)-L-lysine, pyruvate, lysine, and NADH (*98*). The reversal in the release of lysine and the keto acid suggests that there may be a randomness in substrate binding.

1.4.4 Chemical Mechanism of SDH

SDH is a *pro*-R specific for hydride transfer from C-2 of the saccharopine glutaryl moiety to the nicotinamide ring of NAD (*85, 86*). A series of chemical modification experiments suggested the presence of essential cysteine (*93*), histidine (*99*), lysine (*100*), and arginine residues (*101*) that may be involved in substrate binding and/or catalysis.

A chemical mechanism of the SDH has been proposed on the basis of pH-rate profiles and product and dead-end inhibition studies (*86*). Saccharopine is first oxidized to ε-glutariminyl-L-lysine. A general base then activates water for attack to form a carbinolamine intermediate, which collapses to give the products, L-lysine and α-Kg by using general acid, general base chemistry.

In the direction of saccharopine formation, the pH dependence of V/K_{Lys} exhibits a pK of 6.3 for a group that must be unprotonated, and a pK of 8.0 for a group that must be protonated for activity (*86*). Temperature and solvent perturbation studies are consistent with these groups being histidines. The $V/K_{\alpha\text{-}Kg}$ pH profile exhibits a single pK of 8.4 for a group that must be protonated for α-Kg binding (*86*). In the direction of saccharopine cleavage, the V/K_{Sacc} pH profile shows two pK values of 6.0 and 7.1 that must both be unprotonated for catalysis and/or binding of saccharopine (*86*). Although the mechanism proposed is certainly consistent with the data, studies are incomplete and the identity of the groups involved is based on the observed pK values, their temperature dependence, and chemical modification studies; all are notoriously inaccurate.

1.4.5 Substrate Specificity of SDH

SDH from *S. cerevisiae* shows very strict substrate specificity with respect to its amino acid and keto acid substrates (*102*). Only pyruvate has been observed as an alternative substrate in the direction of ε-N-(L-propionyl-2)-L-lysine formation (*103*). In addition, the enzyme exhibits a high degree of coenzyme specificity (*102, 104*). It does use NADPH as a poor substrate, but with a much lower affinity compared to NADH (*95*). Furthermore, binding of NADPH causes an increase in the K_m values for α-Kg and lysine (*95*). Coenzyme fragments, such as AMP, ADP, ADP-Ribose, and ATP, inhibit the enzyme activity, but no inhibition is observed by adenine, 3'-AMP, 2'-deoxy-5'-AMP, IMP, GMP, pyrimidine nucleotides, NMN^+, and NMNH (*95*). Data suggest that the AMP moiety of NAD is responsible for the majority of the binding energy. The lack of inhibitory effect of 2'-deoxy-5'-AMP and low affinities of NADPH suggest that the interaction of the oxygen at the 2' position of the adenosine moiety with the enzyme is important in binding (*95*). No binding of lysine or α-Kg to free enzyme was detected.

Several pyridine nucleotide dehydrogenases that have an ordered kinetic mechanism exhibit substrate inhibition. SDH was reported to exhibit inhibition by high concentrations of α-Kg and lysine in the direction of saccharopine formation, but not by saccharopine in the oxidative direction (*105*).

Hydrophobic amino acids with five and six carbon atoms, leucine, norleucine, and norvaline, were potent inhibitors, whereas branched chain isomers, valine, isoleucine, and α-aminobutyrate inhibited weakly, and no inhibition was observed by aspartate, glutamate, or AAA (*96*). It appears that a hydrophobic interaction between the side chain of an amino acid and the enzyme is important in binding the amino acid reactant.

Inhibition observed with keto acid analogues was more complicated. Noncompetitive inhibition was observed with OAA, pyruvate, α-ketobutyrate, α-ketovalerate, and α-ketocaproate, whether NADH, α-Kg, or lysine was the varied substrate, inconsistent with the proposed kinetic mechanism. Data suggested combination of the dead-end inhibitors with more than one enzyme form, but this aspect will have to await future studies.

1.4.6 Structure and Sequence Allignment

In *S. cerevisiae*, *Y. lipolytica*, and *C. albicans*, an 11-amino acid active site peptide, GRCGSGALIDL, has been identified that is thought to originate from the Rossmann fold responsible for the binding of the adenosine moiety of NADH (*106*). In the Rossmann fold, the Gly is strictly conserved to eliminate steric hindrance in binding the ribose ring, and the terminal Glu (Asp) is conserved because of its function in hydrogen bonding the 2'-OH of the adenosine ribose.

Multiple sequence alignment indicates SDH has a similar sequence in three fungi (*C. albicans, Y. lipolytica,* and *S. pombe*), four animals (*Caenorhabditis elegans, Mus musculus, Homo sapiens,* and *Bos Taurus*), one plant (*Zea mays*), and nine prokaryotes (*20*). Construction of a phylogenetic tree indicates SDH and prokaryotic L-AlaDH have a common ancestor (*20*). L-AlaDH, catalyzes the NADH-dependent reversible reductive amination of pyruvate to L-alanine and is the key factor in the assimilation of L-alanine as an energy source via the tricarboxylic acid cycle during sporulation in *Bacillus* spp. The structure of L-AlaDH has been solved (*89*), and sequence alignment of it and SDH shows that the residues involved in the active site of AlaDH, Arg15, His95, and Lys74, are highly conserved in SDH.

1.5 Summary

Although mechanistic precedence for each of the enzyme-catalyzed reactions discussed above in the AAA pathway is available, none of the mechanisms of the enzymes in the first half of the pathway is known with any certainty. However, some information is available for enzymes in the second half of the pathway. A general mechanism has been proposed for the AAR (*69*), but all mechanistic detail is lacking. For the SR, only structural information is available, with virtually nothing known of its mechanism. Significant, but incomplete, mechanistic data have been collected for the SDH, but no structural information is available. Regulation of the pathway at the enzyme level is not completely clear and little is known about the mechanism of regulation.

Our understanding of the AAA pathway for lysine synthesis at the molecular level has been increasing dramatically, together with a growth in genomic information. However, a complete understanding of the gene-enzyme relationship, mechanisms of the enzymes, regulation of the AAA pathway, and a comparative study of the cloned genes would help to gain an understanding of the functions of the biosynthetic and catabolic genes and enzymes. Knowledge gained using biochemical and molecular techniques with *S. cerevisiae* can be applied to pathogenic fungi to gain a basic understanding of the metabolism of fungal pathogens. Systemic fungal infections are among the most difficult infectious diseases to treat and are life-threatening for individuals who are immune-suppressed, including those with AIDS and other autoimmune diseases, those undergoing chemotherapy, and those who have undergone a transplant. All of the presently available antifungal drugs have side effects, including nausea, vomiting, and diarrhea; toxicities, including hepatotoxicity and renal insufficiency; and drug interactions. It is thus

important to develop new antifungal drugs that are more effective and less toxic. The metabolic pathway for the biosynthesis of lysine in fungi is for the most part unique to these organisms, which has prompted speculation that the enzymes involved in the pathway may be viable targets for selective antifungal agents. Selective inhibition of the enzyme(s) by an appropriate substrate analog(s) may control the growth of fungal pathogens *in vivo*. Similarly, the novelty of several genes in the pathway may permit them to serve as a molecular marker to facilitate rapid identification of fungal pathogens.

Preliminary mechanistic data have been collected for the SDH. However, the proposed kinetic mechanism was considered suspect because of the inconsistency of data, and chemical mechanism studies are incomplete. The identity of the groups involved in the reaction is based on the observed pK_a values, their temperature dependence, and chemical modification studies, which are less than diagnostic. The specificity determinants for binding saccharopine are not clear, nor are those for substrate specificity in either the oxidative deamination or reductive amination reaction directions. In this dissertation, the kinetic and chemical mechanisms of SDH from *S. cerevisiae* have been fully determined, as well as the topography of the active site. Data are also discussed in terms of potential rate limiting steps along the reaction pathway.

Three fourth of this dissertation is reproduced with permission from:

1. Xu, H., Andi, B., Qian, J., West, A. H., and Cook, P. F. (2006) The α-aminoadipate pathway for lysine biosynthesis in fungi, *Cell. Biochem. Biophys. 46*, 43-64. Copyright [2006] Humana Press, Inc.

2. Xu, H., West, A. H., and Cook, P. F. (2006) Overall kinetic mechanism of saccharopine dehydrogenase from *Saccharomyces cerevisiae, Biochemistry 45*, 12156-12166. Copyright [2006] American Chemical Society.

3. Xu, H, West, A. H., and Cook, P. F. (2006) A proposed proton shuttle mechanism of saccharopine dehydrogenase from *Saccharomyces cerevisiae, Biochemistry 46*, 871-882. Copyright [2007] American Chemical Society.

CHAPTER 2

MATERIALS AND METHODS

2.1 Chemicals

All chemicals were of the highest grade commercially available and were used without further purification. L-Saccharopine, L-lysine, D-lysine, L-ornithine, L-valine, L-norvaline, L-methionine, L-leucine, L-isoleucine, L-asparagine, L-glutamine, L-arginine, adenosine, AMP, ADP, ADP-ribose, NMN, 3-APAD, 3-PAAD, thio-NAD, 2',3'-cyclic NADP, α-Kg, pyruvate, glyoxylate, α-ketobutyrate (α-Kb), α-ketovalerate (α-Kv), α-ketomalonate (α-Km), α-ketoadipate (α-Ka), malonate, oxaloacetate (OAA), adipate, glutarate, α-ketoisovalerate (α-Kiv), α-ketopimalate (α-Kp), pyridine 2,4-dicarboxylate, pyridine 2,3-dicarboxylate, pyridine 2,5-dicarboxylate, L-pipecolic acid, imidazole, chloramphenicol, yeast lactate, alcohol, and aldehyde dehydrogenases were obtained from Sigma. β-NAD(P)H, β-NAD(P), Luria-Bertani (LB) broth, and LB agar were purchased from USB. The Ni-NTA agarose resin was from Qiagen. Isopropyl-β-D-1-thiogalactopyranoside (IPTG), *Sma*I, *Nde*I, *Bam*HI, Platinum Pfx polymerase, and T4 DNA ligase were from Invitrogen. Ampicillin (Amp) was from Fisher Biotechnologies. Oxalylglycine (OG) was from Frontier Scientific. Succinate and oxalate were from Fisher Scientific. Mes, Hepes, Ches, and Taps were from Research Organics, Inc. Deuterium oxide (D_2O) (99 atom % D) and ethanol-d_6 (99 atom % D) were purchased from Cambridge Isotope Laboratories, Inc. AG MP-1 and Bio-Gel P-2 resins were from Bio-Rad. All other chemicals and reagents were obtained from commercial sources, were reagent grade, and were used without further purification.

2.2 Molecular Cloning, Cell Growth, and Protein Expression

A 1154 bp DNA fragment encoding SDH was amplified by polymerase chain reaction (PCR) with 200 ng of yeast genomic DNA as the template using the following protocol: one cycle of initial denaturation at 94 °C for 2 min, followed by 35 cycles of denaturation at 94 °C for 45 s, annealing at 50 °C for 45 s, and extension at 72 °C for 3 min. The enzyme used was Platinum Pfx polymerase, which produces blunt end PCR products. The pUC12 cloning vector was digested with *Sma*I to create a blunt-end linear vector that was gel purified. The purified *Lys1* DNA was ligated into linearized pUC12 vector. *Escherichia coli* DH5α cells were transformed with the plasmid, and single colonies were grown on LB/Amp medium. Plasmids from each clone were isolated, and restriction endonuclease mapping was carried out on the plasmids to confirm the presence of the insert.

For subcloning into the expression vector, the *Lys1* insert was excised from the pUC12-*Lys1* plasmid with *Nde*I/*Bam*HI restriction endonucleases and the digested plasmid was electrophoresed on a 1% agarose gel. The fragment containing the *Lys1* gene was gel-purified and subcloned using T4 ligase into the pET16b expression vector, which was previously digested with *Nde*I/*Bam*HI. *E. coli* BL21 (DE3) RIL cells were then transformed, and the new plasmid was designated sdhHX1. The entire gene was then sequenced at the Laboratory for Genomics and Bioinformatics of the University of Oklahoma Health Science Center in Oklahoma City, OK.

The sdhHX1 plasmid-containing strain was grown at 37 °C in LB supplemented with 100 μg/mL amplicillin and 25 μg/mL chloramphenicol. Induction by 1 mM IPTG (final concentration) was accomplished once the OD_{600} reached 0.7-0.9. Cell growth was

then continued at 32 ºC overnight. After centrifugation, the harvested cells were suspended in 100 mM Hepes at pH 7.0 and sonicated on ice for 1.5 minutes, with a 15 s pulse followed by a 30 s rest, using a MISONIX Sonicator XL. After the cell debris was removed by centrifugation at 12000*g* for 15 min, the collected supernatant was mixed with the Ni-NTA resin at 4 ºC, washed with 20 mM imidazole at pH 7.0, and then eluted with buffer containing 300 mM imidazole at pH 7.0. The SDH-containing sample, identified by SDS-PAGE, was concentrated using an Amicon ultrafiltration device with a YM 10 membrane. Protein concentration was determined either by the Bradford method using bovine serum albumin as a standard or by the intrinsic enzyme absorbance at 280 nm using an ε of 40.21 $mM^{-1}cm^{-1}$. The protein concentrations determined by the two methods were identical within error.

2.3 Enzyme Assays

The SDH-catalyzed oxidative deamination reaction was followed by monitoring the increase (or decrease) in absorbance at 340 nm as NAD(P) is reduced or NAD(P)H is oxidized, and by monitoring the increase in absorbance at 363, 358, and 395 nm as 3-APAD, 3-PAAD, and thio-NAD are reduced, respectively, using a Beckman DU640 UV/vis spectrophotometer. The following extinction coefficients were used for NAD(P)H, reduced 3-APAD, 3-PAAD, and thio-NAD: 6.22 $mM^{-1}cm^{-1}$, 9.1 $mM^{-1}cm^{-1}$, 9.3 $mM^{-1}cm^{-1}$, and 11.3 $mM^{-1}cm^{-1}$ (*136*).

All kinetic assays were carried out at 25 °C, and the temperature was maintained by a Neslab RTE-111 circulating water bath. A unit of enzyme activity is defined as the amount of enzyme catalyzing the production or utilization of 1 μmole of dinucleotide substrate analogs per min at 25 °C. Reactions were carried out in semi-micro quartz

cuvettes with a path length of 1 cm in a final volume of 1 or 0.5 ml containing 100 mM buffer (Mes, pH 5.5-6.8; Hepes, pH 6.8-8.2; Ches, pH 8.2-10.0) and variable concentrations of substrates as indicated below. Reactions were initiated by the addition of small amount (10 or 20 μL) of an appropriately diluted enzyme solution to a mixture that contained all other reaction components, and the initial linear portion of the time course was used to calculate the initial velocity. Because the diluted enzyme solution (protein concentrations less than 100 μg/mL) is not stable, 50% glycerol was added to the enzyme solution to minimize any activity loss, and the diluted enzyme solution was prepared fresh daily.

2.4 Initial Velocity Studies

2.4.1 Systematic Analysis

The initial rate in the direction of saccharopine formation was measured as a function of NADH concentration (0.015-0.2 mM), different fixed concentrations of α-Kg (0.1-1 mM), and a fixed concentration of L-lysine (0.5 mM). The experiment was then repeated at several additional L-lysine concentrations (0.71-5 mM). Initial velocity studies were also carried out in the direction of saccharopine oxidation at pH 7.0. In this case, the initial rate was measured as a function of NAD (0.2-2 mM) at different fixed levels of saccharopine (5-50 mM). The amount of enzyme used for each reaction in the direction of saccharopine oxidation was twice that used in the reverse reaction (final concentration 0.014 μM).

When NADPH was used as the coenzyme in the direction of saccharopine formation, a systematic initial velocity study was performed at pH 7.0 in a similar manner as mentioned above. Briefly, the initial rate was measured as a function of the NADPH

concentration and at different fixed levels of α-Kg and a fixed concentration of lysine. The experiment was then repeated at different lysine concentrations. The concentration ranges for NADPH, α-Kg, and lysine are 0.05-0.3, 1-10, and 2-20 mM, respectively. Systematic initial velocity studies were also carried out when pyruvate served as the keto acid substrate. In this case, initial rates were measured as a function of the pyruvate concentration (5-50 mM) at different fixed levels of lysine (30-300 mM), with NADH fixed at 0.2 mM at pH 7.0. The amount of enzyme used for each reaction was 6.5 times that used in SDH reactions with the natural substrates.

In the direction of saccharopine oxidation, initial rates were also measured as a function of the concentration of the coenzyme analogues, NADP, 3-APAD, 3-PAAD, and thio-NAD, respectively, with saccharopine fixed at 6 mM; the pH was maintained at 7.55 or 9.2. Since the concentration of saccharopine used was relatively low (~K_m), the K_{ia} of oxidized dinucleotides were obtained. In order to estimate the apparent K_m values of the keto acid substrates, glyoxylate, α-Kb, α-Kv, α-Km, and α-Ka, initial rates were measured as a function of the concentration of keto acid substrates, with NADH fixed at 0.2 mM, and lysine at 20 or 40 mM, at pH 7.0.

2.4.2 Pairwise Analysis

Initial rates were measured varying one substrate at different fixed concentrations of a second and with the third substrate saturating. For example, the initial rate was measured as a function of NADH at several fixed levels of α-Kg and with lysine fixed at 10K_m. The fixed saturating concentrations of NADH, α-Kg, and L-lysine were 0.2 mM (5K_m), 5 mM (20K_m), and 12.5 mM (10K_m), respectively.

2.5 Determination of K_{eq} and the Haldane Relationship

In a 1 mL reaction mixture, the concentrations of NADH, α-Kg, L-lysine, and saccharopine were fixed at 0.05, 0.1, 0.1, and 2.5 mM, respectively, and the concentration of NAD was varied over the range of 0.1-5 mM in separate reactions. The reaction was initiated by the addition of enzyme. The difference in A_{340} representing the displacement from equilibrium was plotted against the NAD concentration. The K_{eq} is obtained using the concentrations given above and the concentration of NAD that gave a ΔA_{340} of 0 according to eq 2.1.

$$K_{eq} = \frac{[\mathrm{NADH}][\alpha - \mathrm{Kg}][\mathrm{L-lysine}]}{[\mathrm{NAD}][\mathrm{saccharopine}]} \tag{2.1}$$

The K_{eq} was also estimated from the Haldane relationship for a Bi-Ter kinetic mechanism according eq 2.2.

$$K_{eq} = \frac{(\frac{V}{K_{Sacc}})K_{iNADH}K_{ilys}}{(\frac{V}{K_{\alpha-Kg}})K_{iNAD}} \tag{2.2}$$

2.6 Inhibition Studies

2.6.1 Substrate Inhibition Studies

Lysine substrate inhibition studies were carried out by measuring the initial rates as a function of the lysine concentration (5-200 mM), with the concentration of the other two substrates both fixed at their respective K_m values. In the case of α-Kg substrate inhibition, the initial rates were measured as a function of the NADH concentration and

different fixed α-Kg concentrations (0.1-50 mM) and with the lysine concentration fixed at 6 times its K_m value.

2.6.2 Product and Dead-End Inhibition Studies

Inhibition patterns were obtained by measuring the initial rate at different concentrations of one reactant, with the concentration of the other reactants fixed at different levels (see Tables and Figure Legends), and at different fixed concentrations of the inhibitor including zero. In all cases, an initial estimate of the K_i for the inhibitor was obtained by fixing the varied substrate at its K_m value and varying the inhibitor concentration. The appK_i is estimated by Dixon analysis, a plot of $1/v$ vs **I**, extrapolating to $1/v$ equal to 0, and dividing by 2.

2.6.3 Double Inhibition Studies

A double-inhibition study was performed to investigate the existence of the E:NAD:α-Kg dead-end complex. The initial rates were measured as a function of NAD (0-8 mM) at different fixed levels of α-Kg (20-50 mM), with the concentration of the other substrates, NADH and lysine, both fixed at their respective K_m values.

Double-inhibition studies were also performed to determine whether synergism of binding occurs between analogues of α-Kg and lysine. In the direction of saccharopine formation, initial rates were measured as a function of OG (0-0.2 mM) or pyridine 2,4-dicarboxylic acid (0-4 mM), respectively, at different fixed levels of ornithine (0-15 mM), with the concentration of NADH maintained saturating ($10K_m$), while α-Kg and lysine were maintained at their respective K_m values.

2.7 pH profiles and pK_i profiles

In order to determine whether the kinetic mechanism changes with pH and to obtain estimates of the K_m values of all of the substrates as a function of pH, initial velocity patterns were obtained at pH 5.5, 7.0, 8.0, 8.5, 9.5, in a same manner as described in **Materials and Methods 2.4.1**. Initial velocity studies were also carried out in the direction of saccharopine oxidation at the pH extremes (6.0 and 9.6). The pH dependence of V and V/K for all substrates was then obtained under conditions in which one substrate concentration was varied with the others maintained at saturation ($\geq 10K_m$). At different pH, inhibition constants were obtained for inhibitors competitive with NADH, α-Kg, and lysine, respectively, at a fixed concentration of the other two substrates (K_m) and different fixed levels of inhibitor including zero.

The pH was maintained using the following buffers at ≥ 100 mM concentration: Mes 5.5-6.8; Hepes, 6.8-8.2; Ches; 8.2-10.0. Sufficient overlap was obtained upon changing buffers to determine whether the buffer effects the reaction (no effects were detected). The pH was recorded before and after initial velocity data were measured with changes limited to ≤ 0.1 pH unit. The enzyme is stable when incubated for 20 min over the pH range 5.5-9.8. pH profiles were then evaluated graphically for quality of data by plotting log$V$ or log(V/K) against pH, while the inhibition profiles for AMP, OG, and leucine were evaluated by plotting log($1/K_i$) against pH.

2.8 Isotope Effect Studies

2.8.1 Synthesis of 4*R*-NADD (A-side)

The 4*R*-NADD was prepared according to (*107, 108*). The reaction mixture contained 2.8 mM ethanol-d_6, 5.6 mM NAD, 50 units of yeast alcohol dehydrogenase, and 100 units of yeast aldehyde dehydrogenase in 10 ml of 6 mM Taps, at pH 9.0 and 25 °C. The pH was adjusted to 9.0 with KOH throughout the reaction since protons are being produced and the reaction mixture is lightly buffered. The reaction was allowed to proceed overnight, several drops of $CHCl_3$ were added to the mixture to quench the reaction, and the aqueous layer was adjusted to pH 10.0 with KOH and removed for ion-exchange chromatography. The NADD eluted in a large single peak with baseline separation from NAD when eluted isocratically from an 4 x 25-cm AG MP-1 column with 1 M LiCl, pH 10.0. The reported ratio of absorbance at 260 and 340 nm for A-side NADD was 2.15 ± 0.05 (*107*). The ratio obtained for the sample prepared above is 2.2 ± 0.05. The purified A-side NADD was concentrated by rotary evaporation at 25 °C to about 5 mL. The concentrated solution was then desalted via a 1.6 x 60-cm Bio-Gel P-2 column. The concentrations of NADH(D) stock solutions were adjusted spectrophotometrically, using an ε_{340} of 6.22 $mM^{-1}cm^{-1}$.

2.8.2 Primary Substrate Deuterium Kinetic Isotope Effects

Isotope effects were measured by direct comparison of initial velocities, with NADD used as the deuterated substrate. $^{D}V_2$ and $^{D}(V_2/K_{Lys})$ were obtained in triplicate by measuring the initial rate as a function of lysine concentration at saturating levels of either NADH(D) and α-Kg (10 K_m). $^{D}(V_2/K_{NADD})$ and $^{D}(V_2/K_{\alpha\text{-}Kg})$ were obtained in the

same manner, varying NADH(D) or α-Kg, at saturating levels of the other two substrates, respectively. $^{D}V_2$ and $^{D}(V_2/K_{Lys})$ were also measured as a function of pH.

Primary deuterium kinetic isotope effects were also measured for the reaction in which pyruvate replaced α-Kg by direct comparison of initial rates with NADH and NADD. The fixed concentrations used for NADH(D), pyruvate, and lysine are 0.2 mM (~3K_m), 50 mM (~12.5K_m), and 300 mM (~5K_m), respectively.

2.8.3 Solvent Deuterium Isotope Effects and Proton Inventory Experiments

Initial velocities were measured in H_2O and D_2O. For rates measured in D_2O, substrates (NADH, α-Kg and lysine) and buffers were first dissolved in a small amount of D_2O and lyophilized overnight to remove exchangeable protons. The lyophilized powders were then dissolved in D_2O to give the desired concentrations and the pD was adjusted using either DCl or NaOD. A value of 0.4 was added to pH meter readings to calculate pD (*109*). Data were obtained with lysine as the variable substrate at fixed concentrations (10K_m) of NADH and α-Kg. The isotope effects were obtained by direct comparison of initial rates in H_2O and D_2O over the pH(D) range 6.6-8.3, around the pH-independent region of the *V* and *V/K* pH-rate profile. Reactions were initiated by adding 10 μL of enzyme solution in H_2O, such that the final percentage of D_2O is ca. 99%.

In the direction of saccharopine formation, finite isotope effects were observed, and proton inventory experiments were carried out to measure the solvent deuterium kinetic isotope effects more accurately and estimate the number of proton(s) in flight in the rate-determining transition state(s) (*110*). V_2 and V_2/K_{Lys} were measured at pH(D) 7.1 in 100% H_2O, 25% D_2O, 50% D_2O, 75% D_2O, and ~100% D_2O with lysine as the variable substrate at a fixed concentration of NADH and α-Kg (10K_m).

2.8.4 Multiple Solvent/Substrate Deuterium Isotope Effects

The multiple isotope effect was obtained by direct comparison of initial rates in H_2O and D_2O with lysine varied and NADD and α-Kg fixed at $10K_m$. It was also measured by comparison of initial rates using NADH and NADD in D_2O with lysine as the varied substrate. Rates were measured at pH(D) 7.1, the pH-independent region of the *V* and *V/K* pH-rate profile.

Nomenclature. Isotope effects are expressed using the nomenclature developed by Northrop (*111*) and Cook and Cleland (*112*). Primary and solvent deuterium kinetic isotope effects are written with a leading superscript D and D_2O; e.g., a primary deuterium isotope effect on *V/K* is written $^{D}(V/K)$. Multiple isotope effects are written with a leading superscript to depict the isotope varied and a following subscript to depict the fixed isotope; e.g., a solvent deuterium isotope effect measured with A-side NADD would be written $^{D2O}(V/K)_D$. A "sticky" substrate is one that reacts to give product as fast as or faster than it dissociates from the enzyme complex.

2.9 ^{1}H NMR Experiments

2.9.1 Measurement of the Saccharopine Secondary Amine pK_a by NMR

The pK_a value of saccharopine was determined by measuring the ^{1}H NMR chemical shifts of protons β to the secondary amine nitrogen of saccharopine as a function of pH at 21 °C. Solutions in D_2O of 20 mM saccharopine and 20 mM K_2HPO_4 buffer were prepared. The solution was adjusted to different pD values (5.0-11.9) using either DCl or NaOD. All 1D and 2D NMR experiments were performed on a Varian Mercury VX-300 MHz spectrometer with a Varian 4-nuclei auto-switchable PFG probe.

^{1}H NMR spectra were collected using the PRESAT pulse sequence supplied by Varian, Inc. The spectra were collected with a sweep width of 1510.1 Hz, eight transients, and an acquisition time of 5.490 s and processed with 32K points resulting in a 0.09 Hz digital resolution. Assignment of chemical shifts was aided by gCOSY experiments. The gCOSY pulse sequence supplied by Varian, Inc., was used, and data were collected with 1 transient and 128 increments.

2.9.2 Product Identification by NMR

When keto acid analogues were used as slow substrates, products were identified by measuring the ^{1}H NMR chemical shifts of protons β to the secondary amine nitrogen of the new products at 21 °C. Reaction mixtures containing 2 mM NADH, 20 mM keto acid analogues, and 2 mM lysine were prepared in 20 mM K_2HPO_4 buffer, and were adjusted to a pD value of 7.4 using either DCl or NaOD before SDH was added. The purified SDH was dialyzed against 20 mM K_2HPO_4 at pD 7.4. Once the enzyme was added, the reaction mixtures were kept at 4 ºC overnight, allowing sufficient time for the reaction to reach completion (monitored spectrophotometrically). Once the reactions were complete, several drops of $CHCl_3$ were added to the mixtures to precipitate the enzyme, and sufficient heat acid-activated charcoal was then added to remove the dinucleotides. The remaining reaction mixtures were then analyzed by ^{1}H NMR. All NMR experiments were performed on the same instrument mentioned above, and the spectra were collected with a sweep width of 4803.1 Hz, 8 transients, and an acquisition time of 1.998 seconds.

2.10 Data Analysis

Initial velocity data were first analyzed graphically using double-reciprocal plots of initial velocities vs substrate concentrations and suitable secondary and tertiary plots. Data were then fitted using the appropriate equation as discussed below, using the Marquardt-Levenberg algorithm (*113*), supplied with the EnzFitter program from BIOSOFT, Cambridge, U.K. and the Fortran programs of Cleland (*114*). Kinetic parameters and their corresponding standard errors were estimated using a simple weighting method.

Data obtained from the systematic initial velocity studies of SDH using natural substrates at different pH in the direction of saccharopine formation were fitted using eqs 2.3 and 2.4 for a terreactant kinetic mechanism (*115*), while in the direction of saccharopine oxidation at different pH, data were fitted using eq 2.5. The three data sets obtained from the pairwise analysis in the direction of saccharopine formation were fitted using either eq 2.5 for a sequential mechanism or eq 2.6 with the constant term absent. Data conforming to competitive (C), noncompetitive (NC), or uncompetitive (UC) inhibition were fitted using eqs 2.7-2.9. Data for double inhibition by NAD/α-Kg were fitted using eq 2.10. Data for glutarate inhibition against NADH were fitted using eq 2.11. Data for V and V/K deuterium isotope effects were fitted using eq 2.12. Data obtained from systematic initial velocity studies using α-Kg substrate analogues in the direction of saccharopine formation, or using NADPH as the coenzyme substrate were fitted using eq 2.13 for a terreactant kinetic mechanism. When NADP, 3-APAD, 3-PAAD, and thio-NAD were used as coenzyme, respectively, in the direction of saccharopine oxidation, data were fitted using eq 2.14. When concentrations of pyruvate and lysine were varied at

a fixed NADH concentration, data obtained were fitted using eq 2.5 for a bireactant mechanism. Data for double inhibition studies by OG/ornithine and pyridine 2,4-dicarboxylic acid/ornithine were fitted using eq 2.10.

$$v = \frac{V\mathbf{ABC}}{\text{Constant} + (\text{CoefA})\mathbf{A} + (\text{CoefB})\mathbf{B} + (\text{CoefC})\mathbf{C} + K_c\mathbf{AB} + K_b\mathbf{AC} + K_a\mathbf{BC} + \mathbf{ABC}} \tag{2.3}$$

$$v = \frac{V\mathbf{ABC}}{\text{Constant} + (\text{CoefA})\mathbf{A} + K_c\mathbf{AB} + K_b\mathbf{AC} + K_a\mathbf{BC} + \mathbf{ABC}} \tag{2.4}$$

$$v = \frac{V\mathbf{AB}}{K_{ia}K_b + K_a\mathbf{B} + K_b\mathbf{A} + \mathbf{AB}} \tag{2.5}$$

$$v = \frac{V\mathbf{AB}}{K_a\mathbf{B} + K_b\mathbf{A} + \mathbf{AB}} \tag{2.6}$$

$$v = \frac{V\mathbf{A}}{K_a(1 + \frac{\mathbf{I}}{K_{is}}) + \mathbf{A}} \tag{2.7}$$

$$v = \frac{V\mathbf{A}}{K_a(1 + \frac{\mathbf{I}}{K_{is}}) + \mathbf{A}(1 + \frac{\mathbf{I}}{K_{ii}})} \tag{2.8}$$

$$v = \frac{V\mathbf{A}}{K_a + \mathbf{A}(1 + \frac{\mathbf{I}}{K_{ii}})} \tag{2.9}$$

$$v = \frac{v_o}{1 + \frac{\mathbf{I}}{K_i} + \frac{\mathbf{J}}{K_j} + \frac{\mathbf{IJ}}{\alpha K_i K_j}} \tag{2.10}$$

$$v = \frac{\mathrm{V}\mathbf{A}}{K_a(1 + \frac{\mathbf{I}^2}{K_{i\,s}{}^2}) + \mathbf{A}(1 + \frac{\mathbf{I}}{K_{ii}})} \tag{2.11}$$

$$v = \frac{V\mathbf{A}}{K_a(1 + F_i E_{V/K}) + \mathbf{A}(1 + F_i E_V)} \tag{2.12}$$

$$v = \frac{V\mathbf{ABC}}{K_{ia}K_{ib}K_c + K_{ib}K_c\mathbf{A} + K_{ic}K_a\mathbf{B} + K_{ia}K_b\mathbf{C} + K_c\mathbf{AB} + K_b\mathbf{AC} + K_a\mathbf{BC} + \mathbf{ABC}} \tag{2.13}$$

$$v = \frac{V\mathbf{A}}{K_a + \mathbf{A}} \tag{2.14}$$

In eqs 2.3-2.14, v and V are initial and maximum velocities, **A**, **B**, and **C** are substrate concentrations, **I** and **J** are inhibitor concentrations, and K_a, K_b, and K_c are Michaelis constants for substrates A, B, and C, respectively. In eqs 2.3 and 2.4, the constant and coef terms are products of kinetic constants that dependent on the kinetic mechanism and will be defined in the **Discussion 4.1.1**. In eq 2.5, K_{ia} is the dissociation constant of A from the EA complex, while in eq 2.13, K_{ia}, K_{ib}, and K_{ic}.are inhibition constants for A from EA, B from EAB, and C from EAC, respectively. In eqs 2.7-2.9, K_{is} and K_{ii} represent inhibition constants for the slope and intercept, respectively. In eq 2.10, K_i and K_j are dissociation constants for EI and EJ complexes, respectively, and v_0 is the rate in the absence of inhibitors and α is the interaction constant that estimates the influence of one inhibitor upon binding of the other. In eq 2.11, K_{is} is the average dissociation constant for glutarate from the E:glutarate and E:(glutarate)$_2$ complexes, and all other terms are the same as defined above. In eq 2.12, F_i is the fraction of D_2O in the solvent or deuterium label in the substrate, and $E_{V/K}$ and E_V are the isotope effects minus 1 on V/K and V, respectively.

Data for pH-rate profiles that decreased with a slope of 1 at low pH and a slope of -1 at high pH were fitted using eq 2.15. Data for pH-rate profiles with a slope of 1 at low pH were fitted using eq 2.16, while data for pH-rate profiles with a slope of -1 at high pH were fitted using eq 2.17. Data for pH-rate profile that decreased with a slope of 2 at low pH were fitted using eq 2.18. In the direction of saccharopine formation, data for the log$V$ pH-rate profile over the pH range 5.0-7.0 were fitted using eq 2.16, data for V for the pH

range 6.5-10.0 and data for the leucine pK_i profile were fitted using eq 2.19, while data for the AMP pK_i profile were fitted using eq 2.20.

$$\log y = \log\left[C / \left(1 + \frac{H}{K_1} + \frac{K_2}{H} \right) \right] \tag{2.15}$$

$$\log y = \log\left[C / \left(1 + \frac{H}{K_1} \right) \right] \tag{2.16}$$

$$\log y = \log\left[C / \left(1 + \frac{K_2}{H} \right) \right] \tag{2.17}$$

$$\log y = \log\left[C / \left(1 + \frac{H}{K_1} + \frac{H^2}{K_1 K_2} \right) \right] \tag{2.18}$$

$$\log y = \log\left[\frac{Y_L + Y_H \left(\frac{K_1}{H} \right)}{1 + \left(\frac{K_1}{H} \right)} \right] \tag{2.19}$$

$$\log y = \log \frac{\left[\frac{Y_H}{\left(1 + \frac{K_2}{H} \right)} + Y_L \left(\frac{H}{K_1} \right)^2 \right]}{\left[1 + \left(\frac{H}{K_1} \right)^2 \right]} \tag{2.20}$$

In eqs 2.15-2.20, y is the observed value of the parameter as a function of pH (V, V/K, or $1/K_i$), C is the pH-independent value of y, H is the hydrogen ion concentration, K_1 and K_2 represent acid dissociation constants for enzyme or substrate functional groups important in a given protonation state for optimal binding and/or catalysis, and Y_L and Y_H are constant values of V or $1/K_i$ at low and high pH, respectively.

CHAPTER 3

EXPERIMENTAL RESULTS

3.1 Protein Expression and Purification

The expression of SDH is very high under conditions used to induce expression. After the enzyme is washed with 20 mM imidazole, it is eluted from the Ni-NTA column most efficiently by 300 mM imidazole, and the purity of the eluted SDH is about 98% by densitometric scanning (data not shown). The amount of purified enzyme obtained is 35-40 mg from 200 mL cell culture (500 mg wet cell pellet). His-Tagged SDH is active and stable for months when kept at 4°C at concentrations ≥ 0.1 mg/mL and pH 7.0.

3.2 Kinetic Mechanism Determination of SDH

3.2.1 Initial Velocity Studies: Systematic Analysis

Double-reciprocal initial velocity patterns in the direction of saccharopine formation were obtained by varying the concentration of NADH and α-Kg at different fixed concentrations of lysine. The crossover points for all double-reciprocal plots are to the left of the ordinate, Fig. 3.1.1. All of the initial velocity data were fitted to the equation for a fully random terreactant mechanism (eq 2.3) to determine which terms, if any, in the denominator of the rate equation were absent. Data were then fitted to eq 2.4, which describes a kinetic mechanism with ordered addition of A followed by random addition of B and C. Values of the kinetic parameters determined were identical to those obtained using eq 2.3, and the standard error of the fit was also identical.

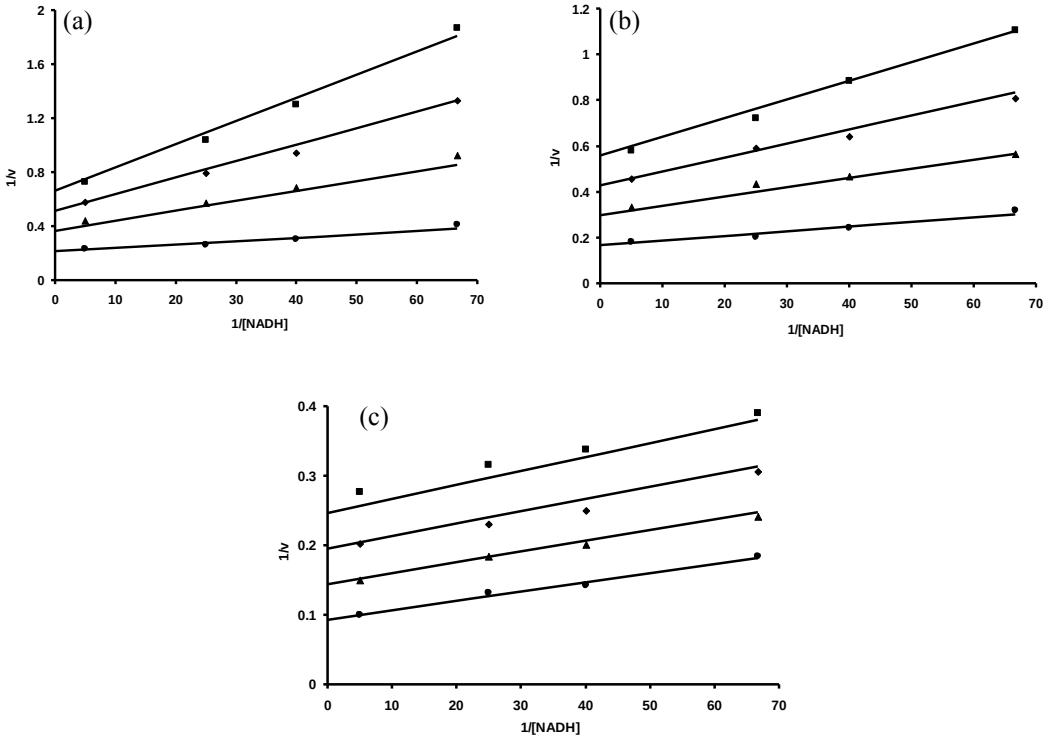


Figure 3.1.1: Systematic initial velocity studies of SDH in the saccharopine formation reaction direction at pH 7.0 -- primary plots. Double-reciprocal plots obtained upon varying the concentrations of NADH at different fixed levels of α-Kg (0.1 mM ■, 0.14 mM ♦, 0.25 mM ▲, and 1 mM ●) and a fixed concentration of lysine (0.71mM (a), 1.25 mM (b), and 5 mM (c)) were measured in 100 mM Hepes at pH 7.0 and 25°C. The points are experimental, while the solid lines are theoretical based on a fit to eq 2.5.

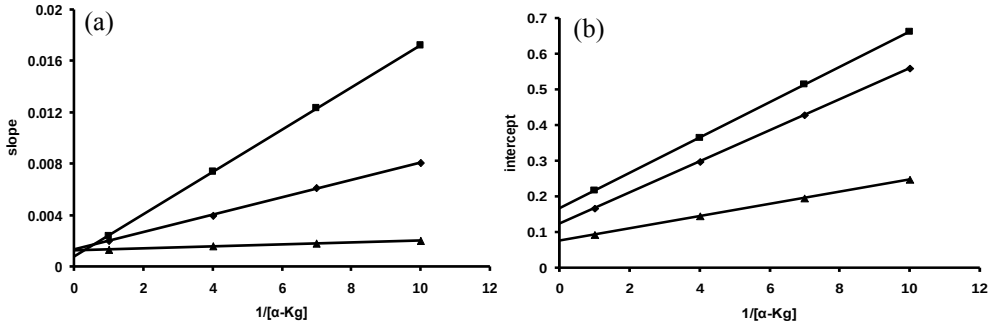


Figure 3.1.2: Systematic initial velocity studies of SDH in the saccharopine formation reaction direction at pH 7.0 -- secondary replots of double-reciprocal plots vs α-Kg concentration. (a) is the secondary slope replot, while (b) is the secondary intercept replot. Lysine concentration was fixed at 0.71 mM ■, 1.25 mM ♦, and 5 mM ▲.

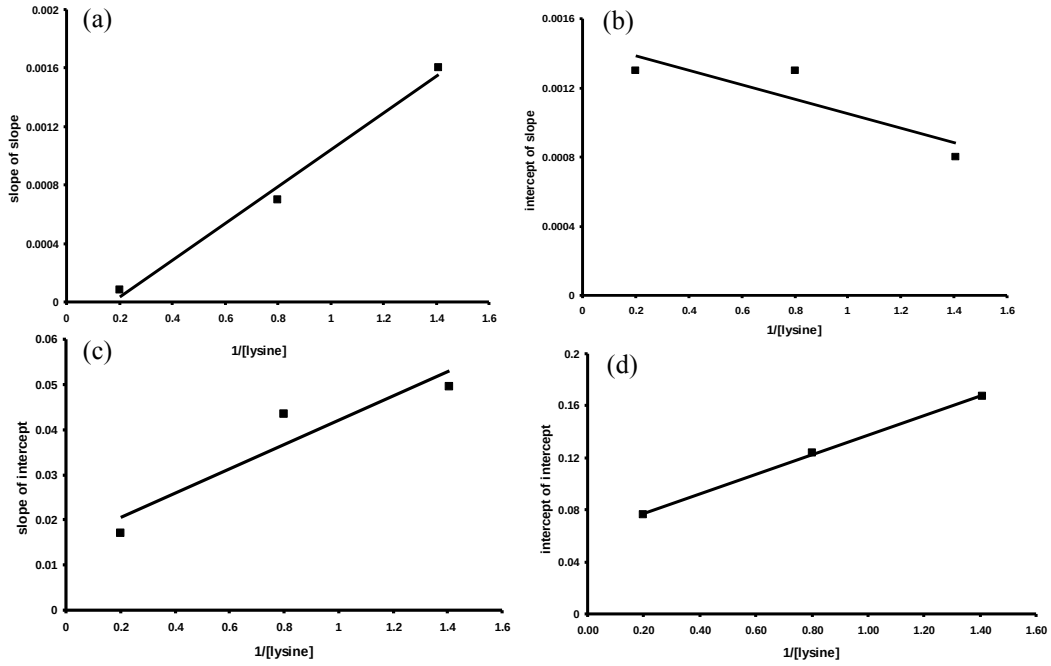


Figure 3.1.3: Systematic initial velocity studies of SDH in the saccharopine formation reaction direction at pH 7.0 -- tertiary replots of double-reciprocal plots vs lysine concentration. (a) is slope of slope replot; (b) is intercept of slope replot; (c) is slope of intercept replot; and (d) is intercept of intercept replot.

Initial rates were also obtained in the direction of saccharopine oxidation at pH 7.0, as a function of the NAD concentration and different fixed levels of saccharopine. The pattern intersects to the left of the ordinate (data not shown). Estimates of all of the kinetic parameters in this reaction direction were obtained by fitting the data to eq 2.5 for a sequential mechanism. All kinetic parameters for both reaction directions are summarized in Table 3.1. Values of K_{NADH}, K_{Lys}, and $K_{\alpha\text{-}Kg}$ are identical, within error, to those reported previously (*1*).

Table 3.1: Kinetic Parameters of Saccharopine Dehydrogenase at pH 7.0.

Forward Reaction	
K_{NAD} (mM)	0.9 ± 0.1
K_{Sacc} (mM)	6.7 ± 1.4
K_{iNAD} (mM)	1.1 ± 0.3
V_1/E_t (s^{-1})	1.1 ± 0.1
$V_1/K_{NAD}E_t$ ($M^{-1}\cdot s^{-1}$)	(1.2 ± 0.1) x 10^3
$V_1/K_{Sacc}E_t$ ($M^{-1}\cdot s^{-1}$)	(1.6 ± 0.3) x 10^2
Reverse Reaction	
K_{NADH} (mM)	0.019 ± 0.002
K_{Lys} (mM)	1.1 ± 0.2
$K_{\alpha\text{-}Kg}$ (mM)	0.11 ± 0.03
constant $(mM)^3$	0.013 ± 0.002
coef A $(mM)^2$	0.71 ± 0.08
V_2/E_t (s^{-1})	20 ± 1
$V_2/K_{NADH}E_t$ ($M^{-1}\cdot s^{-1}$)	(1.6 ± 0.2) x 10^6
$V_2/K_{Lys}E_t$ ($M^{-1}\cdot s^{-1}$)	(2.5 ± 0.4) x 10^4
$V_2/K_{\alpha\text{-}Kg}E_t$ ($M^{-1}\cdot s^{-1}$)	(2.8 ± 0.7) x 10^5

Substrate inhibition

varied substrate	substrate inhibitor	K_i (mM)	inhibition pattern
NADH	L-lysine	27.8 ± 0.3	C
NADH	α-Kg	28 ± 7	UC

3.2.2 Initial Velocity Studies: Pairwise Analysis

To further define the kinetic mechanism, initial velocity patterns obtained by varying one substrate at different fixed concentrations of a second and with the third substrate saturating were obtained and are shown in Fig. 3.2A-C. An intersecting initial velocity pattern was observed for the α-Kg/lysine pair (Fig. 3.2A), while the NADH/α-Kg and NADH/lysine pairs gave parallel patterns (Fig. 3.2B, C). Patterns are consistent with the ordered addition of NADH followed by the random addition of α-Kg and lysine. Kinetic parameters were obtained by fitting the data to eqs 2.5 and 2.6. Values of kinetic parameters were in good agreement with those obtained via the systematic analysis described above.

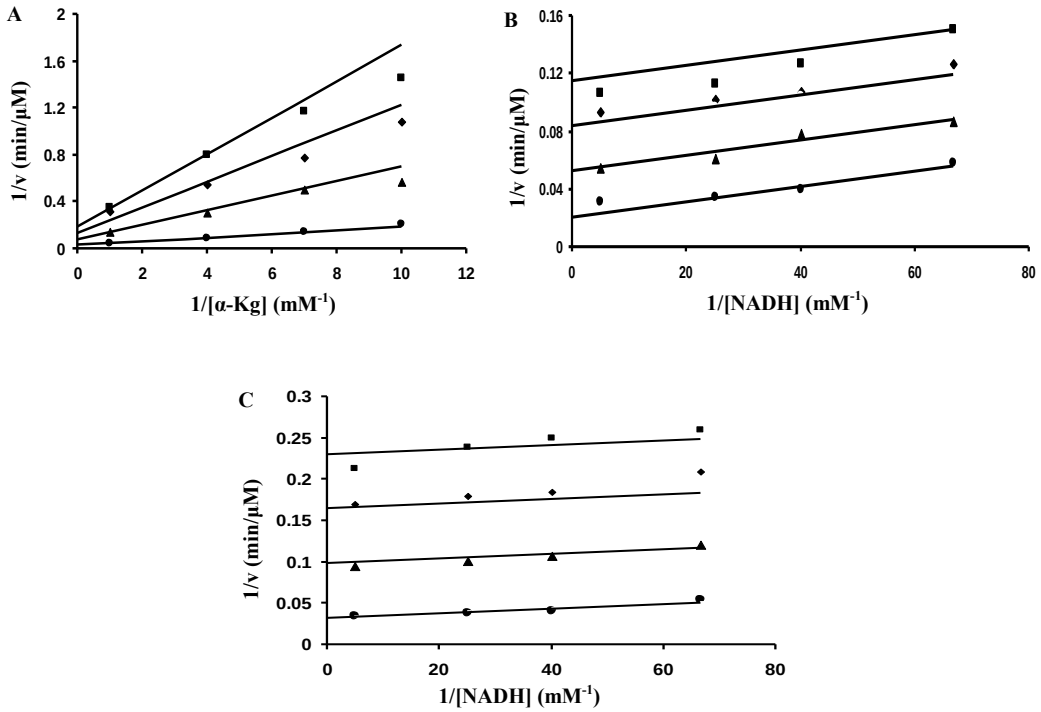


Figure 3.2: Pairwise analysis of the SDH oxidative deamination reaction. Double-reciprocal plots obtained upon varying one substrate at different fixed concentrations of a second and with the third substrate saturating. Rates were measured in 100 mM Hepes at pH 7.0 and 25°C. (A) Initial velocity pattern obtained with the α-Kg/lysine pair with NADH at 0.2 mM ($5K_{NADH}$). (B) Initial velocity pattern obtained for the NADH/α-Kg pair with lysine at 12.5 mM ($10K_{Lys}$). (C) Initial velocity pattern obtained for the NADH/lysine pair with α-Kg at 5 mM ($20K_{\alpha\text{-}Kg}$). The points are experimental, while the solid lines are theoretical based on a fit to eq 2.5 in A and to eq 2.6 in B and C.

3.2.3 Determination of K_{eq}

With all reactants, with the exception of NAD, fixed as discussed in **Materials and Methods 2.5**, the change in A_{340} (once the system has attained equilibrium after enzyme was added to the reaction mixture) was plotted against the NAD concentration. The ΔA_{340} is an indicator of displacement from equilibrium position (Fig. 3.3). The concentration of NAD that gave a ΔA_{340} of 0 is about 0.5 mM. The K_{eq} calculated using fixed concentrations of the other reactants and 0.5 mM NAD (eq 2.1) is 3.9×10^{-7} M, while the K_{eq} calculated from the Haldane relationship is about 2.9×10^{-7} M (eq 2.2).

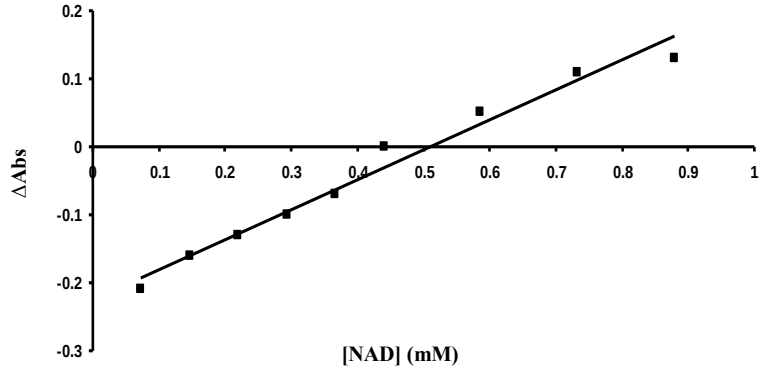


Figure 3.3: Determination of K_{eq} of SDH reaction at pH 7.0. The difference in A_{340} vs the NAD concentration (0.1-1.2 mM). The points are experimental, while the solid line is theoretical based on a fit to the equation for a straight line.

3.2.4 Inhibition Studies: Substrate Inhibition

When the initial rate was measured over a wide range of lysine concentrations (5-200 mM), with the concentrations of the other two substrates fixed at their respective K_m, the double-reciprocal plot exhibits substrate inhibition as the lysine concentration increases above 60 mM (Fig.3.4A). Inhibition by lysine vs NADH is competitive (Fig. 3.4B). Substrate inhibition parameters are summarized in Table 3.1.

The initial velocity pattern obtained with lysine at 6 times its K_m and NADH varied at different fixed concentration of α-Kg exhibits substrate inhibition that is uncompetitive vs NADH (Fig. 3.5A). Data suggest the binding of α-Kg to the E:NAD complex. A double-inhibition experiment obtained with NADH and lysine fixed at their K_m values and NAD and α-Kg varied is consistent with the formation of an E:NAD:α-Kg complex (Fig. 3.5B). The rate in the absence of inhibitors, $v_{0,}$ was 6.7 ± 0.2 μM/min. The dissociation constants for E:NAD and E:α-Kg complexes are 26 ± 5 and 460 ± 160 mM,

respectively. The interaction constant α was 0.12 ± 0.09, indicating synergism of binding for NAD and α-Kg.

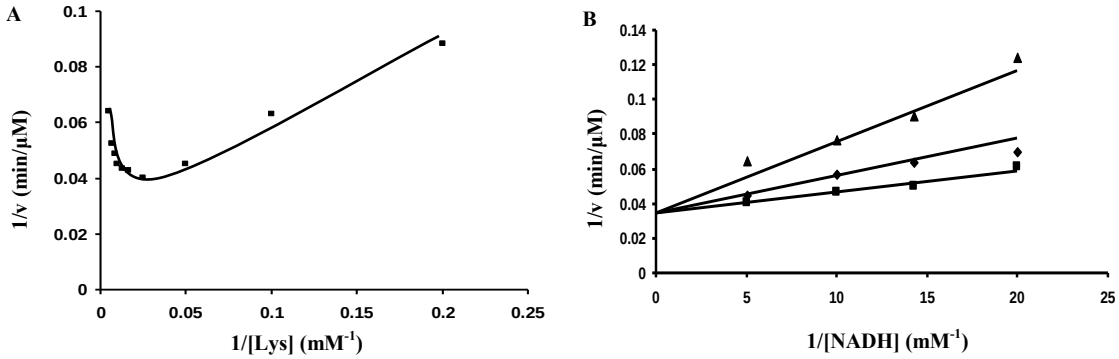


Figure 3.4: Competitive substrate inhibition by lysine against NADH. (A) Plot of the reciprocal initial rate vs the lysine concentration, with the other substrates fixed at their respective K_m. (B) Double-reciprocal plot exhibiting competitive substrate inhibition by lysine [100 mM (■), 200mM (♦), and 400 mM (▲)] vs NADH, with α-Kg fixed at its K_m. Rates were measured in 100 mM Hepes at pH 7.0 and 25°C. The points are experimental, while the solid lines are theoretical based on a fit to eq 2.5 in A and to eq 2.7 in B.

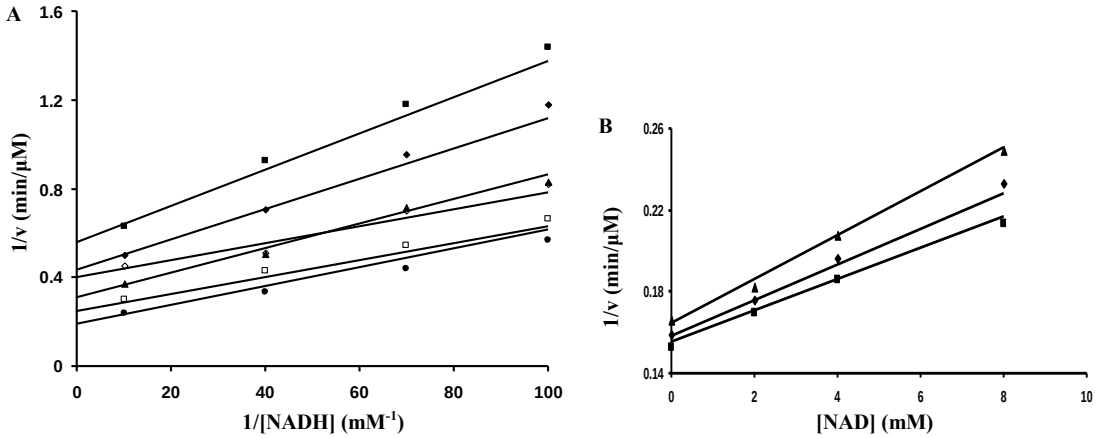


Figure 3.5: Substrate inhibition by α-Kg against NADH. (A) Uncompetitive inhibition by α-Kg vs NADH. The concentrations of α-Kg were 0.1 mM (■), 0.143 mM (♦), 0.25 mM (▲), 1 mM (●), 20 mM (□), and 50 mM (◊). The concentration of lysine is fixed at 5 mM. (B) Double inhibition by NAD and α-Kg. Plot of the reciprocal initial rate vs NAD concentration (0-8 mM) at different levels of α-Kg [20 mM (■), 30 mM (♦), 50 mM (▲)].The points are experimental, while the solid lines are theoretical based on a fit to eq 2.9 in A and to eq 2.10 in B.

Table 3.2: Inhibition Kinetic Constants for Product Inhibitors of SDH.

varied substrate	fixed substrate	inhibitor	K_{is} (mM)	K_{ii} (mM)	Inhibition pattern
NADH	lysine (K_m) α-Kg ($2K_m$)	Sacc	--	1.00 ± 0.05	UC
lysine	NADH (K_m) α-Kg ($2K_m$)	Sacc	1.5 ± 0.1	1.42 ± 0.08	NC
α-Kg	NADH (K_m) lysine (K_m)	Sacc	0.95 ± 0.05	11 ± 4	NC
NADH	lysine ($2K_m$) α-Kg ($2K_m$)	NAD	1.56 ± 0.03	--	C
lysine	NADH ($3K_m$) α-Kg ($2K_m$)	NAD	44 ± 4	4.0 ± 0.1	NC
α-Kg	NADH ($3K_m$) lysine ($2K_m$)	NAD	28 ± 8	107 ± 96	NC
NAD	Sacc ($1.5K_m$)	NADH	0.0032 ± 0.0004	--	C
Sacc	NAD (K_m)	NADH	0.033 ± 0.003	0.0105 ± 0.0003	NC
NAD	Sacc ($1.5K_m$)	lysine	19 ± 3	33 ± 4	NC
Sacc	NAD (K_m)	lysine	2.84 ± 0.06	--	C
Sacc	NAD ($20K_m$)	α-Kg	6.0 ± 0.7	64 ± 6	NC

3.2.5 Inhibition Studies: Product Inhibition

Product inhibition data in both reaction directions are summarized in Table 3.2. In the direction of saccharopine formation, saccharopine is uncompetitive vs NADH and noncompetitive vs lysine and α-Kg, while NAD is competitive vs NADH and noncompetitive vs lysine and α-Kg. In the opposite direction, NADH is competitive vs NAD and noncompetitive vs saccharopine, while lysine is noncompetitive vs NAD and

competitive vs saccharopine. Product inhibition by α-Kg is only observed at high NAD concentrations ($\geq 20K_m$), and it is noncompetitive vs saccharopine.

3.2.6 Inhibition Studies: Dead-End Inhibition

Inhibition by leucine, chosen as a dead-end analogue of lysine, was competitive vs lysine, uncompetitive vs NADH, and noncompetitive vs α-Kg. OG was chosen as a dead-end analogue of α-Kg, and it exhibited a competitive inhibition vs α-Kg, uncompetitive inhibition vs NADH, and noncompetitive vs lysine. OAA was also chosen as a dead-end analogue of α-Kg, but it is competitive vs lysine, and noncompetitive vs NADH and α-Kg.

When glutarate is used as a dead-end inhibitor, it is competitive vs lysine and noncompetitive vs NADH and α-Kg. The secondary slope replot for glutarate inhibition vs NADH, however, is parabolic, while the intercept replot is linear, indicating S-parabolic noncompetitive inhibition (Fig. 3.6A-C).

Pyruvate is an alternative keto acid substrate but only when both lysine and pyruvate concentrations are very high. Under conditions where inhibition studies are carried out, pyruvate is treated as a dead-end α-Kg substrate analogue. Surprisingly, it shows competitive inhibition vs both lysine and α-Kg and uncompetitive inhibition vs NADH. All dead-end inhibition data are summarized in Table 3.3.

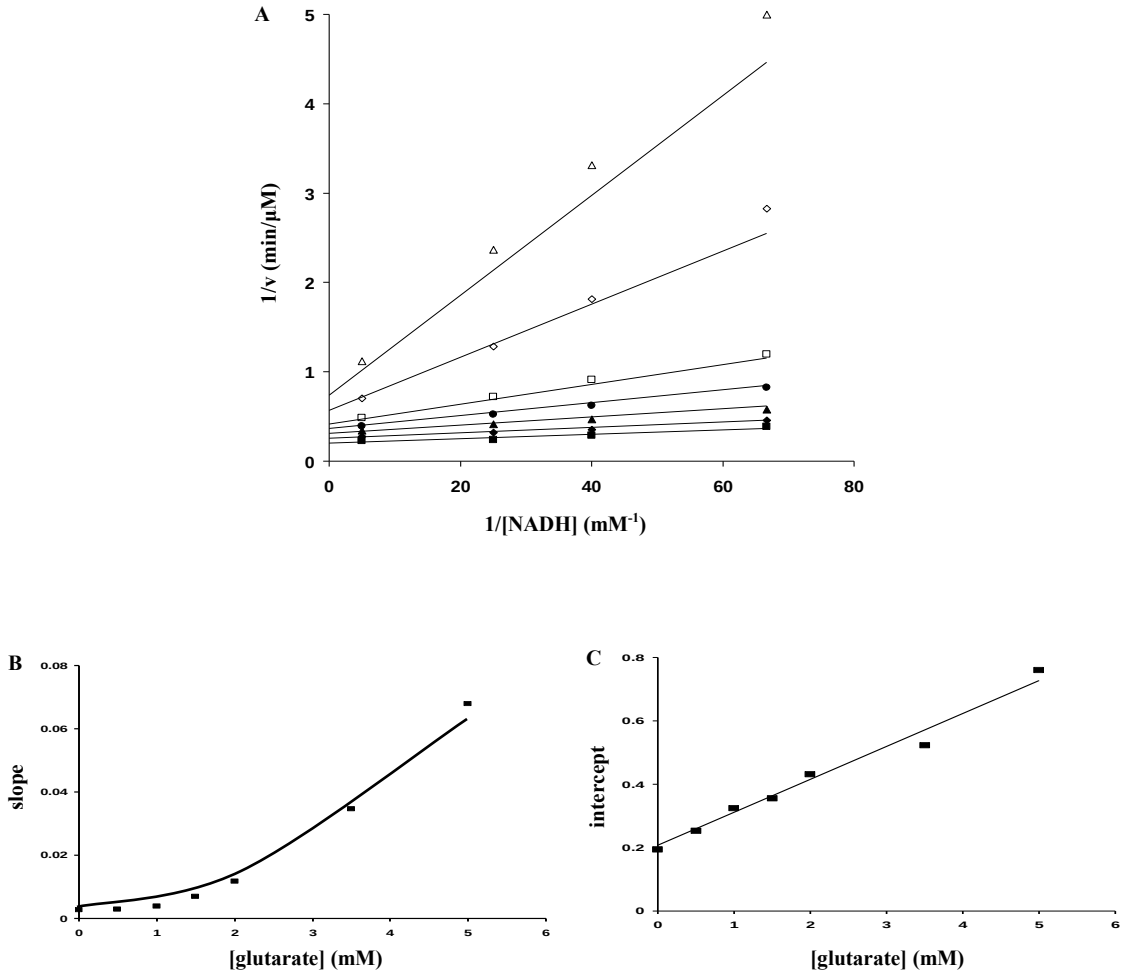


Figure 3.6: S-parabolic noncompetitive inhibition by glutarate against NADH. (A) Primary plot exhibiting the S-parabolic noncompetitive inhibition by glutarate [0 mM (■), 0.5 mM (♦), 1 mM (▲), 1.5 mM (●), 2 mM (□), 3.5 mM (◊), and 5mM (Δ)] vs NADH, with lysine and α-Kg fixed at their respective K_m. (B) Secondary plot of the slope vs the glutarate concentration. (C) Secondary plot of the intercept vs the glutarate concentration. Rates were measured in 100 mM Hepes at pH 7.0 and 25°C. The points are experimental or from a graphical analysis, whereas the solid lines are theoretical based on the kinetic parameters from a fit to eq 2.11.

Table 3.3: Inhibition Kinetic Constants for Dead-End Inhibitors of SDH.

varied substrate	fixed substrate	inhibitor	K_{is} (mM)[a]	K_{ii} (mM)[a]	Inhibition pattern
NADH	lysine ($2K_m$) α-Kg ($2K_m$)	leucine	--	0.45 ± 0.01 (0.240 ± 0.005)	UC
lysine	NADH ($3K_m$) α-Kg ($2K_m$)	leucine	0.44 ± 0.03 (0.17 ± 0.01)	--	C
α-Kg	NADH ($3K_m$) lysine ($2K_m$)	leucine	1.12 ± 0.26 (0.64 ± 0.15)	0.23 ± 0.02 (0.10 ± 0.01)	NC
NADH	lysine ($2K_m$) α-Kg ($2K_m$)	OG	--	0.06 ± 0.02 (0.020 ± 0.007)	UC
lysine	NADH ($3K_m$) α-Kg ($2K_m$)	OG	0.154 ± 0.004 (0.070 ± 0.002)	0.36 ± 0.01 (0.060 ± 0.002)	NC
α-Kg	NADH ($3K_m$) lysine ($2K_m$)	OG	0.100 ± 0.002 (0.070 ± 0.001)	--	C
NADH	lysine ($2K_m$) α-Kg ($2K_m$)	OAA	4.7 ± 1.8	11.8 ± 2.6	NC
lysine	NADH ($3K_m$) α-Kg ($2K_m$)	OAA	6.1 ± 0.5	--	C
α-Kg	NADH ($3K_m$) lysine ($2K_m$)	OAA	6.4 ± 0.5	29 ± 8	NC
NADH	lysine ($2K_m$) α-Kg ($2K_m$)	pyruvate	--	11.21 ± 0.04	UC
lysine	NADH ($3K_m$) α-Kg ($2K_m$)	pyruvate	17.9 ± 0.5	--	C
α-Kg	NADH ($3K_m$) lysine ($2K_m$)	pyruvate	19 ± 1	--	C
NADH	lysine ($2K_m$) α-Kg ($2K_m$)	glutarate	1.1 ± 0.2[b]	1.9 ± 0.4	S-Parabolic NC
lysine	NADH ($3K_m$) α-Kg ($2K_m$)	glutarate	2.3 ± 0.4	--	C
α-Kg	NADH ($3K_m$) lysine ($2K_m$)	glutarate	1.0 ± 0.1	2.3 ± 0.5	NC

[a] The values in parentheses are the corrected values for the fixed substrates where applicable. [b] Average K_i for binding two molecules of glutarate to E.

3.3 Chemical Mechanism Determination of SDH

3.3.1 pK_a of the Saccharopine Secondary Amine: Determination by NMR

^{1}H NMR spectra of saccharopine were obtained at pH 6.86 and referenced to HDO (4.68 ppm). Chemical shifts are as follows: δ 3.6 [t, 1H, J = 6.7 Hz, C(2)-H], δ 3.5 [t, 1H, J = 5.8 Hz, C(8)-H], δ 2.9 [t, 2H, J = 7.9 Hz, C(6)-H_2], δ 2.3 [t, 2H, J = 7.2 Hz, C(10)-H_2], δ 1.95 [dd, 2H, J = 7.2, 5.8 Hz, C(9)-H_2], δ 1.78 [m, 2H, C(3)-H_2], δ 1.64 [p, 2H, J = 7.9 Hz, C(5)-H_2], δ 1.38 [m, 2H, C(4)-H_2]. The ^{1}H NMR chemical shifts of saccharopine were assigned by gCOSY at pH 6.86 and 11.9. The correlations at pH 6.86 and 11.9 were identical. The correlations at pH 6.86 are listed in Table 3.4.

Table 3.4: Results of Saccharopine gCOSY Experiments.

Chemical Shift	Correlation
3.62 C(2)-H	1.78 C(3)-H_2
3.48 C(8)-H	1.95 C(9)-H_2
2.93 C(6)-H_2	1.64 C(5)-H_2
2.26 C(10)-H_2	1.95 C(9)-H_2
1.95 C(9)-H_2	3.48 C(8)-H, 2.26 C(10)-H_2
1.78 C(3)-H_2	3.62 C(2)-H, 1.38 C(4)-H_2,
1.64 C(5)-H_2	2.93 C(6)-H_2, 1.38 C(4)-H_2
1.38 C(4)-H_2	1.78 C(3)-H_2, 1.64 C(5)-H_2

The chemical shifts of peaks corresponding to C(2)-H, C(8)-H, and C(6)-H_2 changed significantly as the pD was increased (Fig. 3.7A). The largest changes were seen in C(8)-H and C(6)-H_2 (reflecting the protons β to the secondary amine) which moved 0.59 and 0.58 ppm, respectively, upfield as the pH was increased from 6.86 to 11.90. A plot of the chemical shift vs pH was used to estimate the pK_a value of the secondary amine of saccharopine (Fig. 3.7B). Data were fitted by eq 2.19, which gave an estimated pK_a of 10.5 ± 0.2. The pK_a in H_2O is 10.1 ± 0.2 [obtained by subtracting 0.4 (*109*)] in the range of 10-11 from model compounds (*116*).

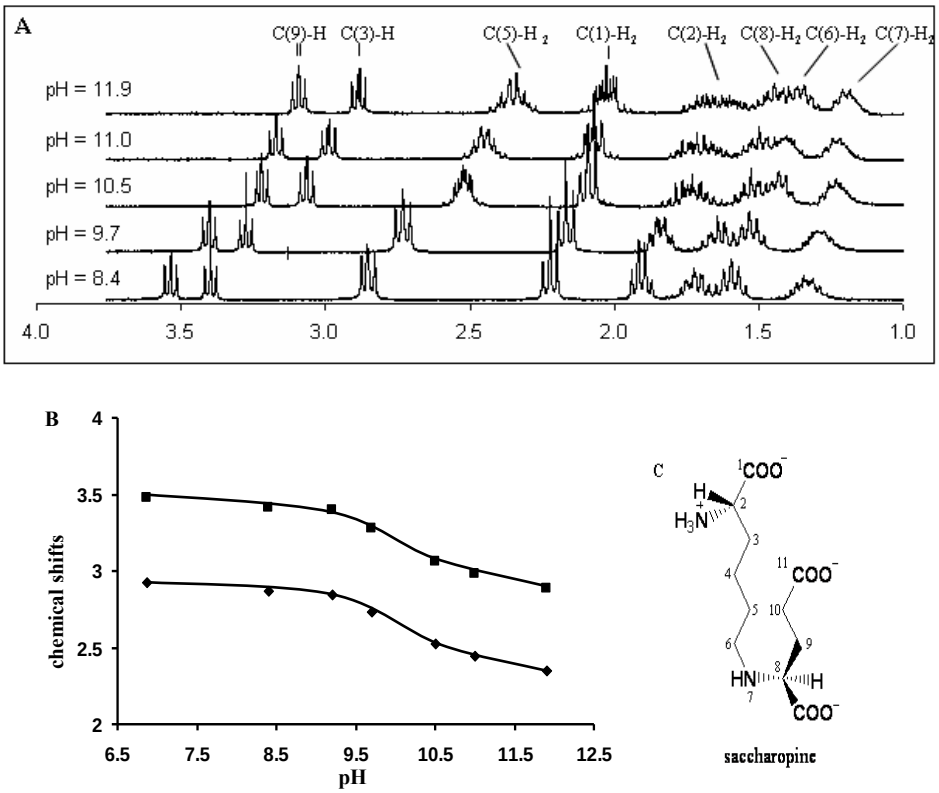


Figure 3.7: pH dependence of the ^{1}H NMR spectrum of saccharopine. (A) ^{1}H NMR spectra of saccharopine measured at the indicated pH values. Chemical shifts are referrenced to the carbons of saccharopine. (B) pH dependence of the chemical shift of protons β to the secondary amine of saccharopine. Data are presented for the C(8)-H (■) and C(6)-H_2 (▲) positions. (C) Structure of saccharopine with main chain atoms labeled.

3.3.2 pH Dependence of Kinetic Parameters

The pH dependence of kinetic parameters potentially provides information on the optimum protonation state of enzyme and/or reactant functional groups required for enzyme conformation, binding, and catalysis. To be certain the kinetic mechanism of the enzyme does not change with pH and to obtain estimates of the K_m values of all of the substrates as a function of pH, initial velocity patterns and diagnostic dead-end inhibition patterns were obtained at pH 5.0, 7.0, 8.0, 8.5, and 9.5. In the direction of saccharopine formation, initial velocity patterns and leucine dead-end inhibition patterns are consistent with the kinetic mechanism in which NADH binds first to free enzyme, followed by

random addition of α-Kg and lysine at pH 7.0, and the mechanism also applies at pH 8.0. However, the mechanism changes at the pH extremes (5.0, 8.5, and 9.5) to an ordered one with NADH binding first, followed by rapid equilibrium addition of α-Kg before lysine. In the direction of lysine formation, initial velocity and dead-end inhibition patterns obtained at the pH extremes (6.0 and 9.6) are consistent with a sequential ordered mechanism in which NAD is the first substrate bound and saccharopine binds second (data not shown).

The pH dependence of the kinetic parameters for SDH was determined, and the results are shown in Figs 3.8 and 3.9. In the direction of lysine formation, V_1/E_t and $V_1/K_{NAD}E_t$ decrease at low pH with a limiting slope of +1, giving a pK_a value of about 7.3 - 7.4 (Fig. 3.8A, B), while $V_1/K_{Sacc}E_t$ decreases at low pH with a limiting slope of +2, giving pK_a values of 6.2 and 7.2 (Fig. 3.8C). The pK_a of the saccharopine secondary amine is 10.1, outside the pH range used for the $V_1/K_{Sacc}E_t$ pH-rate profile. NAD is the first reactant bound, and the pH dependence of $V_1/K_{NAD}E_t$ (the on-rate constant for binding NAD) reflects a group important for binding NAD. Since NAD and saccharopine have no pK_a values over the pH range that was studied, the pK_a of 7.2-7.4 exhibited in V_1/E_t, $V_1/K_{NAD}E_t$, and $V_1/K_{Sacc}E_t$ may reflect the same enzyme side chain important in catalysis and binding (see **Discussion 4.2.2**). The group on enzyme with the pK_a of 6.2 in the $V_1/K_{Sacc}E_t$ pH-rate profile likely contributes to the binding of saccharopine, since it is not observed in the V_1/E_t pH-rate profile. pK_a values are summarized in Table 3.5. Estimates of the pH-independent values of the kinetic parameters are as follows: V_1/E_t, (9.5 ± 0.9) s^{-1}, $V_1/K_{NAD}E_t$, (8.6 ± 1.6) x 10^3 $M^{-1}s^{-1}$, and $V_1/K_{Sacc}E_t$, (4.4 ± 0.4) x 10^3 $M^{-1}s^{-1}$.

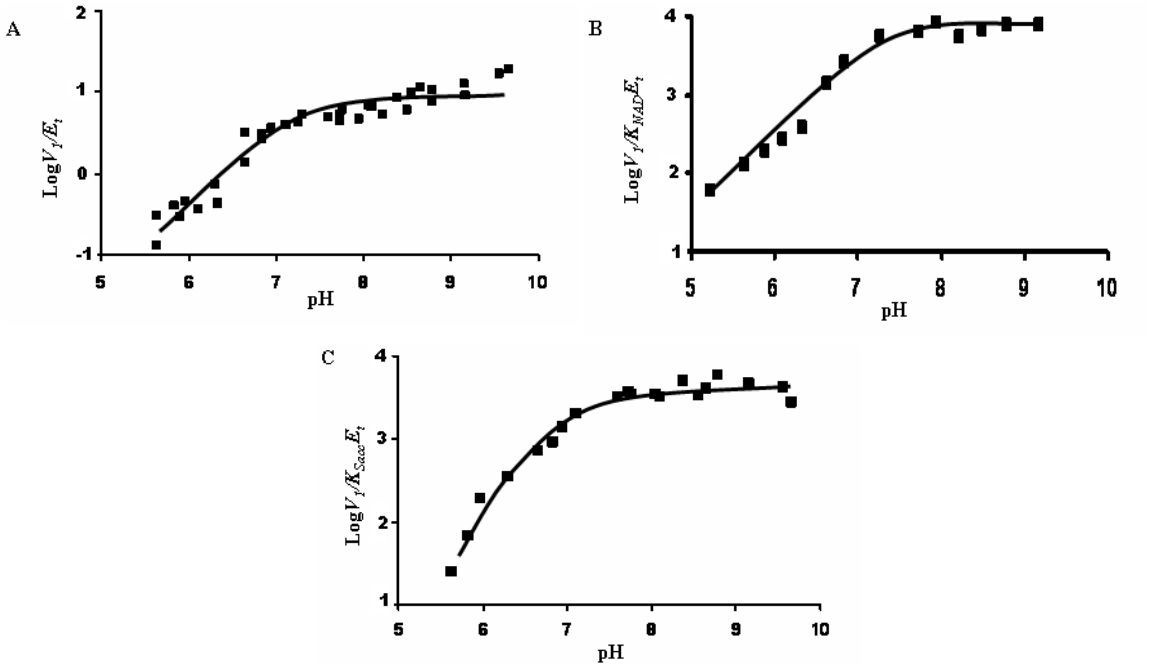


Figure 3.8: pH dependence of kinetic parameters for the SDH reaction from *S. cerevisiae* in the direction of saccharopine formation. Data were obtained at 25 °C for V_1/E_t (A), $V_1/K_{NAD}E_t$ (B), and $V_1/K_{Sacc}E_t$ (C). The points shown are the experimentally determined values, while the curves are theoretical based on fits of the data using eq 2.14 for V_1/E_t and $V_1/K_{NAD}E_t$, and eq 2.18 for $V_1/K_{Sacc}E_t$.

Table 3.5: pH Dependence of Kinetic Parameters for SDH from *S. cerevisiae.*

Parameter	pK_a ± SE	
	Acid side	Basic side
V_1	7.3 ± 0.2	--
V_1/K_{NAD}	7.4 ± 0.2	--
V_1/K_{Sacc}	6.2 ± 0.3 7.2 ± 0.2	--
V_2	5.8 ± 0.2	8.4 ± 0.5
V_2/K_{NADH}	--	9.6 ± 0.2
$V_2/K_{\alpha\text{-}Kg}$	--	8.9 ± 0.1
V_2/K_{Lys}	7.2 ± 0.5[a]	--
pK_{iOG}	--	--
pK_{iLeu}	--	6.2 ± 0.7[b] 9.2 ± 0.3[c]

[a] average value. [b] pK_a for the EH complex. [c] pK_a for the EH:leucine complex.

In the reverse reaction direction, V_2/E_t decreases at low pH with a limiting slope of +1 giving a pK_a value of about 5.8 and decreases at high pH to a new constant value exhibiting a pK_a of about 8.4 (Fig.3.9A). The pK_a of 5.8 suggests an enzyme group

important for catalysis, while the group with a pK_a of about 8.4 suggests an enzyme group important, but not essential, for catalysis. The V_2/KE_t values for NADH and α-Kg both decrease at high pH with a slope of -1 giving pK_a values of 9.6 and 8.9, respectively (Fig. 3.9B, C). V_2/K_{NADH} is the on-rate constant for NADH, and the pK_a of about 9.6 reflects a group on enzyme important for binding the reduced cofactor. (Note that the group with a pK_a of 7.2 important for NAD binding is not observed in the $V_2/K_{NADH}E_t$ profile.) The V_2/KE_t for lysine exhibits a bell-shaped pH-rate profile, which decreases at low pH with a slope of +1 and at high pH with a slope of -1 (Fig. 3.9D). Because the difference in these two pK_a values is less than 0.6, they were considered identical, and an average pK_a of about 7.2 was estimated. pK_a values are summarized in Table 3.5. The pH-independent values of kinetic parameters are as follows: V_2/E_t, (58 ± 3) s^{-1}, $V_2/K_{NADH}E_t$, (1.41 ± 0.06) x 10^6 $M^{-1}s^{-1}$, $V_2/K_{\alpha\text{-}Kg}E_t$ (2.16 ± 0.08) x 10^5 $M^{-1}s^{-1}$, and $V_2/K_{Lys}E_t$, (1.44 ± 0.07) x 10^5 $M^{-1}s^{-1}$.

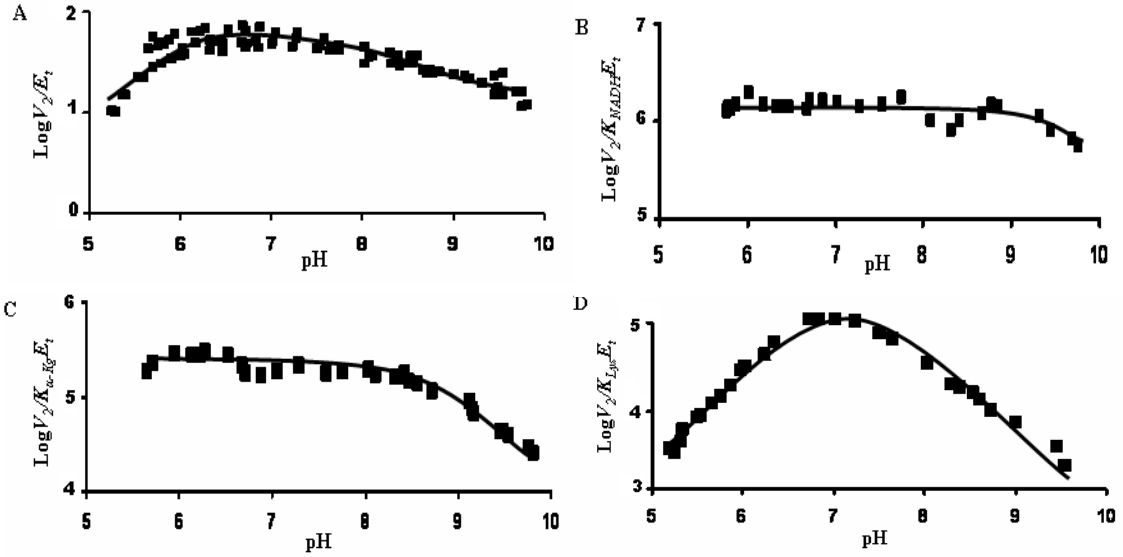


Figure 3.9: pH dependence of kinetic parameters for the SDH reaction from *S. cerevisiae* in the direction of lysine formation. Data were obtained at 25 °C for V_2/E_t (A), $V_2/K_{NADH}E_t$ (B), $V_2/K_{\alpha\text{-}Kg}E_t$ (C), and $V_2/K_{Lys}E_t$ (D). The points shown are the experimentally determined values, while the curves are theoretical based on fits of the data using eq 2.17 for $V_2/K_{NADH}E_t$ and $V_2/K_{\alpha\text{-}Kg}E_t$ and eq 2.15 for $V_2/K_{Lys}E_t$, while the V_2/E_t profile was fitted as described in **Materials and Methods 2.10**.

3.3.3 pH Dependence of the K_i for Oxalylglycine and Leucine

The pH dependence of the dissociation constant for competitive inhibitors vs α-Kg and lysine was determined in order to obtain an estimate of intrinsic pK value(s) of group(s) required for optimum binding of reactants. OG was utilized as a dead-end analogue of α-Kg to measure its pK_i profile. At pH 5.45 and 9.58, it is competitive vs α-Kg, and its pK_i profile is shown in Fig. 3.10A. It shows an increase in its K_i as the pH is decreased below 6, and increased above 8. Over the pH range studied, leucine is a competitive inhibitor against lysine. Its pK_i decreases from a constant value below pH 6 to another constant value above pH 9.0 (Fig. 3.10B). A pK_a of about 6.2 is estimated for the enzyme complex EH:NADH:α-Kg, and this pK_a is perturbed to about 9.2 in the EH:NADH:α-Kg:leucine complex (Table 3.5). The pH-independent dissociation constant for leucine is 0.09 ± 0.01 mM for EH:NADH:α-Kg:leucine, and increases to 30 ± 6 mM in the E:NADH:α-Kg:leucine complex.

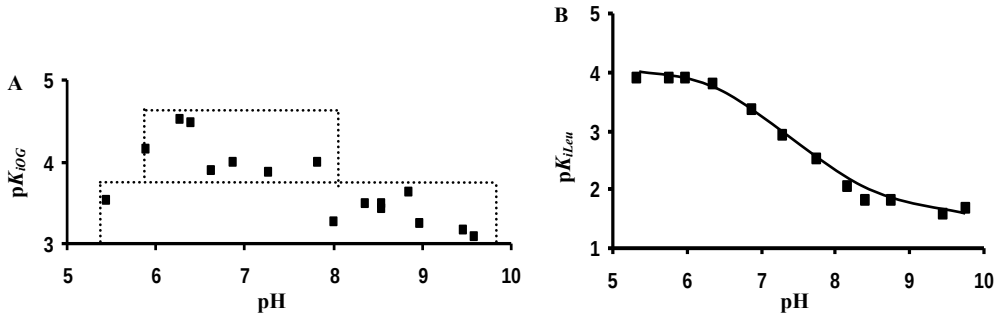


Figure 3.10: pH dependence of the reciprocal of the inhibition constant for oxalylglycine (A) and leucine (B). The points shown are the experimentally determined values, while the curve in (B) is theoretical based on the fit of the data using eq 2.19.

3.3.4. Isotope Effects

3.3.4.1 Primary Substrate Deuterium Kinetic Isotope Effects

Primary deuterium kinetic isotope effects were measured by direct comparison of initial rates at pH 7.1 with A-side NADH(D) used as the labeled substrate. Finite effects were observed in all parameters, with the exception of V_2/K_{NADH}. $^{D}V_2$ = 1.45 ± 0.07, $^{D}(V_2/K_{NADH})$ = 0.92 ± 0.08, $^{D}(V_2/K_{\alpha\text{-}Kg})$ = 1.9 ± 0.1, and $^{D}(V_2/K_{Lys})$ = 1.56 ± 0.05. Isotope effects on V_2 and V_2/K_{Lys} were also obtained as a function of pH and are shown in Table 3.6. Since the isotope effects tend to unity as the pH is increased, data are also plotted as the log(IE minus 1) (Fig. 3.11) to better estimate the pK_a for the process.

Table 3.6: pH Dependence of Primary Deuterium Kinetic Isotope Effect for SDH.

	$^{D}V_2$	$^{D}(V_2/K_{Lys})$
pH 5.6	1.20 ± 0.07	1.66 ± 0.12
pH 6.1	1.44 ± 0.13	1.76 ± 0.10
pH 7.1	1.45 ± 0.07	1.56 ± 0.05
pH 7.9	1.3 ± 0.05	1.20 ± 0.08
pH 8.4	1.16 ± 0.03	1.03 ± 0.04

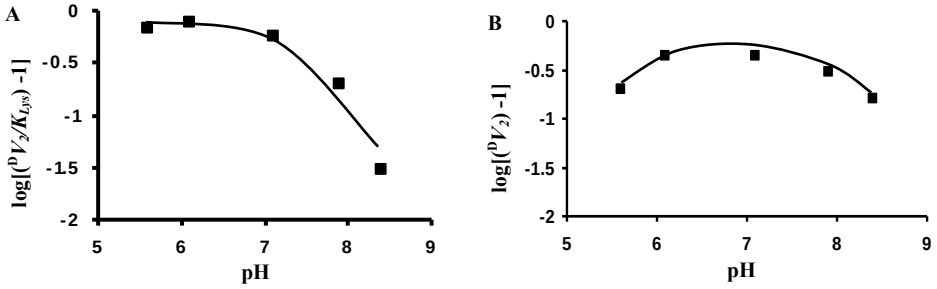


Figure 3.11: pH dependence of primary substrate deuterium kinetic isotope effects of SDH. Data were plotted as the logarithm of the isotope effect minus 1. (A) V_2/K_{Lys}. (B) V_2. The points shown are the experimentally determined values, while the curves are theoretical based on fits of the data using eq 2.17 for V_2/K_{Lys} and eq 2.15 for V_2.

3.3.4.2 Solvent Deuterium Isotope Effects and Proton Inventory Studies

The pH(D) dependence of kinetic parameters was measured over the pH(D) range 6.5-8.5 to determine whether a solvent deuterium kinetic isotope effect is observed on V_2 and V_2/K_{Lys}. The pH(D) independent values of V_2 and V_2/K_{Lys} gave values of $^{D2O}V_2$ and $^{D2O}V_2/K_{Lys}$ of 2.2 ± 0.1 and 1.9 ± 0.1, respectively. The pH(D) profile is shown in Fig. 3.12. Proton inventories (*110*) measured at pH(D) 7.1 is shown in Fig. 3.13. The proton inventories can be described as dome-shaped or bulging upward for V_2 and V_2/K_{Lys}. The concavity is pronounced in the case of V_2, and shallow in the case of V_2/K_{Lys}.

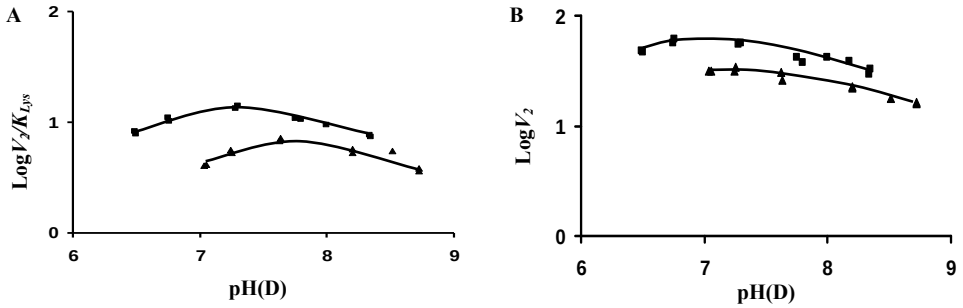


Figure 3.12: pH(D) profile of SDH. (A) log(V_2/K_{Lys}) (B) log(V_2). Kinetic parameters were obtained in H_2O (■) and in D_2O (▲). The points shown are the experimentally determined values, while the curves are drawn by eye.

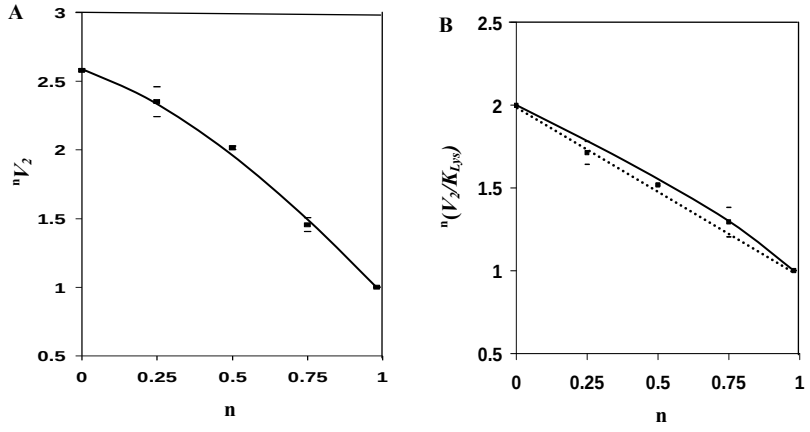


Figure 3.13: Proton Inventories for SDH. Solvent deuterium dependence of $^{n}(V_2)$ (A) and $^{n}(V_2/K_{Lys})$ (B) (ratio of V_2 and V_2/K_{Lys} at n fraction of D_2O to that at 99.9% D_2O) on the fraction of deuterium (n) in solvent. Velocities were measured at pH(D)-independent value of 7.1 in 100% H_2O, 25% D_2O, 50% D_2O, 75% D_2O, and ~100% D_2O. Points are experimental values, and curves are drawn by eye. The dotted line in B is theoretical for a linear proton inventory.

3.3.4.3 Multiple Solvent/Substrate Deuterium Isotope Effects

Multiple isotope effects allow one to determine whether two isotope effects reflect the same or different steps. A multiple kinetic deuterium isotope effect is obtained when A-side NADD is used in both H_2O and D_2O (80%) with $^{D2O}(V_2)_D = 1.76 \pm 0.08$ and $^{D2O}(V_2/K_{Lys})_D = 1.86 \pm 0.08$. The multiple kinetic deuterium isotope effect obtained by using NADH(D) in D_2O (90%) gives $^{D}(V_2)_{D2O} = 1.50 \pm 0.15$ and $^{D}(V_2/K_{Lys})_{D2O} = 1.55 \pm 0.14$.

3.4 Substrate Specificity of SDH

3.4.1 Initial Velocity Studies with NAD/NADH Analogues

In the physiological reaction direction, NADP, 3-APAD, 3-PAAD, and thio-NAD all can serve as the oxidant in the oxidative deamination reaction, while in the reverse reaction direction, NADPH can substitute for NADH. In the direction of saccharopine oxidation, initial rates were obtained as a function of the concentrations of NAD analogues and fixed concentration of saccharopine (6 mM) at pH 7.55 and 9.2. Estimates of the kinetic parameters are provided in Table 3.7.

Double-reciprocal initial velocity patterns in the direction of reductive amination using NADPH as the reductant were obtained by varying the concentrations of NADPH and α-Kg at different fixed concentrations of lysine at pH 7.0 and 25 ˚C. The crossover points for all double-reciprocal plots are to the left of the ordinate (data not shown). All of the initial velocity data were fitted to eq 2.13 for a terreactant mechanism. Substrate inhibition by α-Kg and lysine was observed as α-Kg and lysine concentration increased

above 50 mM and 100 mM, respectively (data not shown). Kinetic parameters are summarized in Table 3.8 and compared to data obtained previously with NADH (*124*).

Table 3.7: Kinetic Parameters for Alternative Coenzyme Substrates of SDH.

	K_i (mM)	V_{app} (μM/min)
NAD	1.1 ± 0.3 (K_i) [a] 0.9 ± 0.1 (K_m) [a]	--
NADP	2.3 ± 0.4 [b] 5.7 ± 0.9 [c]	2.5 ± 0.2 [b]
3-APAD	8.9 ± 1.7 [b] 8 ± 1 [c]	63 ± 7 [b]
3-PAAD	0.88 ± 0.06 [b] 2.1 ± 0.4 [c]	10.4 ± 0.2 [b]
thio-NAD	0.48 ± 0.05 [b] 0.6 ± 0.1 [c]	11.5 ± 0.6 [b]

[a] value from reference at pH 7.0 (*124*).
[b] data obtained at pH 7.55 and [c] data obtained at pH 9.2.

Table 3.8: Kinetic Parameters of SDH in the Saccharopine Formation Reaction Direction at pH 7.0.

	NADH [a]	NADPH
$K_{coenzyme}$ (mM)	0.019 ± 0.002	0.48 ± 0.17
$K_{\alpha\text{-}Kg}$ (mM)	0.11 ± 0.03	12 ± 4
K_{Lys} (mM)	1.1 ± 0.2	22 ± 9
$K_{icoenzyme}$ (mM)	0.018 ± 0.004	0.04 ± 0.01
$K_{i\alpha\text{-}Kg}$ (mM)	0.6 ± 0.1	6.0 ± 1.4
K_{iLys} (mM)	--	9.4 ± 2.0
V/E_t (s^{-1})	20 ± 1	22 ± 6
$V/K_{coenzyme}\ E_t$ ($M^{-1}\cdot s^{-1}$)	(1.6 ± 0.2) x 10^6	(4.6 ± 2.0) x 10^4
$V/K_{\alpha\text{-}Kg}\ E_t$ ($M^{-1}\cdot s^{-1}$)	(2.8 ± 0.7) x 10^5	(1.8 ± 0.8) x 10^3
$V/K_{Lys}\ E_t$ ($M^{-1}\cdot s^{-1}$)	(2.5 ± 0.4) x 10^4	(1.0 ± 0.5) x 10^3

Product and Dead-end Inhibitor	Varied Substrate	K_i (mM) pH 7.0	Inhibition Pattern
NAD	NADH	1.56 ± 0.03 [a]	C
NADP	NADPH	3.5 ± 0.6	C
L-leucine	NADPH	5.6 ± 0.3	UC
L-leucine	NADH [b]	69 ± 2	UC

[a] value from reference at pH 7.0 (*124*);
[b] for pyruvate reaction.

3.4.2 Inhibition Studies to Determine the Kinetic Mechanism with NADP

In the direction of saccharopine formation, product inhibition by NAD is competitive vs NADH. Similarly, product inhibition by NADP is competitive vs NADPH when NADPH serves as the coenzyme, while dead-end inhibition by leucine (lysine analogue) is uncompetitive vs NADPH.

3.4.3 Initial Velocity Studies with Keto Acid Substrate Analogues

In addition to pyruvate, five keto acids have been identified as alternative substrates for the SDH-catalyzed reaction in the direction of saccharopine formation. These include glyoxylate, α-Kb, α-Kv, α-Km, and α-Ka. Kinetic parameters obtained by measuring the initial rate at fixed NADH and lysine are summarized in Table 3.

Initial velocity patterns obtained with pyruvate as the substrate, and varying the concentrations of pyruvate and lysine with NADH fixed at 0.2 mM (~3K_m) intersects to the left of the ordinate (data not shown), consistent with the proposed sequential kinetic mechanism (*124*). All kinetic parameters are listed in Table 3.9.

Table 3.9: Kinetic Parameters of SDH using Keto Acid Substrates at pH 7.0.

Substrate	K_m (mM)	V/E_t (s^{-1})	V/KE_t (M^{-1} s^{-1})
α-Ketoglutarate [a]	0.11 ± 0.03	20 ± 1	(2.8 ± 0.7) x 10^5
Pyruvate [b]	4.1 ± 0.2	2.55 ± 0.02	381 ± 3
Glyoxylate [c]	6.4 ± 0.6	1.85 ± 0.09	289 ± 31
α-Ketobutyrate [c]	153 ± 34	27.4 ± 4.8	179 ± 31
α-Ketovalerate [c]	94 ± 13	9.5 ± 0.9	101 ± 10
α-Ketomalonate [c]	24 ± 1	12.5 ± 0.5	521 ± 21
α-Ketoadipate [c]	5.3 ± 0.2	4.43 ± 0.05	836 ± 9

[a] value from reference (*124*);
[b] K_m value of lysine for pyruvate reaction is 62 ± 1 mM;
[c] The lysine concentrations used are 225 mM and 40 mM for glyoxylate and α-Kv reactions, respectively, and 20 mM for α-Kb, α-Km, and α-Ka reactions.

With glyoxylate as the substrate, a background rate was observed when the absorbance at 340 nm was monitored in the absence of enzyme. The stock glyoxylate solution (500 mM) has a slight yellow color, and this was thought to account for the absorbance at 340 nm. The increased presence of D_2O decreased the background rate, suggesting it is related to the dehydration of glyoxylate. A solvent deuterium isotope effect has been observed for dehydration of glyoxylate (*137*). Thus, the SDH reaction in the presence of glyoxylate was corrected for the background rate. Kinetic parameters are shown in Table 3.9.

Although there appeared to be an OAA-dependent decrease in A_{340} in the presence of NADH, lysine, and SDH, the rate was due to pyruvate contaminating the OAA solution, a result of nonenzymatic decarboxylation, as shown using lactate dehydrogenase.

3.4.4 Confirmation of Product of Reaction with Alternative α-Keto Acid Substrates by ^{1}H NMR

When keto acid analogues were used as alternative substrates, products were identified by measuring the ^{1}H NMR chemical shifts of protons β to the secondary amine nitrogen in the products. A control spectrum with lysine exhibits chemical shifts at 3.7 and 3.0 ppm, close to product peaks at 3.5 and 2.9 ppm, corresponding to C(8)-H and C(6)-H_2 of saccharopine, respectively (*138*). However, there is no overlap of the chemical shifts of the keto acid analogues and products. Therefore, experiments were carried out with the keto acid analogue in excess and with lysine limiting. Completeness of the reaction was monitored using the absorbance at 340 nm in a separate reaction using

similar conditions. In all cases the chemical shifts corresponding to the product C(8)-H and C(6)-H_2 resonances were observed, confirming product formation.

3.4.5 Deuterium Kinetic Isotope Effects

Primary deuterium kinetic isotope effects with pyruvate in place of α-Kg were measured by direct comparison of initial rates at pH 7.0 with A-side NADH(D). Finite effects were observed on all kinetic parameters, and are listed in Table 3.10.

Table 3.10: Isotope Effects for SDH at pH 7.0.

Isotope Effects	α-Kg [a]	Pyruvate
^{D}V	1.45 ± 0.07	1.29 ± 0.09
$^{D}(V/K_{NADH})$	0.92 ± 0.08	2.2 ± 0.1
$^{D}(V/K_{keto\ acid})$	1.9 ± 0.1	1.9 ± 0.1
$^{D}(V/K_{Lys})$	1.56 ± 0.05	2.3 ± 0.2

[a] value from reference (*124*).

3.4.6 Dead-end Inhibition by NAD/NADH Analogues

Inhibition by dinucleotide analogues AMP, ADP, ADP-ribose, NMN, 2',3'-cyclic NADP, and NADP, was competitive vs NADH at pH 7.0. All inhibition constants are summarized in Table 3.11, and structures of all dinucleotide analogues are shown in Fig. 3.14.

3.4.7 pH Dependence of the K_i for AMP

The pH dependence of the dissociation constant of AMP was determined in order to obtain an estimate of intrinsic p*K* value(s) of group(s) required for optimum binding of NADH. Over the pH range studied, AMP is a competitive inhibitor against NADH, and

the pK_{iAMP} profile is shown in Fig. 3.15. The pK_i decreases from a constant value at pH 7.0 to another constant value below a pH of 6.0, and decreases as pH increases above 7.5. The decrease at low pH exhibits a slope of 2 indicating two groups must be unprotonated for optimum binding of AMP, while the decrease at high pH is with a slope of -1 indicating a group must be protonated for optimum binding of AMP. An average pK_a value of about 7.1 is estimated for all three of the groups.

Table 3.11: Inhibition Constants of NAD analogue inhibitors at pH 6.9.

Substrate/Inhibitor	K_i (mM)
NADH	0.018 ± 0.004 [a]
Adenosine	0.42 ± 0.04
AMP	0.055 ± 0.006
ADP	0.093 ± 0.006
ADP-ribose	0.29 ± 0.01
NMN	7.2
NADP	1.2 ± 0.4
2',3'-cyclic NADP	1.5 ± 0.1
NADP [b]	3.5 ± 0.6
NAD	1.56 ± 0.03 [a]

[a] value from reference (*124*);
Varied substrate is NADH with the exception of [b] where NADPH is the varied substrate.

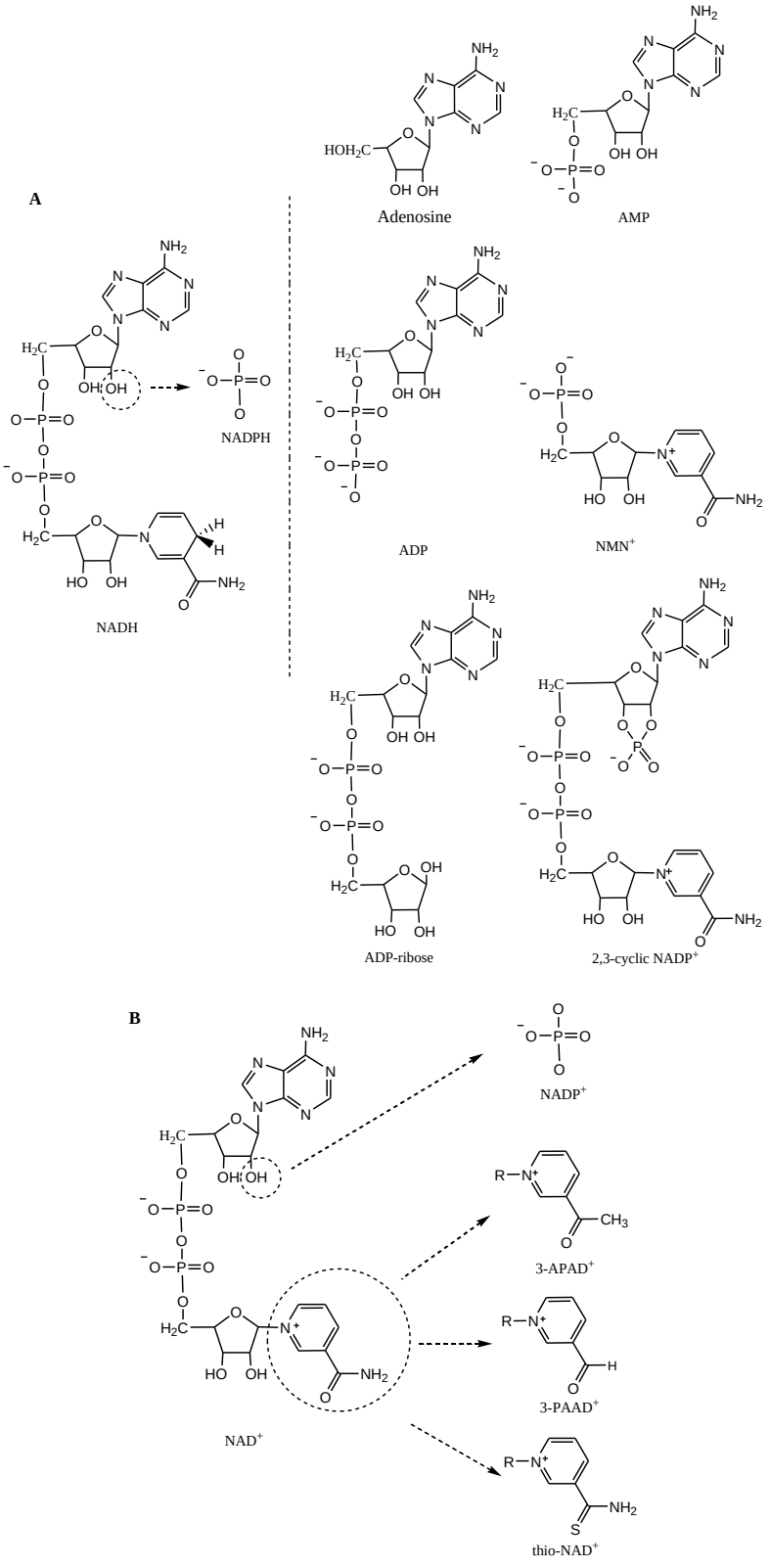


Figure 3.14: Structures of coenzyme analogues. (A) NAD analogue inhibitors (B) NAD analogue substrates.

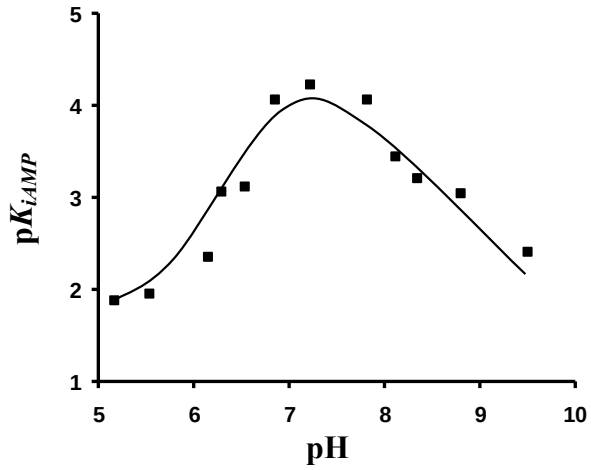


Figure 3.15: pH dependence of the reciprocal of the inhibition constant for AMP. The points shown are the experimental determined values, while the curve is theoretical based on the fit of the data using eq 2.20.

3.4.8 Dead-end Inhibition by Keto Acid Analogues

A number of α-Kg analogues exhibit competitive inhibition patterns against α-Kg at pH 7.0 in the direction of saccharopine formation, Table 3.12. In addition, pyridine 2,5-dicarboxylate and L-pipecolic acid gave no observed inhibition at a concentration of 50 mM. Structures of the α-Kg analogues are shown in Fig. 3.16B-C.

3.4.9 Dead-end Inhibition by Amino Acid Analogues

SDH shows a very strict substrate specificity towards its amino acid substrate, L-lysine. A number of lysine analogues show competitive inhibition vs L-lysine, including L-ornithine and D-lysine. L-Asparagine gave no inhibition at a concentration of 50 mM. Since L-leucine, a competitive inhibitor of L-lysine, binds better at pH values below 6, the K_i for amino acid analogues with aliphatic side chains such as L-valine and L-isoleucine were measured at pH 6.0 and 7.0. All K_i values are summarized in Table 3.13, and structures of all L-lysine analogues are shown in Fig. 3.16A.

Table 3.12: Inhibition Constants of α-Kg Substrate Analogue Inhibitors at pH 7.0.

α-Kg analogue inhibitors	K_i (mM)
Oxalate	36 ± 4
α-Keto Dicarboxylic Acids	
α-Ketomalonate	24 ± 1 (K_m)
Oxaloacetate	6.4 ± 0.5 [a] (NC)
α-Ketoglutarate [b]	0.6 ± 0.1 (K_{ib}) [a]
Oxalylglycine	0.100 ± 0.002 [a]
α-Ketoadipate	5.3 ± 0.2 (K_m)
α-Ketopimelate	18 ± 2
Dicarboxylic Acids	
Malonate	24 ± 2
Succinate	21 ± 1
Glutarate	1.0 ± 0.1 [a] (NC)
Adipate	50 ± 2
Other	
α-Ketoisovalerate	36 ± 1
Pyridine 2,4-dicarboxylate	1.10 ± 0.01
Pyridine 2,3-dicarboxylate	18.3 ± 0.4

[a] value from reference (*124*);
[b] K_m for α-Kg is 0.11 ± 0.03 mM (*124*).

Table 3.13: Inhibition Constants of Lysine Substrate Analogue Inhibitors.

dead-end inhibitor	K_i (mM) pH 6.0	K_i (mM) pH 7.0
L-Lysine	1.7 ± 0.2 (K_m) [a]	1.1 ± 0.2 (K_m) [a]
D-Lysine	--	5.5 ± 0.4
L-Ornithine	3.6 ± 0.1 (pH 7.6)	5.0 ± 0.1
L-Valine	62 ± 5	140
L-Norvaline	0.71 ± 0.04	1.13 ± 0.05
L-Methionine	0.96 ± 0.03	3.12 ± 0.08
L-Leucine	0.125 ± 0.002 [a]	0.44 ± 0.03 [a]
L-Isoleucine	10.7 ± 0.4	22 ± 2.0
L-Arginine	--	16.4 ± 0.4
L-Glutamine	--	16.0 ± 0.8
L-Asparagine	--	No inhibition

[a] value from reference (*124*).

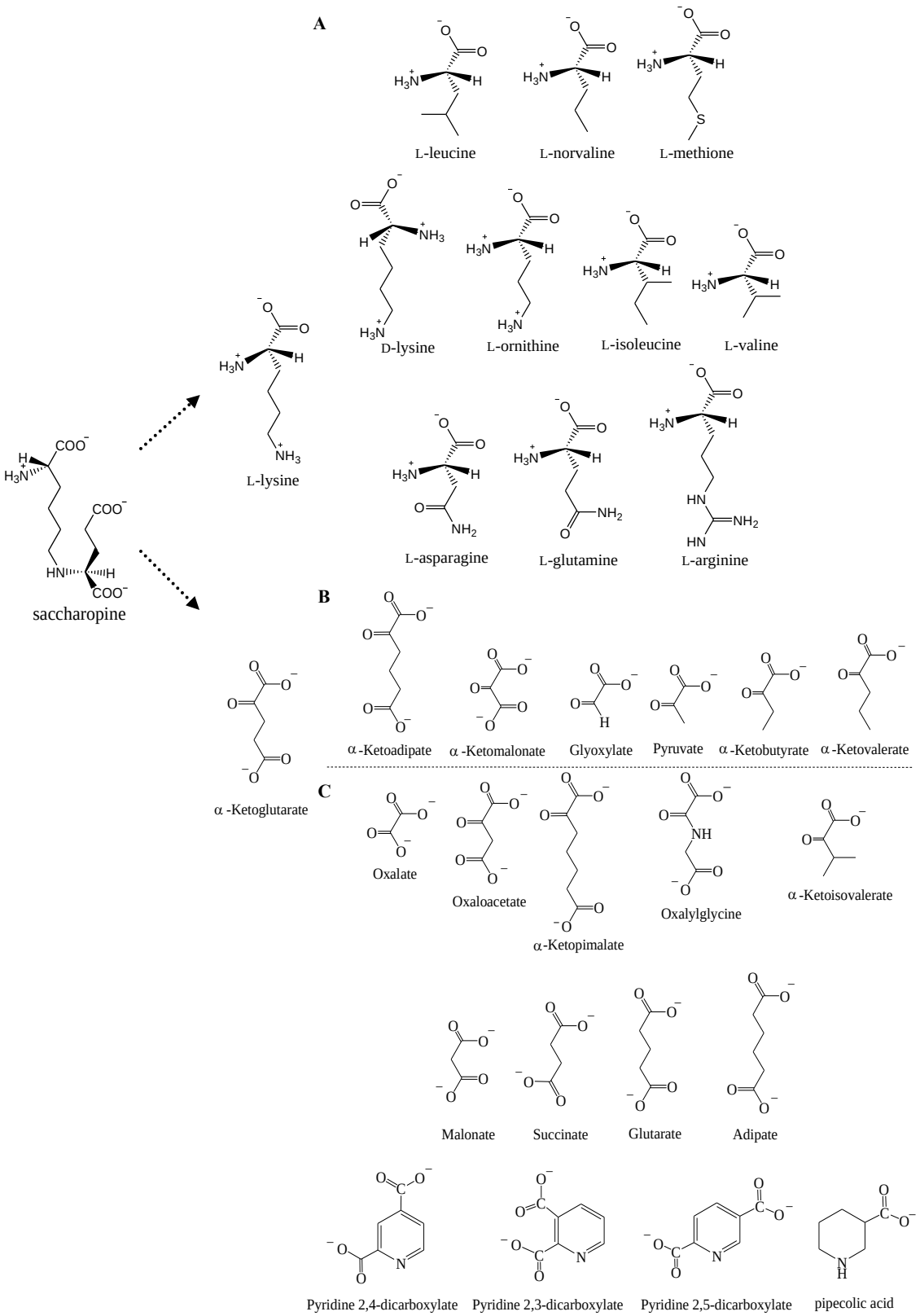


Figure 3.16: Structures of α-Kg and L-lysine analogues. (A) lysine analogue inhibitors (B) keto acid substrates (C) α-Kg analogue inhibitors.

3.4.10 Double Inhibition Studies

In order to determine whether the binding of lysine and α-Kg affect one another, double-inhibition experiments with competitive inhibitors of the two substrates were carried out. The initial rate was measured at saturating NADH, with α-Kg and lysine fixed at their respective K_m values, and varying the concentrations of OG and ornithine, Fig. 3.17. The rate in the absence of inhibitors, $v_{0,}$ was 11.8 ± 0.2 μM/min, while the appK_i values for E:NADH:OG and E:NADH:ornithine complexes are 0.050 ± 0.002 and 4.6 ± 0.2 mM, respectively. The interaction constant, α, was 0.7 ± 0.1, indicating slight synergism of binding between OG and ornithine. A double-inhibition pattern obtained with ornithine and the bulky pyridine 2,4-dicarboxylic acid gave quite different results, with K_i values for E:NADH:pyridine 2,4-dicarboxylic acid and E:NADH:ornithine complexes of 1.99 ± 0.06 and 5.0 ± 0.1 mM, respectively. A value of 2.4 ± 0.4 for α was estimated indicating antagonism of binding.

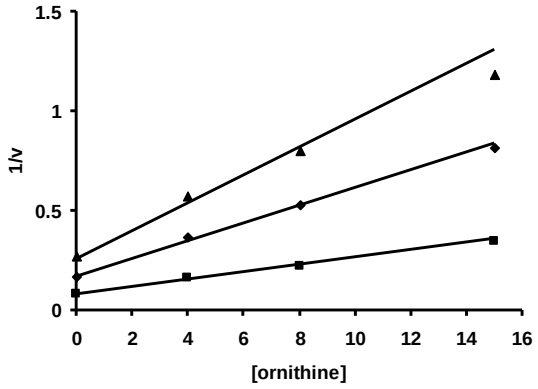


Figure 3.17: Double inhibition by oxalylglycine and ornithine. Plot of the reciprocal initial rate versus the ornithine concentration (0-15 mM) at different levels of oxalylglycine [0 mM (■), 0.05 mM (♦), and 0.1 mM (▲)]. The points are experimental, while the solid lines are theoretical based on a fit to eq 2.10.

CHAPTER 4

DISCUSSION

4.1 Kinetic Mechanism Determination of SDH

4.1.1 Initial Velocity Studies

In general, for a sequential terreactant mechanism, the initial velocity patterns obtained by varying concentrations of any two substrates with the third fixed at a nonsaturating concentration are all intersecting. If the second substrate to add in an ordered mechanism is fixed at a saturating concentration, the initial velocity pattern obtained by varying the first substrate at different fixed levels of the last becomes parallel (*117*); while three intersecting patterns would be consistent with a fully random mechanism whatever the concentration of the fixed reactant. Random binding of A and B to E followed by binding of C to EAB also gives intersecting patterns when any of the substrates is saturating and the other two are varied. However, ordered binding of A followed by random addition of B and C will give two parallel patterns when A and C or A and B are varied at saturating levels of B and C, respectively (*117*).

In the direction of reductive amination of α-Kg catalyzed by SDH, saturation with NADH and varying α-Kg/lysine gave an intersecting pattern, while two parallel patterns were observed for the NADH/α-Kg and NADH/lysine pairs at saturating concentrations of lysine and α-Kg, respectively (Fig. 3.2A-C). These initial velocity patterns suggest the ordered addition of NADH, followed by the random addition of lysine and α-Kg. The binding of NADH to free enzyme has also been demonstrated by isothermal titration calorimetry (ITC) (see **Appendix II**). No direct binding between lysine or α-Kg to the

free enzyme was detected by ITC, which would result from a high K_d or the lack of a defined binding site in the absence of NADH.

When data from a systematic analysis of initial velocities varying all reactant concentrations were fitted to eq 2.3 for a fully random terreactant mechanism, the B and C terms in the denominator of the rate equation were not defined, which suggests that the EB (E:α-Kg) and EC (E:lysine) binary complexes are not present. Data are consistent with the above mechanism that suggests that lysine and α-Kg cannot add until NADH does.

The intersecting initial velocity pattern obtained in the direction of saccharopine oxidation indicates a sequential mechanism for the addition of NAD and saccharopine, consistent with data obtained in the opposite direction. The initial velocity data in the absence of added inhibitors do not define the order of addition. Data obtained from initial velocity studies in the direction of saccharopine formation alone do not discriminate between the ordered and random addition of reactants, and thus, the kinetic mechanism was further defined via product and dead-end inhibition studies.

4.1.2 Substrate Inhibition Studies

A number of pyridine nucleotide-linked dehydrogenases are inhibited by high concentrations of the substrates. Generally, the substrate inhibition is considered to be caused by forming a dead-end enzyme:oxidized coenzyme:oxidized substrate complex or a dead-end enzyme:reduced coenzyme:reduced substrate complex. Substrate inhibition resulting from the combination of a substrate with central complexes has also been reported (*118*).

It has been reported that in the reductive amination reaction direction, SDH is inhibited by high concentrations of lysine and α-Kg (both show uncompetitive inhibition against NADH) but not by NADH, while NAD and saccharopine show no substrate inhibition in the physiologic reaction direction (*105*). If the lysine substrate inhibition arises from the formation of a dead-end E:NAD:substrate complex, one would expect uncompetitive inhibition by lysine vs NADH. The observed competitive inhibition by lysine vs NADH indicates that lysine binds to free enzyme at high concentrations, forming a dead-end E:lysine complex.

The substrate inhibition by α-Kg is uncompetitive with respect to NADH at saturating lysine, suggesting a combination to the E:NAD product complex. For α-Kg to cause any substrate inhibition, the E:NAD complex must exist in the steady state, which suggests that the release of NAD from E:NAD contributes to the overall rate limitation at saturating substrate concentrations (V/E_t). Uncompetitive substrate inhibition is common in the nonphysiological direction of a steady-state ordered mechanism (*119*). Whether the inhibition by α-Kg results from the formation of a E:NAD:α-Kg dead-end complex was further tested via a double-inhibition experiment measuring the initial rate at fixed low NADH and lysine and varying the NAD concentration at different inhibitory levels of α-Kg (Fig. 3.5B). The inhibition by NAD alone in Fig. 3.5B is observed as the line with ■ reflecting the E:NAD complex, while the inhibition by α-Kg alone (ordinate) reflects the binding of α-Kg to the E:NAD that exists in the steady state in the absence of added NAD. The slope effect indicates an enhancement of inhibition as a result of synergism of binding between NAD and α-Kg. A value of 0.12 is obtained for α, suggesting an 8-fold increase in the affinity of α-Kg in the presence of NAD, compared to its absence. Under

the conditions examined, saccharopine substrate inhibition was not observed over a concentration range of 5-50 mM, in 100 mM Hepes and pH 7.0.

4.1.3 Product Inhibition Studies

The order of product release in the direction of saccharopine formation was examined using product inhibition by NAD and saccharopine. If the overall reaction is reversible and NAD is the last product to leave, the inhibition by NAD would be competitive with respect to NADH and noncompetitive vs the other two substrates. Indeed, inhibition patterns predicted by these assumptions were obtained (Table 3.2). The competitive inhibition by NAD vs NADH at low lysine and α-Kg indicates that NAD is the last product to leave in the direction of reduction amination. The noncompetitive inhibition by NAD vs the other two reactants is consistent with NAD binding to free enzyme. Thus, the order of product release would be saccharopine followed by NAD. The high K_{ii} value obtained for the noncompetitive inhibition by NAD against α-Kg is likely due to the low concentration of free enzyme (12%), as a result of the high NADH ($3K_m$) and lysine ($2.5K_m$) concentrations used. Correction for the enzyme concentration gives a value of 13 mM, in reasonable agreement with the K_{is} value of 28 mM (Table 3.2).

According to the proposed mechanism, if saccharopine is the first product to dissociate, one would predict noncompetitive inhibition by saccharopine against all three substrates. However, uncompetitive inhibition by saccharopine vs NADH was observed. The lack of a slope effect can be explained by the combination of saccharopine with E:NADH in dead-end fashion, or with E:NAD with no reversal of the reaction, or both. The noncompetitive patterns observed for saccharopine vs lysine or α-Kg can be explained on the basis of the combination with E:NAD and E:NADH. The inability of

saccharopine to reverse the reaction is fully consistent with the K_{eq} of 2.9 x 10^{-7} M measured for the reaction at pH 7.0. The uncompetitive substrate inhibition by α-Kg and double inhibition by NAD/α-Kg suggest the presence of E:NAD in the steady state, and this is the normal complex with which saccharopine combines as a reactant. It is not unreasonable that saccharopine would bind to the E: NAD and E: NADH complexes because of the structural similarity of the dinucleotide substrates. Both combinations of saccharopine would give an uncompetitive pattern vs NADH and noncompetitive patterns vs lysine and α-Kg. In addition, the high K_{ii} value obtained for the noncompetitive inhibition by saccharopine against α-Kg is likely due to the low concentration of the E:NAD complex to which saccharopine binds, as a result of the low NADH (K_{NADH}) and lysine (K_{Lys}) concentrations used.

In the direction of saccharopine oxidation, all products were used as product inhibitors. The inhibition by α-Kg was only observed when NAD is saturating ($20K_m$) and resulted largely from the formation of the abortive E:NAD:α-Kg complex (see discussion of double-inhibition experiments above). The combination of α-Kg with E:NAD would be expected to give competitive inhibition vs saccharopine, and the combinations of α-Kg with E:NADH and E:NADH:lysine enzyme forms would give noncompetitive inhibition. The observed noncompetitive inhibition pattern is thus consistent with the proposed mechanism. The high K_{ii} value results from the low concentrations of E:NADH and E:NADH:lysine complexes present in the steady state (saccharopine fixed at $1.5K_{Sacc}$).

The product NADH exhibits competitive inhibition against NAD, suggesting that NADH and NAD bind to free enzyme. NADH exhibits noncompetitive inhibition vs

saccharopine, consistent with NADH binding before saccharopine along the reaction pathway, in accordance with the proposed mechanism, that is, the addition of NAD before saccharopine.

Lysine is competitive vs saccharopine under conditions where NAD is fixed at its K_m. It thus appears that no significant E:NADH or E:NADH:α-Kg is present in the steady state under these conditions. This is consistent with the lack of substrate inhibition by saccharopine. The noncompetitive inhibition vs NAD then results from the combination of lysine with E (see lysine substrate inhibition above) and E:NAD when higher lysine concentrations are used.

4.1.4 Dead-end Inhibition Studies

Dead-end inhibitors structurally resembles the substrate and compete with the substrate for a binding site on the enzyme; however, they do not undergo chemical transformation like the substrate. As a result, it is often more straightforward to interpret data from dead-end inhibition, and these experiments are invaluable in establishing the order of substrate binding (*120*).

Leucine was chosen as a dead-end analogue of lysine and was competitive vs lysine, indicating that it competes with lysine for its binding site on the enzyme. The uncompetitive inhibition observed vs NADH is consistent with leucine binding to a form of enzyme that exists when NADH is saturating. The noncompetitive inhibition against α-Kg results from the combination with an enzyme form that α-Kg binds and one that is present at saturating α-Kg, viz., the E:NADH and E:NADH:α-Kg enzyme forms. All of the leucine dead-end patterns are consistent with the random addition of lysine and α-Kg once NADH is bound.

OG was chosen as a dead-end analogue of α-Kg. It was competitive vs α-Kg, indicating that it competes with α-Kg for its binding site on the enzyme. The uncompetitive inhibition observed vs NADH is consistent with OG binding to a form of the enzyme that exists when NADH is saturating. The noncompetitive inhibition against lysine results from the combination of E:NADH and E:NADH:lysine enzyme forms. All of the OG dead-end patterns are consistent with the random addition of lysine and α-Kg once NADH is bound.

OAA was also chosen as a dead-end analog of α-Kg. However, OAA exhibited behavior similar to that of leucine. It was competitive vs lysine, suggesting that it binds to the same enzyme form(s) as does lysine. However, it was noncompetitive vs both α-Kg and NADH, suggesting that it binds to E as well as the E:NADH and E:NADH:α-Kg enzyme forms.

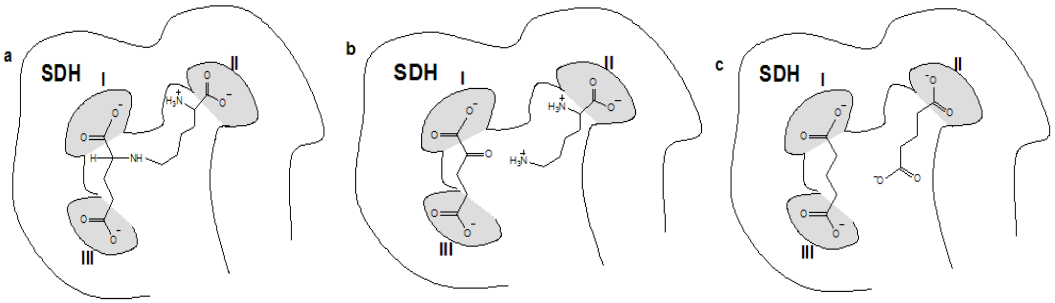
Glutarate as a dead-end inhibitor is competitive vs lysine and noncompetitive vs α-Kg, as are leucine and OAA. However, it exhibits S-parabolic noncompetitive inhibition vs NADH. Thus, in addition to binding to E:NADH and E:NADH:α-Kg, glutarate binds to E, as does OAA. The parabolic slope effect indicates the formation of a E:(glutarate)$_2$ complex, likely as a result of occupying both the lysine- and α-Kg-binding sites. This is a reasonable result because glutarate can be seen as a mimic of both halves of saccharopine. Attempts to fit the data using eq 4.1 were unsuccessful, giving a K_{i1} higher than the concentration range used for glutarate and a K_{i2} lower than the concentration range used.

$$v = \frac{\mathrm{V}\mathbf{A}}{K_a(1+\frac{\mathbf{I}}{K_{i1}}+\frac{\mathbf{I}^2}{K_{i1}K_{i2}})+\mathbf{A}(1+\frac{\mathbf{I}}{K_{ii}})} \qquad (4.1)$$

In eq 4.1, K_{i1} and K_{i2} are dissociation constants for glutarate from the E:glutarate and E:(glutarate)$_2$ complexes, respectively. A fit to eq 2.11, a modified version of eq 4.1, with the $\mathbf{I}/K_{i1}$ term missing, gives good estimates and indicates that the first molecule of glutarate bound has a very low affinity, while the second glutarate molecule bound increases the affinity of the first dramatically, trapping it on the enzyme. As a result, an average K_{is} is obtained for dissociation of both molecules from the E:(glutarate)$_2$ complex.

Pyruvate was reported as a slow alternative keto acid substrate (*98, 103*). Enzyme activity with pyruvate was observed in these studies only when the lysine concentration was fixed at 40 times the value of K_{Lys} obtained for the normal reaction using α-Kg, and a pyruvate concentration is 200 times higher than α-Kg needed for the normal reaction. As a result, pyruvate is treated as a dead-end analogue of α-Kg. Surprisingly, it shows competitive inhibition vs both lysine and α-Kg and uncompetitive inhibition vs NADH, indicating that it binds to both E:NADH:α-Kg and E:NADH:lysine enzyme forms, so that it, like glutarate, binds to both subsites occupied by saccharopine.

The binding mode of the two glutarate molecules in the E:(glutarate)$_2$ complex and the competitive inhibition patterns observed for pyruvate vs both lysine and α-Kg are reasonable considering that their structure mimics both reactants, in part, i.e., α-keto acid and dicarboxylic acid. A schematic representation of the saccharopine-binding pocket is shown in Scheme 4.1. There are likely three subsites (I, II, and III) for the interaction of the three carboxylates of saccharopine (Scheme 4.1A). Production of lysine and α-Kg would then give their binding modes as in Scheme 4.1B. Binding of glutarate may then be accommodated at both sites as shown in Scheme 4.1C. It is also possible that binding sites I and II could be used by one molecule of glutarate and III for a second.



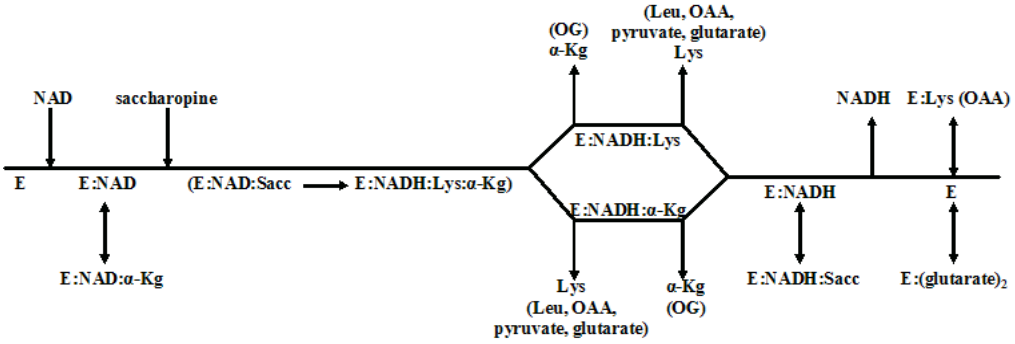
Scheme 4.1: Schematic of the saccharopine-binding pocket to illustrate possible inhibition binding modes. A and B show a possible binding pocket for saccharopine, lysine, and α-Kg. C shows possible binding modes for glutarate.

On the basis of the initial velocity studies in the absence and presence of product and dead-end inhibitors, SDH has a relatively flexible and large substrate-binding pocket for saccharopine and its products, lysine and α-Kg. The binding of NADH causes a conformational change, increasing the affinity of the enzyme for lysine and α-Kg as indicated by the difference in the substrate inhibition constant and the K_m (steady-state dissociation constant) for lysine. An overall kinetic mechanism can thus be proposed and is shown in Scheme 4.2. For the fully defined kinetic mechanism, the rate equation in the direction of saccharopine formation (eq 2.4) can be defined in terms of kinetic constants as shown in eq 4.2

$$v = \frac{V\mathbf{ABC}}{K_{ia}K_{ib}K_c + K_{ib}K_c\mathbf{A} + K_b\mathbf{AC} + K_c\mathbf{AB} + K_a\mathbf{BC} + \mathbf{ABC}} \tag{4.2}$$

In eq 4.2, K_{ia} and K_{ib} are dissociation constants of A from EA and B from EAB complexes, respectively, and all other terms are the same as defined above. A refit of all initial velocity data in the direction of saccharopine formation using eq 4.2 gives K_{ia} a

value of 0.018 ± 0.004 mM and K_{ib} a value of 0.6 ± 0.1 mM. All other constants are given in Table 3.1.



Scheme 4.2: Proposed kinetic mechanism for SDH. E represents SDH. Kinetic data suggest that the reaction is irreversible in agreement with the K_{eq} of the reaction.

4.1.5 Quantitative Analysis of Dead-end Inhibition Data

For dead-end inhibitors, the correction of the observed K_i values for the fixed substrate concentrations should give the same K_i value whatever substrate is varied. Thus, for inhibition by OG and leucine, the observed K_{is} and K_{ii} values must be corrected for the concentration of the fixed substrates. We give an example of how this is done below. Given eq 4.2, each of the terms in the denominator represents an enzyme form. The EA and EAC forms of the enzyme bound OG, represented by $K_{ib}K_c\mathbf{A}$ and $K_b\mathbf{AC}$, respectively, and these terms would be multiplied by $(1 + \mathbf{I}/K_{i1})$ and $(1 + \mathbf{I}/K_{i2})$, respectively, where **I** is OG and K_{i1} and K_{i2} are dissociation constants for E:NADH:OG, and E:NADH:Lys:OG, respectively. However, because $K_{i1} = K_{i2}$ in this case (see below), eq 4.3 is correct. The presence of the inhibitor adds a $(1 + \mathbf{I}/K_i)$ term to each of the denominator terms representing EA and EAC enzyme forms to which B binds, $K_{ib}K_c\mathbf{A}$ and $K_b\mathbf{AC}$, to give eq 4.3, where K_i is the intrinsic dissociation constant for inhibitors

$$v = \frac{V\mathbf{ABC}}{K_{ia}K_{ib}K_c + (K_{ib}K_c\mathbf{A} + K_b\mathbf{AC})(1+\frac{\mathbf{I}}{K_i}) + K_c\mathbf{AB} + K_a\mathbf{BC} + \mathbf{ABC}} \tag{4.3}$$

With **B** varied, eq 4.3 in double-reciprocal form is given by eq 4.4

$$\frac{1}{v} = \left[\frac{K_{ia}K_{ib}K_c}{V\mathbf{AC}} + \left(\frac{K_{ib}K_c}{V\mathbf{C}} + \frac{K_b}{V}\right)\left(1+\frac{\mathbf{I}}{K_i}\right)\right]\left(\frac{1}{\mathbf{B}}\right) + \left[\frac{K_a}{\mathbf{A}} + \frac{K_c}{\mathbf{C}} + \frac{1}{V}\right] \tag{4.4}$$

The expression for the slope of eq 4.4 vs **I** is given in eq 4.5

$$\text{slope} = \left(\frac{K_{ia}K_{ib}K_c}{V\mathbf{AC}} + \frac{K_{ib}K_c}{V\mathbf{C}} + \frac{K_b}{V}\right) + \left(\frac{K_{ib}K_c}{VK_i\mathbf{C}} + \frac{K_b}{VK_i}\right)\mathbf{I} \tag{4.5}$$

and with slope equal to 0

$$\mathbf{I} = \text{app}K_{is} = -K_i\left(\frac{\frac{K_{ia}K_{ib}K_c}{V\mathbf{AC}} + \frac{K_{ib}K_c}{V\mathbf{C}} + \frac{K_b}{V}}{\frac{K_{ib}K_c}{V\mathbf{C}} + \frac{K_b}{V}}\right) \tag{4.6}$$

where the appK_{is} values are those given in Table 3.3.

With **A** varied, eq 4.3 in double-reciprocal form is given by eq 4.7

$$\frac{1}{v} = \left(\frac{K_{ia}K_{ib}K_c}{V\mathbf{BC}} + \frac{K_a}{V}\right)\left(\frac{1}{\mathbf{A}}\right) + \left[\left(\frac{K_{ib}K_c}{V\mathbf{BC}} + \frac{K_b}{V\mathbf{B}}\right)\left(1+\frac{\mathbf{I}}{K_i}\right) + \frac{K_c}{V\mathbf{C}} + \frac{1}{V}\right] \tag{4.7}$$

The expression for the intercept of eq 4.7 vs **I** is given in eq 4.8

$$\text{intercept} = \left(\frac{K_{ib}K_c}{V\mathbf{BC}} + \frac{K_b}{V\mathbf{B}} + \frac{K_c}{V\mathbf{C}} + \frac{1}{V} \right) + \left(\frac{K_{ib}K_c}{VK_i\mathbf{BC}} + \frac{K_b}{VK_i\mathbf{B}} \right)\mathbf{I} \tag{4.8}$$

and with intercept equal to 0

$$\mathbf{I} = \text{app}K_{ii} = -K_i \left(\frac{\frac{K_{ib}K_c}{V\mathbf{BC}} + \frac{K_b}{V\mathbf{B}} + \frac{K_c}{V\mathbf{C}} + \frac{1}{V}}{\frac{K_{ib}K_c}{V\mathbf{BC}} + \frac{K_b}{V\mathbf{B}}} \right) \tag{4.9}$$

With **C** varied, the expression for K_{is} and K_{ii} can be derived in a similar manner and the true K_i can be calculated. Values of K_{i1} and K_{i2} are obtained by correcting the slope (K_{is}) and intercept (K_{is}) values measured for the noncompetitive inhibition vs lysine (Table 3.3). Note that these values, 0.07 mM and 0.06 mM are identical within error, justifying the use of eq 4.3 above. The corrected values of K_i are given in parentheses in Table 3.3, and all are in very good agreement with one another.

Similar corrections have been done for leucine inhibition patterns and could be carried out for all other dead-end inhibition patterns, but this serves to illustrate the process. Data are then consistent with the proposed kinetic mechanism.

4.1.6 Previously Published Data

Previously, an ordered kinetic mechanism was proposed for SDH (*96, 97*). Data suggested that when α-Kg was used as the keto acid substrate, the mechanism was defined as ordered with NAD bound first, followed by saccharopine, and products were released in the order lysine, α-Kg, and NADH. However, when α-Kg was substituted by the alternative slow keto acid substrate pyruvate, the mechanism was still ordered but

with the order of product release pyruvate, lysine, and NADH (*98*). In addition, one of the pairwise initial velocity patterns obtained by the authors, NADH/lysine at saturating levels of α-Kg, was not consistent with the proposed ordered mechanism (*95*). Noncompetitive inhibition patterns observed with OAA, pyruvate, α-ketobutyrate, α-ketovalerate, and α-ketocaproate were observed previously (*96*), whether NADH, α-Kg, or lysine was the varied substrate, and these patterns are also inconsistent with a sequential ordered kinetic mechanism. The ordered mechanism proposed previously differs from that proposed on the basis of studies presented here. Previous results fit well into the mechanism that we propose. The keto acid substrates bind to E:NADH and E:NADH:lysine complexes, consistent with the random addition of the keto acid substrate and lysine. In addition, however, a number of dead-end complexes exist that were not observed previously, and some mono- and dicarboxylic acid inhibitors can apparently bind to both subsites of the saccharopine-binding site (Scheme 4.1).

Differences between the previous studies and those in this dissertation may be caused by a number of reasons. The specific activity of the His-tagged SDH in this study is 243.9 units/mg, more than twice the value of 130 units/mg reported in previous studies (*95*). Hepes buffer was used in all of the studies presented, rather than the phosphate buffer used previously, to eliminate possible inhibition by phosphate. A systematic analysis of initial velocities that covers limiting and saturating concentrations of all three reactants at once was performed in this study in addition to the pairwise analysis. Finally, the kinetic mechanism was probed in both reaction directions as opposed to the reductive amination direction alone.

Interestingly, inhibition patterns obtained differ between the two studies, and this appears to be largely a result of the conditions utilized. For example, a lack of inhibition by glutarate as a dead-end analogue was reported previously (*96*), and this is almost certainly due to the limited glutarate concentration range examined and the unique type of inhibition in which two molecules of glutarate are apparently needed for significant affinity. All of the inhibition patterns obtained in these studies can be reconciled on the basis of the promiscuity of the saccharopine-binding site. Overall, the present studies present a complete description of the kinetic mechanism of SDH at pH 7.0.

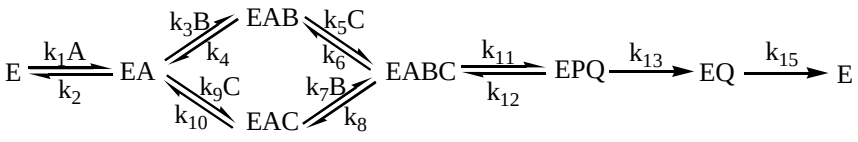
4.2 Chemical Mechanism Determination of SDH

4.2.1 Isotope Effects

The study of deuterium isotope effects has enabled investigators to obtain information about the nature of the transition state in reactions catalyzed by specific dehydrogenases, e.g., formate dehydrogenase (*121*) and alanine dehydrogenase (*78*). In many cases, it has given an indication of the relative rates of the catalytic steps in the mechanism compared to the overall rate of the reaction.

4.2.1.1 Primary Substrate Deuterium Kinetic Isotope Effects

The kinetic mechanism of SDH in the direction of saccharopine formation at neutral pH can be written



(4.10)

where A, B, C, P, and Q represent NADH, α-Kg, lysine, saccharopine, and NAD, respectively. The rate constants k_1 and k_2 are for binding and dissociation of A; k_3, k_4, k_7, and k_8 are for binding and dissociation of α-Kg, and k_5, k_6, k_9, and k_{10} are for binding and dissociation of lysine; k_{11} and k_{12} are the forward and reverse net rate constants for the catalytic pathway; while k_{13} and k_{15} are for release of saccharopine and NAD, respectively.

The substrate deuterium sensitive step, hydride transfer, contained in k_{11}, the net rate constant for catalysis, may exhibit an isotope effect upon deuteration of NADH at the C-4 *pro*-R hydrogen of the dihydronicotinamide ring if it contributes to rate limitation. Conditions for measurement of *V/K* for a given reactant require all other reactants to be present at saturation. Thus, the expressions for *V*, V/K_b, and V/K_c are given by eqs 4.11-4.14, while V/K_a is equal to k_1.

$$\frac{V}{K_b} = \frac{\frac{k_7 k_{11}}{k_8}}{1 + \frac{k_{11}}{k_8} + \frac{k_{12}}{k_{13}}} = \frac{\frac{k_7 k_{11}}{k_8}}{1 + c_{fb} + c_r} \tag{4.11}$$

$$\frac{V}{K_c} = \frac{\frac{k_5 k_{11}}{k_6}}{1 + \frac{k_{11}}{k_6} + \frac{k_{12}}{k_{13}}} = \frac{\frac{k_5 k_{11}}{k_6}}{1 + c_{fc} + c_r} \tag{4.12}$$

$$V = \frac{k_{11}}{1 + \left(\frac{k_{11}}{k_{13}} + \frac{k_{11}}{k_{15}}\right) + \frac{k_{12}}{k_{13}}} = \frac{k_{11}}{1 + c_{vf} + c_r} \tag{4.13}$$

In eqs 4.11-4.13, c_{fb} and c_{fc} (forward commitments to catalysis for B and C) are $\frac{k_{11}}{k_8}$, and $\frac{k_{11}}{k_6}$, respectively, c_r (reverse commitment to catalysis) is $\frac{k_{12}}{k_{13}}$, and c_{vf} (the catalytic ratio) is $\left(\frac{k_{11}}{k_{13}}+\frac{k_{11}}{k_{15}}\right)$ (*111*).

4.2.1.1.1 Substrate Dependence of Primary Deuterium Isotope Effects

In an ordered kinetic mechanism, V/K_a, is the on-rate constant for binding of the first substrate and is not sensitive to substitution of deuterium for protium, and thus the isotope effect on V/K_a is unity. The magnitude of $^{D}(V/K_b)$ and $^{D}(V/K_c)$ provides information on the preference of the two pathways in eq 4.10. The larger the value of $^{D}(V/K)$, the lower the value of the commitment factors, c_f and c_r. The lower commitment factor indicates the least favored pathway in a random mechanism (*122*). For example, if $^{D}(V/K_c) > {}^{D}(V/K_b)$, $c_{fc} < c_{fb}$, B is stickier than C, and the pathway preference is E to EB to EBC. If $^{D}(V/K_b) = {}^{D}(V/K_c)$, there are two possibilities. First, neither substrate B nor substrate C is sticky, suggesting that the kinetic mechanism is rapid equilibrium random. Second, both substrate B and substrate C are equally sticky, indicating a steady-state random addition of B and C, with $k_6 = k_7$ (*123*).

For the SDH reaction, $^{D}(V_2/K_{NADH})$ is 0.92 ± 0.08 at pH 7.1 and 25 °C, within error, identical to 1, consistent with the proposed ordered addition of NADH before α-Kg and lysine (*124*). Since $^{D}(V_2/K_{\alpha\text{-}Kg})$ and $^{D}(V_2/K_{Lys})$ are both finite, their order of addition must be random, consistent with the proposed mechanism, and since $^{D}(V_2/K_{\alpha\text{-}Kg})$ is greater than $^{D}(V_2/K_{Lys})$, the preferred pathway is E:NADH to E:NADH:Lys to E:NADH:Lys:α-

Kg at pH 7.1. Since ${}^{D}V_2 \approx {}^{D}(V_2/K_{Lys})$, the off-rate for lysine from E:NADH:Lys:α-Kg is likely about the same as that of NAD from E:NAD. That E:NAD exists in the steady state is known as a result of uncompetitive substrate inhibition by α-Kg (*124*). The off-rate for α-Kg from E:NADH:Lys:α-Kg is greater than that of lysine from the same complex.

4.2.1.1.2 pH Dependence of Primary Deuterium Isotope Effects

Kinetic parameters depend on pH as a result of titration of groups responsible for reactant binding, catalysis, or maintaining the correct conformation of the enzyme. Information on the kinetic and chemical mechanism can be obtained if the isotope effects are measured at the optimum pH and a pH where the kinetic parameter is decreasing by a factor of 10 per pH unit (*123*). In the case where the isotope-sensitive step is not solely rate-determining and substrate is sticky, the observed isotope effect can be enhanced by changing the pH and eliminating substrate stickiness by making the catalytic pathway slow. For the SDH reaction, the maximum isotope effect is observed at low pH (1.7-1.8), and the effect decreases as the pH is increased above the pK_a observed in the V_2/K_{Lys} pH-rate profile.

At low pH, the isotope effect on V_2/K_{Lys} increases compared to that measured at neutral pH and becomes equal to ${}^{D}(V_2/K_{\alpha\text{-}Kg})$. It thus appears that lysine is sticky, while α-Kg is not. The stickiness factor, $\frac{k_{11}}{k_6}$, can be estimated using the value of 1.8 for the maximum isotope effect and the eq 4. 14.

$$ {}^{D}\left(\frac{V}{K}\right) = \frac{{}^{D}\left(V/K\right)_{\max} + c_f}{1 + c_f} \qquad (4.14) $$

Substituting 1.56 and 1.8 for $^{D}(V/K)$ and $^{D}(V/K)_{max}$, a c_f of about 0.4 is calculated, suggesting that at neutral pH, once lysine is bound, it dissociates from the enzyme 2.5 times faster than the rate of the catalytic pathway. The maximum value of 1.8 is not the intrinsic isotope effect, since the hydride transfer step is not completely limiting for the overall reaction (see below).

The value of $^{D}(V_2/K_{Lys})$ decreases to about unity as the pH increases over the pH range where V_2/K_{Lys} is decreasing by a factor of 10 per pH unit. V_2 does not vary significantly as the pH is decreased to 6.1, nor does $^{D}V_2$. However, the isotope effect does decrease toward unity as the pH is increased, as does $^{D}(V_2/K_{Lys})$, even though V_2 decreases only slightly as the pH increases. In addition, $^{D}V_2$ decreases as the pH is decreased below 6.0. Data suggest that the pH- and isotope-dependent steps are not the same in the direction of saccharopine formation (*125*) and that an isotope independent step contribute to V_2 at low pH. Data will be discussed in the context of the mechanism below.

4.2.1.2 Solvent Deuterium Isotope Effects and Proton Inventory Studies

The pH(D) dependence of kinetic parameters was measured for lysine with NADH and α-Kg maintained at saturation, over the pH(D) range 6.5-8.5 to determine whether a solvent deuterium kinetic isotope effect was observed. As predicted, the profile in D_2O is shifted to higher pD as a result of the equilibrium solvent deuterium isotope effect on the pK_a values (*109*) (Fig. 3.12). The solvent kinetic deuterium isotope effects, obtained as the ratio of the pH(D)-independent values of the kinetic parameters, are significant, with estimated $^{D2O}V_2$ and $^{D2O}V_2/K_{Lys}$ values of 2.2 ± 0.1 and 1.9 ± 0.1,

respectively, suggesting a significant contribution from proton transfer step(s) to rate limitation of the overall reaction.

4.2.1.3. Multiple Solvent/Substrate Deuterium Isotope Effects

Multiple isotope effects potentially allow one to define the interrelationship between two isotope-sensitive steps (*126*). Isotope effects that reflect the same transition state are independent of one another, since they reflect the same step. If the step is completely rate-limiting, the isotope effect will not change in the presence of the second isotope, while if it is not completely rate-limiting, the isotope effect will increase. If substrate and solvent deuterium isotope effects do not reflect the same step, deuteration of the substrate decreases the observed solvent isotope effect by making the deuterium-sensitive step more rate-limiting. Two kinds of multiple isotope effects are used in these studies, a solvent deuterium isotope effect measured with NADD and a primary substrate deuterium isotope effect measured in D_2O. There is no significant decrease in the solvent deuterium isotope effect on V_2 and V_2/K_{Lys} when obtained using NADD compared to that using NADH. In addition, there is no change in the isotope effect upon measuring $^{D}V_2$ and $^{D}(V_2/K_{Lys})$ in 90% D_2O compared to that in H_2O. These data suggest a concerted proton and hydride transfer that is completely rate-limiting for the overall reaction. However, the isotope effect on $V_2/K_{\alpha\text{-}Kg}$ is greater than that observed for V_2/K_{Lys} at pH 7.1, $^{D}(V_2/K_{Lys})$ increases as the pH is decreased, and $^{D2O}(V_2)_D$ is decreased compared to $^{D2O}(V_2)_H$. Thus, hydride transfer cannot be the sole rate-limiting step. The data can be reconciled by suggesting proton transfer in the hydride transfer step and in some other step. The one in the hydride transfer step results in an increase in the primary deuterium isotope effect, while the one in another step causes it to decrease, giving no net change in

the isotope effect. In addition, the lack of change in the solvent deuterium isotope effect indicates that the effect is likely reflected differently by the two solvent-sensitive steps with NADH and NADD, but the weighted average is the same in both cases. The origin of the proton transferred in the hydride transfer step is likely a proton transferred from the protonated secondary amine of saccharopine to an enzyme base as the hydride is transferred. There are several possibilities for the (an)other proton transfer step(s), including hydrolysis of the imine that results from the oxidation of saccharopine.

4.2.1.4. Proton Inventory Studies

An estimate of the number of protons important to the overall reaction and the number of proton transfer steps that contribute to rate limitation can be obtained from the proton inventory method (*110*). If a single proton is transferred in the rate-limiting transition state, a plot of the rate constant vs atom fraction of deuterium (n) will be linear. If more than one proton is transferred in a single transition state, the plot will be bowl-shaped (concave upward), while if protons are transferred in multiple transition states, the plot will be a dome-shaped plot (concave downward). Dome-shaped proton inventories require offsetting normal and inverse contributions to the solvent isotope effect and can have several mechanistic origins (*110*). The replot of V_2 vs the percent D_2O at pH 7.1 gives a bulging dome-shaped plot (Fig. 3.13A), suggestive of contribution from proton transfer with a significant inverse contribution effect likely from a medium effect. However, the slight curvature observed in the case of *V/K* is more consistent with isotope effects in two or more sequential transition states, but with the absence of significant medium effect (Fig. 3.13B). Data are thus consistent with the multiple isotope effects and suggest that rate-limiting proton transfer exists in at least two sequential transition states,

for example, substrate (de)protonation, hydride transfer, water elimination, or an enzyme conformational change. Of these, hydride transfer and formation of the imine from the carbinolamine are most likely. The medium effect seen in V_2, but not V_2/K_{Lys}, suggests that it is caused by a step(s) not included in V_2/K_{Lys} under conditions of saturating substrate concentration, i.e., either product release or a conformational change once substrates are bound, e.g., isomerization of E:NAD, E:NADH, or E:NADH:α-Kg. This will be further discussed below.

4.2.2 Interpretation of the pH Dependence of Kinetic Parameters

The pH dependence of log(*V/K*) vs pH is obtained at a limiting concentration of one of the reactants and saturating levels of all others, with free substrate and the enzyme form to which it binds predominant in the steady state. The log*V* vs pH profile is obtained at saturating concentrations of all substrates with the enzyme form(s) that build(s) up in the steady state predominant. The *V* profile will thus reflect groups on the enzyme required for catalysis, while the *V/K* profile will reflect the protonation state of group(s) on the enzyme and/or reactant responsible in a given protonation state for binding and/or catalysis (*120*). In the case of an ordered mechanism, the *V/K* for the first substrate is the rate constant for binding reactant to enzyme and will thus reflect groups important for binding, which may also contribute to catalysis, for example, if a catalytic group hydrogen bonds to or is in the vicinity of the substrate.

The determination of a steady-state partial random mechanism at pH 7.0-8.0 and a rapid equilibrium ordered mechanism at low and high pH for SDH allow the pH profiles to be interpreted in terms of enzyme forms or species that predominate under any given conditions. In the direction of lysine formation, free enzyme and NAD predominate for

the V_1/K_{NAD} profile, while the E:NAD enzyme form and saccharopine predominate for the V_1/K_{Sacc} profile. Finite primary deuterium and solvent deuterium kinetic isotope effects and proton inventory studies suggest that central complexes (primarily E:NAD:Sacc and E:NADH:imine, where imine is the oxidized form of saccharopine) predominate for the V_1 profile. In the reverse reaction direction, the free enzyme and NADH predominate for the V_2/K_{NADH} profile; while E:NADH:lysine and α-Kg predominate for the $V_2/K_{\alpha\text{-Kg}}$ profile at 5.0 < pH < 8.5, and at pH values lower and higher, E:NADH and α-Kg predominate. In the case of the V_2/K_{Lys} profile, E:NADH:α-Kg and lysine predominate, while central complexes and E:NAD, or E:NADH, or E:NADH:α-Kg predominate for the V_2 pH profile (see discussion of isotope effects above).

The V_1/K_{NAD} is equal to the on-rate constant for NAD binding, and the pK_a of 7.4 reflects a group that must be deprotonated for optimum binding of NAD. The V_1/K_{Sacc} pH-rate profile exhibits pK_a values of 6.2 and 7.2, while the V_1 pH-rate profile shows a pK_a of 7.2. The pK_a of 7.2 likely reflects the same enzyme group in E:NAD and central complexes, which likely serves as a general base in the overall reaction needed to activate water in the hydrolysis of the imine formed upon oxidation of saccharopine. The second group in V_1/K_{Sacc} pH-rate profile with a pK_a of 6.2 which needs to be deprotonated likely contributes to the binding of saccharopine only, since it is not observed in the V_1 pH-rate profile. Since neither NAD nor saccharopine have pK_a values in the pH range studied, the pK_a must represent ionization of a group on the enzyme. Therefore, there are two groups on the enzyme with pK_a values of 6.2 and 7.2 that must be deprotonated for binding of saccharopine and catalysis, respectively. A group on the enzyme with a pK_a of about 7.2-7.4 is likely the same one that affects V_1, V_1/K_{NAD}, and V_1/K_{Sacc}, a catalytic group that also

affects the binding of NAD. The protonation state of this group does not affect binding of NADH, and it is thus likely to be a cationic acid located in the vicinity of the positively charged nicotinamide ring of NAD.

In the direction of saccharopine formation, the SDH has a random kinetic mechanism with NADH bound to free enzyme first, followed by random addition of α-Kg and lysine at neutral pH. The $V_2/K_{NADH}\,E_t$ decreases at high pH with a slope of -1 giving pK_a value of 9.6 ± 0.2. Since NADH is the first substrate bound, and considering that the pK_a of the pyrophosphate moiety of NADH is about 1-2, it is suggested that the group on the enzyme with a pK_a of 9.6 likely contributes to the binding of NADH and must be protonated for optimal binding, likely interacting with the negatively charged phosphoryl oxygens of NADH via an ionic interaction. This group was not seen in the V_1/K_{NAD} pH-rate profile in the forward direction reaction, because the parameter was not measured above pH 9.0 in that reaction direction; the K_m for saccharopine has become about 10 mM at pH values above 9.

The $V_2/K_{\alpha\text{-}Kg}$ profile shows a single group with a pK_a of 8.9 that must be protonated for optimum binding. In addition, V_2 decreases to a new constant value at high pH exhibiting a pK_a of about 8.4. These pK_a values are identical, within error. The kinetic mechanism of SDH changes from random to rapid equilibrium ordered when the pH is above 8.0 or below 5.5. The $V_2/K_{\alpha\text{-}Kg}$ pH-rate profile is independent of pH from 5.5 to about 8.0, but the rate constant decreases when the pH is increased above 8.0, at the point where the mechanism changes. Between pH 5.5 and 8.0, the predominant enzyme form is E:NADH:Lys, while above 8, the E:NAD form predominates. The decrease in $V_2/K_{\alpha\text{-}Kg}$ likely reflects a kinetic pK_a resulting from the change in kinetic mechanism due to a

slower pathway with α-Kg binding before lysine. In agreement with the $V_2/K_{\alpha\text{-}Kg}$, V_2 also decreases at high pH, giving a partial change in activity, likely reflecting the same kinetic mechanism change. The group with a pK_a of 7.2 in the V_2/K_{Lys} profile is not observed in the $V_2/K_{\alpha\text{-}Kg}$ pH-rate profile. Under these conditions lysine is bound, and the group with a pK_a of 7.2 is likely locked in its correct protonation state. Since the group seen on the acid side functions to deprotonate the lysine ϵ-amine, it is reasonable the group would not be observed with lysine bound. Overall, data are consistent with the steady-state random nature of the mechanism with the E:NADH to E:NADH:Lys pathway preferred and faster than that with E:NADH:α-Kg.

The bell-shaped pH profile for V_2/K_{Lys} observed in the reverse reaction direction shows that a group with a pK_a of about 7.2 must be unprotonated and a group with a pK_a of about 7.2 must be protonated for binding lysine to the E:NADH:α-Kg complex and catalysis. Since lysine has no ionizing groups corresponding to 7.2, they must reflect the ionization of groups on the enzyme. A group on the enzyme with a pK_a of 7.2 exhibited in V_1, V_1/K_{NAD}, and V_1/K_{Sacc} profiles must be deprotonated for catalysis in the direction of lysine formation. On the basis of the acid-base chemistry required in the oxidative deamination reaction, the group with a pK_a of 7.2 is believed to represent a general base required to abstract a proton from H_2O as it attacks the carbon of the imine formed upon oxidation of saccharopine. In the opposite direction reaction, the same group, seen in the V_2/K_{Lys} pH-rate profile, must be protonated to donate a proton to the hydroxyl of the carbinolamine intermediate to facilitate H_2O elimination. The second group observed on the acid side of the V_2/K_{Lys} profile with a pK_a of 7.2 is responsible for deprotonating the ϵ-amine of lysine, so that it can act as a nucleophile to form an imine with the α-oxo group

of α-Kg. In the slow reaction direction (formation of lysine), the observed pK_a in the V_1/K_{Sacc} pH-rate profile is 6.2. This pK_a is likely the intrinsic pK_a for the binding group, while it is perturbed to higher pH in the opposite direction (V_2/K_{Lys} pH-rate profile), suggesting lysine is sticky (see pK_{iLeu}).

V_2 also decreases at low pH with a limiting slope of +1 giving a pK_a value of 5.8, indicating that another group on the enzyme must be deprotonated for optimum activity. It is possible that this pK_a reflects a pH-dependent conformational change in the enzyme once all substrates are bound; perhaps the same conformational change seen as a medium effect in the proton inventory of V_2. In agreement with this suggestion, the primary deuterium isotope effect decreases from 1.6 at pH 6.1 to 1.2 at pH 5.6, suggestive of a step other the hydride transfer becoming rate-limiting at low pH.

4.2.3 Interpretation of pK_i profiles

The pK_i profile for leucine, a competitive inhibitor of lysine, indicates a group with a pK_a of 6.2 must be protonated for optimal binding of leucine. This is the same pK_a observed in the V_1/K_{Sacc} pH-rate profile that must be unprotonated to bind saccharopine. The group must also be unprotonated to accept a proton from the ϵ-amine of lysine. The difference between lysine and leucine is that one has a positive charge and the other is hydrophobic. Since the group must be protonated to allow binding of the hydrophobic side chain of leucine, it is likely that it is a neutral acid (Asp or Glu). The perturbation of the pK_a observed in the V_2/K_{Lys} pH-rate profile is in agreement with the stickiness of lysine, as discussed above under the pH dependence of primary deuterium isotope effect. Given the large standard error on the pK_a values, the isotope effects provide a better quantitative estimate of stickiness. In addition, the pK_a perturbation likely reflects an

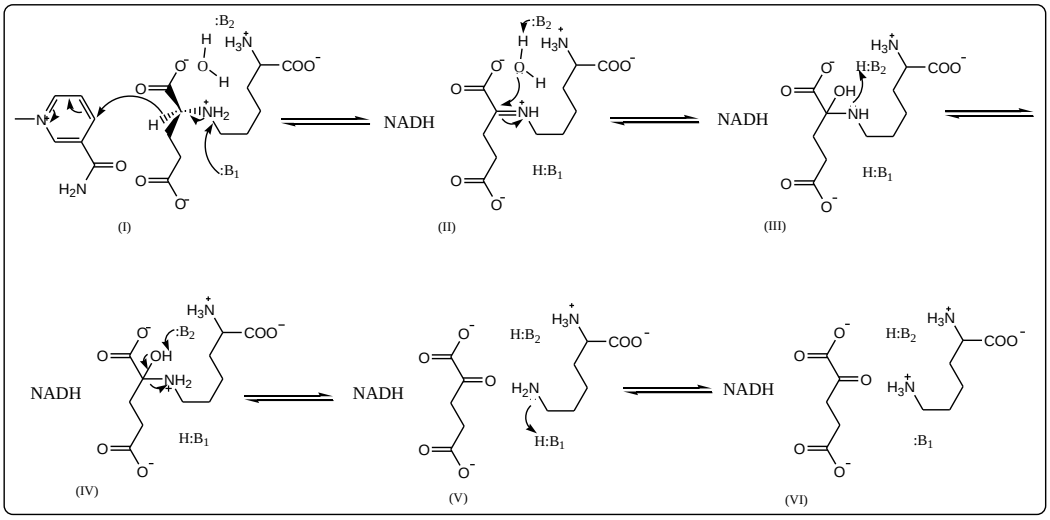
environmental change as lysine binds to the enzyme. Consistent with this suggestion, when leucine is bound, the pK_a of the binding group increases to about 9.2, consistent with a neutral acid in a more hydrophobic environment.

The pK_{iOG} profile within the pH range 6.0-8.0 where the overall kinetic mechanism is random and OG binds to E:NADH:Lys is largely pH-independent with an average K_i value of 100 μM. As the pH is increased above 8 and below 6 where the kinetic mechanism changes to equilibrium ordered, the pK_i also becomes pH-independent with an average K_i value of about 500 μM. The approximately 5-fold change in the K_i value (see the boxes in Fig. 3.10A) over these two pH ranges likely reflects the change in mechanism itself and the difference in affinity of OG for E:NADH:Lys and E:NADH. There is a transition between the two pH-independent regions, but the scatter in the data makes it difficult to see where the transition occurs. The boxes drawn in Fig. 3.10A are simply to highlight the two pH-independent regions.

4.2.4 Proposed Chemical Mechanism

The pH-rate profiles and isotope effect experiments discussed above are consistent with a proton shuttle chemical mechanism as shown in Scheme 4.3. Two groups serve as acid-base catalysts in the reaction, but one of them catalyzes most of the steps. In the direction of lysine formation, once NAD and saccharopine bind (**I**, in Scheme 4.3), the group with a pK_a of 6.2, likely Asp or Glu as suggested on the basis of the difference in V_2/K_{Lys} and pK_{iLeu} pH-rate profiles, accepts a proton from the secondary amine of saccharopine as it is oxidized. This protonated general base then does not function until lysine is formed at the completion of the reaction. The concerted proton and hydride transfer is corroborated by the D/D_2O multiple isotope effect. The general

base with a pK_a of 7.2, likely a cationic acid such as Lys or His (on the basis of the differences in V_1/K_{NAD} and V_2/K_{NADH} pH-rate profile), accepts a proton from H_2O as it attacks the Schiff base carbon (**II**) to form the carbinolamine intermediate (**III**). It is likely this step that reflects the solvent isotope effect on the step outside hydride transfer. The same residue then serves as a general acid and donates a proton to the carbinolamine nitrogen to give the protonated carbinolamine (**IV**). The carbinolamine collapses, facilitated by the proton shuttle accepting a proton from the carbinolamine hydroxyl to generate α-Kg and lysine (**V**). The amine nitrogen is then protonated by the group that originally accepted a proton from the secondary amine of saccharopine (**VI**).



Scheme 4.3: Proposed chemical mechanism for SDH. **I**. the formed central complex E:NAD:saccharopine once NAD and saccharopine bind. **II**. Schiff base intermediate. **III**. carbinolamine intermediate. **IV**. protonated carbinolamine. **V**. the generated central complex E:NADH:α-Kg-Lys. **VI**. protonated lysine. With the exception of saccharopine, no stereochemistry is implied.

Isotope effect data suggest a difference in the pH-dependent and isotope-dependent step (hydride transfer) at high pH. Data most likely reflect a pathway in which the general base with a pK_a of 7.2 becomes deprotonated along the reaction pathway,

committing reactants to go on to products. A protonated carbinolamine (**IV**) is formed from lysine and α-Kg (**V**). The base then accepts a proton from the carbinolamine nitrogen to generate the neutral carbinolamine (**III**). Deprotonation of the base at this point causes the reaction to be committed to forming saccharopine. This step precedes the hydride transfer step and would still require protonation of the leaving hydroxide to generate the imine. This proton could be generated by the imine itself in II or from some other secondary proton donor. These details await additional experiments to sort out.

As we were completing the chemical mechanism study, the structure of apo-SDH was solved (Albert M. Berghuis, McGill University, Canada, personal communication). The active site could be located using a binary complex of AlaDH with pyruvate bound; AlaDH is the closest homolog of SDH (*20*). On the basis of a superposition of the binary complex structures of AlaDH (E:NAD and E:pyruvate) and the apo-structure of SDH, the active site of the two enzymes has significant similarity. There are several Arg residues that may be in proper position to ion pair the three carboxylates of saccharopine, in agreement with the proposed role of arginine (*101*). The neutral acid suggested in our study that deprotonates saccharopine and lysine may be Asp 281, which located in the approximate vicinity predicted for the lysine side chain. In addition, the group with a pK_a of about 7.2 in the proposed mechanism is likely Lys77, which is close to Lys 13, which may function as a Lys-Lys pair to serve as the general acid-base in the reaction. The Lys-Lys pair would account for the low pK_a observed in the pH-rate profiles for V_1, V_1/K_{NAD}, V_1K_{Sacc}, and V_2/K_{Lys}. If protonated, the binding of NAD would be hindered as a result of the positive charge in the vicinity of the nicotinamide ring.

A couple of additional points should be mentioned. The proton to be transferred to the group with a pK_a of 6.2 requires that there be a better match of the pK_a values of the base and proton donor. The latter have solution values of 10-10.5 (saccharopine secondary amine and lysine ϵ-amine), > 4 pH units higher than the base. As a result, there must be a shift in the pK_a of the base to a higher value and the proton donor to a lower value, likely by about 2 pH units for each. The pK_a perturbation likely results from neutralization of the charge of the binding groups in the active site (substrate carboxylates and Arg), which will make the site more hydrophobic, resulting in an increase in the putative enzymic carboxylate pK_a and a decrease in the pK_a of the proton donor (lysine ϵ-amine or saccharopine secondary amine). The pK_a of 9.2 observed in the pK_{iLeu} profile once leucine is bound is consistent with the pK_a perturbation. Another important point is that although the group with a pK_a of 6.2 is unprotonated at the beginning and end of the reaction, the group with a pK_a of 7.2 is in opposite protonation states at the beginning and end of the reaction and must be deprotonated for a new round of catalysis, and the proton is most likely exchanged with bulk solvent after the active site is open and products are released.

4.3 Substrate Specificity of SDH

The substrate specificity exhibited by most enzymes is a hallmark of biological systems, which distinguishes them from non-biological catalysts. A survey of substrate analogues was undertaken to determine which substrate functional groups are responsible for substrate binding, to determine the stereochemistry involved in substrate/inhibitor

binding, and to potentially define the geometry of the substrate binding site. These aspects are discussed below.

4.3.1. NAD/NADH Analogues

4.3.1.1 Kinetic Mechanism with NADP/NADPH

In contrast to the previously published results (*95*), NADP does serve as a substrate, albeit poorly, in the direction of saccharopine oxidation. Under the conditions we examined, 6.5 times more enzyme was needed with NADP compared to assay conditions with NAD as the natural substrate at pH 7.55 and 9.2 (*124*). The K_{ia} value of NADP increased about 2-fold, which is the same extent as the increase of K_{ia} of NADPH comparing to that of NADH, suggesting that the presence of the phosphate at the C2 of the adenosine moiety of the coenzyme decreases its affinity only slightly.

In the direction of saccharopine formation, substitution of NADPH for NADH results in the formation of saccharopine. Systematic initial velocity studies were carried out by varying the concentrations of NADPH and α-Kg at different fixed concentrations of lysine at pH 7.0 and 25 ˚C. Double-reciprocal patterns all intersects to the left of the ordinate, indicating a sequential kinetic mechanism. When data obtained were fitted to eq 2.13 for a terreactant mechanism defined using NADH as a substrate (*124*), all terms in the denominator of the rate equation were present, and all parameters were well defined, consistent with a similar mechanism with NADPH. To test this hypothesis further, inhibition studies were carried out and are discussed below.

As a competitive inhibitor of lysine, leucine competes with lysine for its binding site on the enzyme (*124*). An uncompetitive inhibition pattern is observed vs NADPH, indicating that leucine or lysine binds to an enzyme form that exists when NADPH is

saturating, suggesting that NADPH is the first substrate bound to the free enzyme in a sequential kinetic mechanism. The order of product release in the direction of saccharopine formation was examined using product inhibition by NADP. The competitive inhibition by NADP vs NADPH at low α-Kg and lysine concentrations indicates that NADP binds to the free enzyme, competing with NADPH, suggesting it is the last product released in the direction of saccharopine formation.

The K_i value of NADPH increased about 2-fold compared to that of NADH. However, the presence of the 2'-phosphate resulted in about an order of magnitude increase in the Michaelis constants for all of the substrates. K_m is equal to the product of the steady state concentration of substrate and the enzyme forms that are present at near zero substrate concentration divided by the concentration of enzyme forms that are present at saturating substrate concentration. Thus, the increase in K_m likely reflects either an increase in the off-rate for NADP, which would increase the concentration of enzyme forms at near zero substrate, or a decrease in the affinity of the E:NADPH complex for lysine and α-Kg. Given the data in Table 3.8, it is the latter that is affected; note the 10-fold increase in $K_{i\alpha\text{-}Kg}$ when NADPH is the substrate compared to that with NADH. Data are consistent with a difference in the conformation of the E:NADH and E:NADPH complexes.

When initial rates were measured with NADPH as the coenzyme, the double-reciprocal plot exhibited substrate inhibition as the concentrations of α-Kg and lysine were increased above 50 mM and 100 mM, respectively. The observed substrate inhibition by α-Kg suggests the existence of the dead-end E:NADP:α-Kg complex, as is true with NADH as the substrate (*124*). In order to form this complex, the E:NADP form

must exist in the steady-state, which suggests that the release of NADP from E:NADP contributes to the overall rate limitation. The substrate inhibition by lysine suggests the existence of the dead-end E:Lys complex at high lysine concentrations, as is true with NADH as the substrate (*124*).

4.3.1.2 Substrate Analogues of NAD

In addition to NADP, the dinucleotide analogues 3-APAD, 3-PAAD, and thio-NAD that contain modified nicotinamide rings, all support the oxidative deamination reaction. Because the concentrations of saccharopine used were roughly estimated to be around K_m values, K_{ia} values, dissociation constants for each of the dinucleotide analogues from the E:dinucleotide complex, and apparent V_{max} values were obtained. The K_{ia} values obtained at pH 7.55 and 9.2 indicate that there is no pH dependence over this range, as is true for NAD. 3-PAAD and thio-NAD bind to free enzyme with about the same affinity as NAD, suggesting that the amide NH_2 of the nicotinamide ring does not contribute much in terms of coenzyme binding. The K_{ia} value of 3-APAD is increased 10-fold, suggesting that the binding pocket of the nicotinamide ring is relatively hydrophilic, and cannot accommodate the hydrophobic methyl group of 3-APAD very well.

4.3.1.3 Inhibitory Nucleotide Analogues

K_i values for dead-end inhibitors provide information on the importance of substrate binding since they occupy the same binding site as the substrate. With NAD(P)H as the varied substrate, NAD, NADP and 2',3'-cyclic NADP all have about the same K_i, suggesting little or no effect of the 2'-phosphate on dinucleotide binding. NMN

binds poorly to the dinucleotide-binding site, with a 5-fold lower affinity. Some of the lower affinity can be explained by the 75-fold tighter binding of NADH than NAD, and the tighter binding of NAD at pH values above 7.2 (*124*). Consistent with this suggestion, ADP-ribose binds to free enzyme with a 5-fold increased affinity. This is still about 20-fold lower than the affinity for NADH, indicative of the preference for the reduced nicotinamide ring. Elimination of the nicotinamide portion of the molecule as in ADP gives a 3-fold increase in affinity compared to ADP-ribose, but still 5-fold lower than NADH; while AMP has only a 3-fold lower affinity compared to NADH. Nonetheless, AMP binds 30-fold tighter than NAD. Adenosine binds with an 8-fold lower affinity compared to AMP, indicative of the importance of the α-phosphate.

Data indicate that the majority of the binding energy of NAD comes from the AMP portion. In the case of ADP-ribose, the β-phosphate groups account for the lower affinity, suggesting that the binding pocket is slightly hydrophobic and/or negatively charged. Since NAD binds with an about 2-order of magnitude lower affinity compared to NADH, data suggest distinctly different conformations generated upon binding the two dinucleotides.

4.3.1.4 pH Dependence of the K_i for AMP

The pK_i profile for AMP, a competitive inhibitor of NADH, indicates that two groups with pK_a values of about 7.1 must be unprotonated, and one group about the same apparent pK_a must be protonated for optimal binding of AMP. Since AMP has only one pK_a over the pH range 5-10 with a value of 6.2-6.4 for 5'-phosphate, one of the groups with a pK_a of 7.0 that must be unprotonated and the group with a pK_a of 7.2 that must be protonated must come from the enzyme. On the basis of the proposed chemical

mechanism of SDH, the two groups seen in the pK_{iAMP} profile are most likely Asp 281 and Lys 77 (*138*). The former, with a pK_a of about 6.2, is important for binding of saccharopine and likely serves as a general base in the oxidation step, while the group with a pK_a of about 7.2, is likely responsible for activating water in hydrolysis of the imine formed upon oxidation of saccharopine, and is known to affect the binding of NAD.

4.3.2 Keto Acid Analogues

4.3.2.1 Kinetic Mechanism with Pyruvate

The kinetic mechanism of SDH with pyruvate as the keto acid substrate has been fully characterized by initial velocity, dead-end inhibition, and primary deuterium kinetic isotope effect studies. The Initial velocity pattern obtained by varying the concentrations of pyruvate and lysine at a fixed level of NADH intersects to the left of the ordinate (data not shown), suggesting a sequential mechanism. Uncompetitive inhibition by leucine vs NADH indicates that NADH is the first substrate bound. Data suggest that the kinetic mechanism with pyruvate is the same as that observed with the natural substrate, α-Kg.

When both NADH and NADD were used for the pyruvate reaction, finite isotope effects were observed for all kinetic parameters. Given that $^{D}(V/K_{NADH})$, $^{D}(V/K_{pyruvate})$, and $^{D}(V/K_{Lys})$ are identical, within error, and initial velocity data suggest ordered addition of NADH before lysine and pyruvate, data suggest an equilibrium mechanism. However, the isotope effect on V decreases compared to the α-Kg reaction, suggesting that release of the product NAD still contributes to rate-limitation.

4.3.2.2 Substrate Analogues of Keto Acid

Several α-keto acids can replace α-Kg, including glyoxylate, α-Kb, α-Kv, α-Km, and α-Ka, Table 3.9. The V/KE_t values for all of the alternative substrates relative to α-Kg are decreased by 300- (α-Ka) to 2700- (pyruvate) fold, suggesting that the γ-carboxylate of α-Kg is important for proper binding of the α-keto acid substrate. However, OAA is not a substrate, and α-Ka is a substrate, but with a 5-fold lower V/E_t value, indicating that the position of the side chain carboxylate is important. The V/E_t for α-Kb is identical to that with α-Kg, while that of α-Kv is decreased by only about 2-fold. Data suggest that the optimum length of the side chain is 3 carbons (from the α-keto group up to and including the side chain carboxylate). In addition, α-Km can serve as a substrate but not OAA, suggesting that the binding pocket of the keto acid can accommodate a negative charge at the C3 but not the C4 position.

4.3.2.3 Inhibitory Keto Acid Analogues

The specificity of the keto acid substrate-binding pocket was assessed using mimics of α-Kg. Two classes of inhibitors, aliphatic and aromatic, were chosen as probes of the α-Kg binding site of SDH. With the exception of pyridine 2,5-dicarboxylate and L-pipecolic acid, which exhibit no inhibition at high concentrations, and OAA and glutarate, which exhibit noncompetitive inhibition, all other compounds are competitive inhibitor of α-Kg. Glutarate and OAA give noncompetitive inhibition as a result of combination with E:NADH and E:NADH:Lys complexes (*138*). From these data, Table 3.12, the topography of the keto acid binding site is assessed with respect to the spatial relationship and distance between the C1-C2 unit and the C5 carboxylate.

Oxalylglycine, the tightest binding inhibitor discovered to date, is structurally most similar to α-Kg, and suggests optimization of the site for a 5-carbon α-oxo dicarboxylic acid. Oxalate, α-Km, OAA, α-Kg, OG, α-Ka, and α-Kp constitute a series of α-keto dicarboxylic acids and can be compared to α-Kg as such, Fig. 3.16B-C. The log of the affinity constant for each of the keto acid analogues can be plotted against the chain length corresponding to numbers of C atoms, Fig. 4.1. The binding affinity of OAA and α-Ka, which are a methylene group shorter and longer than α-Kg, respectively, have decreased about 50-fold in affinity compared to α-Kg. Similarly, the binding affinity of α-Km and α-Kp, with two methylene groups shorter and longer than α-Kg, respectively have decreased about 200-fold in affinity, while in the case of oxalate, with three fewer methylene groups, the binding affinity has been decreased by about 360-fold. Thus, binding of a 3 carbon chain is optimal, and the distance between the C1-C2 unit and the C5 carboxylate is an important factor for determining the affinity of SDH for the α-keto acid substrate. However, of the 5 α-keto acid analogues of α-Kg, only α-Km and α-Ka can serve as an alternative substrate. The keto acid substrate binding pocket can thus accommodate the geometry of α-Ka, suggesting that the flexibility of the α-Ka side chain allows binding of the δ-carboxylate to the group on enzyme that interacts with the γ-carboxylate of α-Kg, while in the case of α-Km, the α-carboxylate is far enough away to eliminate its interaction with the same group. In addition, the α-oxo groups of α-Ka and α-Km are oriented such that hydride transfer from the nicotinamide ring of NADH is allowed.

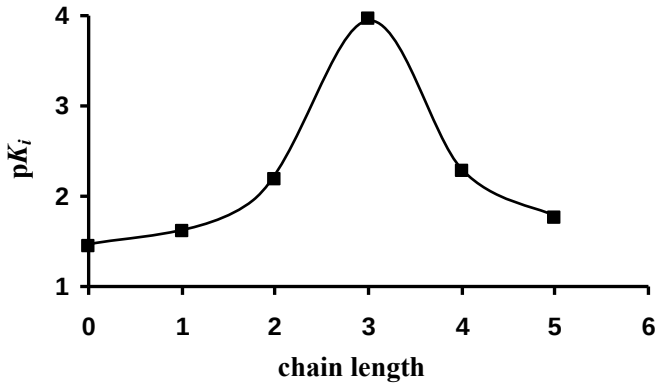


Figure 4.1: Binding affinity of keto acid substrates against chain length from C3 and including the side chain carboxylate. From left to right are oxalate, α-Km, OAA, α-Kg, α-Ka, and α-Kp, respectively. Points are experimental values, and curve is drawn by eye.

Malonate, succinate, glutarate, and adipate, dicarboxylic acids, can also be considered as a series, Fig. 3.16C. Glutarate has the lowest K_i value, suggesting that a carboxylate at the 1 and 5 positions provides the tightest binding, consistent with the above consideration of α-keto acid analogues. Increasing or decreasing the chain length by a methylene or more decreases affinity by more than an order of magnitude. In addition, the inhibition constants of α-Kg and α-Ka, which have the α-oxo group, are decreased compared to those of glutarate and adipate, which have the same chain length, but no α-oxo group; the α-oxo contributes a factor of 10 in affinity. With malonate/α-Km as the inhibitors, there is no effect of the α-oxo group suggesting that the two carboxylates are likely bound to the α-carboxylate and α-oxo binding sites of α-Kg. Similarly, with succinate/OAA, an increase by a factor of 3 is observed for the α-oxo acid. Since the α-oxo contributes a factor of 10 in binding energy, the β-carboxylate of OAA must decrease the affinity by about 3-fold. This is likely a result either of binding the β-carboxylate to the α-oxo site or the hydrophobic nature of the site in the vicinity of C4 of α-Kg.

The importance of the C5 carboxylate group can be further illustrated by a series of α-keto analogues with hydrophobic side chains; the K_i or K_m values of α-Kiv, α-Kv, and α-Kb are 36, 94, and 153 mM, respectively. However, all are alternative substrates, likely as a result of a lack of interaction with the group that binds the γ-carboxylate of α-Kg.

Finally, pyridine carboxylates provide information on the geometry of the bound α-Kg. If one assumes that the nitrogen atom of the pyridine ring mimics the oxygen atom of the α-keto group, a carboxylate in the 2-position is required. Addition of a second carboxylate, mimicking the γ-carboxylate of α-Kg can best be accommodated at the 4-position as in pyridine 2,4-dicarboxylate, which has the lowest K_i value (1.1 mM at pH 7.0). In addition, the K_i values of pyridine 2,4-dicarboxylate and glutarate are identical, within error, suggesting that the bulky aromatic ring does not affect binding when properly positioned. The distance between the two carboxylates of pyridine 2,4-dicarboxylate is 3.77 Å, very close to that of glutarate in its extended conformation, 3.83 Å (Cambridge Structural Database). Pyridine 2,3-dicarboxylate has a K_i value similar to those of malonate and succinate, which is not unreasonable, because the aromatic ring of the pyridine may orient these two carboxylates such that this part of structure mimics the 3- and 4-carbon dicarboxylic acids. Data suggest that the keto acid binding pocket is relatively large and flexible, and can accommodate the bulky aromatic ring of the pyridine.

4.3.3 Amino Acid Analogues

4.3.3.1 Inhibitory Amino Acid Analogues

SDH exhibits an absolute specificity toward its amino acid substrate L-lysine. D-Lysine is not a substrate, and binds with 5-fold lower affinity compared with L-lysine, consistent with the stereospecificity. To gain insight into the structural requirements for amino acid binding, lysine analogues were tested for their effectiveness to inhibit the reaction. The frame of reference is the K_d for lysine from the central complex. The primary deuterium kinetic isotope effects on V and (V/K_{Lys}) at pH 7.0 are identical, within error, and thus the K_d value for L-lysine is identical to its K_m, i.e., 1.1 ± 0.2 mM (*139*).

The inhibition constant of L-ornithine, a competitive inhibitor of L-lysine, with one fewer methylene group, is lower at pH 7.0 than that at pH 7.6, consistent with optimal binding as a result of interaction with the neutral form of an enzyme carboxylate (*138*). Interestingly, when ornithine was substituted for lysine, the inhibition constant is increased by about 5-fold compared to the K_d of lysine, suggesting that the length of hydrophobic portion of amino acid carbon side chain is essential for optimal binding. L-Arginine and L-glutamine are poor inhibitors vs L-lysine, and L-asparagine causes no inhibition at 50 mM, indicating that the amino acid substrate binding site is hydrophobic, in agreement with previous results (*138*).

The inhibition constants for aliphatic amino acids, L-valine, L-isoleucine, L-methionine, L-norvaline, and L-leucine, as competitive inhibitors against L-lysine at pH 7.0, are increased by at least 2-fold compared to the value at pH 6.0, consistent with the previously reported pH dependence of the pK_i for leucine, which binds optimally at pH values below 6.0 (*138*). The pH dependence reflects a close proximity of the leucine

hydrophobic side chain to an enzyme carboxylate. Hydrophobic amino acids with a linear 3 or 4 carbon side chain are good inhibitors.

L-Leucine binds to the amino acid binding site with a higher affinity than the natural substrate L-lysine, suggesting the binding pocket can accommodate a branch at the γ-carbon. Consistent with this idea, L-methionine, with a large S atom substituent at δ-carbon, has the same binding affinity as L-lysine. However, a branch at the β-carbon, as is present in L-valine and L-isoleucine, increases the inhibition constant dramatically, indicating a tighter binding site at the C1 and C2 positions.

4.3.4 Double Inhibition Studies

In the direction of saccharopine formation, the double-inhibition pattern obtained with OG and ornithine is shown in Fig. 3.17. The inhibition by ornithine alone is observed as the line at zero OG, reflecting the E:NADH:ornithine complex, while the inhibition by OG alone (ordinate) reflects the E:NADH:OG complex. The slope effect indicates the enhancement of inhibition as a result of synergism of binding between OG and ornithine. A value of 0.7 obtained for α suggests a 1.4-fold increase in the affinity of OG in the presence of ornithine, compared to its absence. Since OG and ornithine are competitive inhibitors of α-Kg and lysine, respectively, the observed synergism of binding between OG and ornithine suggests a slight synergism of binding between α-Kg and lysine. However, when concentration was increased, OG began to compete with ornithine for the lysine binding site (data not shown), consistent with the proposed kinetic mechanism (*124*). In contrast, results obtained with pyridine 2,4-dicarboxylic acid and ornithine double inhibition gives a value of 2.4 for α, suggesting antagonism of binding. The difference in the double-inhibition patterns of OG and pyridine 2,4-dicarboxylic acid

is due to difference in structure of the bulky pyridine and the optimally bound OG. The bulky aromatic ring of pyridine 2,4-dicarboxylic acid likely interferes with the binding of ornithine, while in the case of OG, structurally very similar to α-Kg, a better indication of the interaction of α-Kg and lysine is obtained.

4.4 Conclusion

4.4.1 Kinetic Mechanism

Kinetic data have been measured for SDH from *S. cerevisiae*, suggesting the ordered addition of NAD followed by saccharopine in the physiologic reaction direction. In the opposite direction, NADH adds to the enzyme first, while there is no preference for the order of binding of α-Kg and lysine. In the direction of saccharopine formation, data also suggest that, at high concentrations, lysine inhibits the reaction by binding to free enzyme. In addition, uncompetitive substrate inhibition by α-Kg and double inhibition by NAD and α-Kg suggest the existence of an abortive E:NAD:α-Kg complex. Product inhibition by saccharopine is uncompetitive vs NADH, suggesting a practical irreversibility of the reaction at pH 7.0 in agreement with the overall K_{eq}. Saccharopine is noncompetitive vs lysine or α-Kg, suggesting the existence of both E:NADH:Sacc and E:NAD:Sacc complexes. NAD is competitive vs NADH, and noncompetitive vs lysine and α-Kg, indicating the combination of the dinucleotides with free enzyme. Dead-end inhibition studies are also consistent with the random addition of α-Kg and lysine. Leucine and oxalylglycine serve as lysine and α-Kg dead-end analogues, respectively, and are uncompetitive against NADH and noncompetitive against α-Kg and lysine, respectively. OAA, pyruvate, and glutarate, behave as dead-end analogue of lysine,

which suggests that the lysine-binding site has a higher affinity for keto acid analogues than does the α-Kg site or that dicarboxylic acids have more than one binding mode on the enzyme. In addition, OAA and glutarate also bind to free enzyme as does lysine at high concentration. Glutarate gives S-parabolic noncompetitive inhibition vs NADH, indicating the formation of a E:(glutarate)$_2$ complex as a result of occupying both the lysine- and α-Kg-binding sites. Pyruvate, a slow alternative keto acid substrate, exhibits competitive inhibition vs both lysine and α-Kg, suggesting the combination to the E:NADH:α-Kg and E:NADH:lysine enzyme forms. The equilibrium constant for the reaction has been measured at pH 7.0 as 3.9 x 10^{-7} M by monitoring the change in NADH upon the addition of the enzyme. The Haldane relationship is in very good agreement with the directly measured value.

4.4.2 Chemical Mechanism

The proton shuttle chemical mechanism is proposed on the basis of the pH dependence of kinetic parameters, dissociation constants for competitive inhibitors, and isotope effects. In the direction of lysine formation, once NAD and saccharopine bind, a group with a pK_a of 6.2 accepts a proton from the secondary amine of saccharopine as it is oxidized. This protonated general base then does not participate in the reaction again until lysine is formed at the completion of the reaction. A general base with a pK_a of 7.2 accepts a proton from H_2O as it attacks the Schiff base carbon of saccharopine to form the carbinolamine intermediate. The same residue then serves as a general acid and donates a proton to the carbinolamine nitrogen to give the protonated carbinolamine. Collapse of carbinolamine is then facilitated by the same group accepting a proton from the carbinolamine hydroxyl to generate α-Kg and lysine. The amine nitrogen is then

protonated by the group that originally accepted a proton from the secondary amine of saccharopine, and products are released. In the reverse reaction direction, finite primary deuterium kinetic isotope effects were observed for all parameters with the exception of V_2/K_{NADH}, consistent with a steady-state random mechanism and indicative of a contribution from hydride transfer to rate limitation. The pH dependence, as determined from the primary isotope effect on ${}^{D}V_2$ and ${}^{D}(V_2/K_{Lys})$, suggests that a step other than hydride transfer becomes rate-limiting as the pH is increased. This step is likely protonation/deprotonation of the carbinolamine nitrogen formed as an intermediate in imine hydrolysis. The observed solvent isotope effect indicates that proton transfer also contributes to rate limitation. A concerted proton and hydride transfer is suggested by multiple substrate/solvent isotope effect, as well as a proton transfer in another step, likely hydrolysis of the carbinolamine. In agreement, dome-shaped proton inventories are observed for V_2 and V_2/K_{Lys}, suggesting that proton transfer exists in at least two sequential transition states.

4.4.3 Substrate Specificity and Binding Pockets

Saccharopine dehydrogenase is the only enzyme in the α-aminoadipate pathway for lysine biosynthesis in fungi for which mechanistic data have been obtained and for which a structure has recently been determined (Albert M. Berghuis, personal communication). This allows an elucidation of the molecular basis for the specificity of SDH for all of its substrates. A survey of NADH, α-Kg, and lysine analogues has been undertaken to define the geometry of the active site and to identify functional groups on all three substrates important for substrate binding. The following can be concluded.

1. The majority of the binding energy of dinucleotides comes from the AMP portion of the molecule.

2. Distinctly different conformations are generated upon binding of the oxidized and reduced dinucleotides, and upon binding of NADH or NADPH.

3. The binding pocket for the nicotinamide ring is largely hydrophilic.

4. A side chain with 3 carbons (from the α-keto group up to and including the side chain carboxylate), with 2 carbons between the C1-C2 unit and the C5 carboxylate is optimal for binding of α-keto acids; the α-oxo group contributes a factor of 10 in affinity.

5. The keto acid binding pocket is relatively large and flexible, and can accommodate the bulky aromatic ring of pyridine dicarboxylic acid and a negative charge at the C3 but not the C4 position.

6. The amino acid substrate binding pocket is hydrophobic, and the optimal length of the hydrophobic portion of the amino acid side chain is 3 or 4 carbons.

7. The amino acid binding pocket can accommodate a branch at the γ-carbon, but not at the β-carbon.

Appendices

APPENDIX I

Multiple Sequence Alignments

CLUSTAL W multiple sequence alignment of saccharopine dehydrogenases (SDH) and alanine dehydrogenases (ADH) (6.5 % identity and 10.6 % similarity)

```
                          10        20        30        40        50        60
                           |         |         |         |         |         |
(SDH)Scerevis --------------MAAVTLHLRAETKPLEARAALTPTTVKKLIAKGFKIYVED--SPQ
(SDH)Calbican -------------MSKSPVILHLRAETKPLEARAALTPSTTKQLLDAGFEIYVEE--SSQ
(SDH)Ylipolyt --------------MTAPVKLHLRAETKPLEHRSALTPTTTRKLLDAGFEVFVEK--SPL
(SDH)Cneoform MAATAPESATTSANTRPRQPIWLRCEKKPFEHRSALTPTTAKTLLDSNFDVYVEK--DPQ
(SDH)Spombe   ---------------MVAPHLWLRAETKPLEERSALTPRTAKILADAGFQITIER--SSQ
(SDH)Afumigat ---------------MSSNKIWLRAETKPAEARSALTPTTCKALMDAGYEVTVER--SRQ
(ADH)Plapideu ------------------MEIGVPKEIKNQEFRVGLSPSSVRTLVEAGHTVFIETQAGIG
(ADH)Bsubtili ------------------MIIGVPKEIKNNENRVALTPGGVSQLISNGHRVLVETGAGLG
                                  : :  * *  * * .*:*     *   .. : :*   .
Prim.cons.    MAATAPESATTSA23M22V222LRAETKPLEARSALTPTTVK3LLDAGFEVYVE32ASPQ

                          70        80        90       100       110       120
                           |         |         |         |         |         |
(SDH)Scerevis STFNINEYRQAGAIIVPAGSWKT-APRDRIIIGLKEMPETDTFPLVHEHIQFAHCYKDQA
(SDH)Calbican STFDIKEYEAVGAKIVPEGSWKT-APKERIIFGLKELPENETFPLIHEHIQFAHCYKDQA
(SDH)Ylipolyt RIFDDQEFVDVGATLVEEGSWVS-APEDRMIIGLKELPE-ESFPLSHEHIQFAHCYKDQG
(SDH)Cneoform RIFDDREFEAVGCKIVPHNTWPS-APVDVPIIGLKELPE-STDPLPHTHIQFAHCYKQQA
(SDH)Spombe   RAFKDKEFERLGFPMVPEGSWRH-APKDAYIIGLKELPENDNSPLKHTHIQFAHCYKNQE
(SDH)Afumigat RIFD---VVQIGAPLVEEGSWVKDAPKDAYILGLKELPE-DDFPLEHVHISFAHCYKQQA
(ADH)Plapideu AGFADQDYVQAGAQVVPSAKDAW--SR-EMVVKVKEPLPAEYDLMQKDQLLFT--YLHLA
(ADH)Bsubtili SGFENEAYESAGAEIIADPKQVW--DA-EMVMKVKEPLPEEYVYFRKGLVLFT--YLHLA
                *        *  ::   .          :. :**    .   : :  : *:  * .
Prim.cons.    RIFDD2EYEQ2GA2IVPEGSWV3DAPKDRMIIGLKELPENETFPL8HEHIQFAHCYKDQA

                         130       140       150       160       170       180
                           |         |         |         |         |         |
(SDH)Scerevis GWQNVLMRFIKGHGTLYDLEFLEN-DQGRRVAAFGFYAGFAGAALGVRDWAFKQTHSDDE
(SDH)Calbican GWQDVLKRFPQGNGILYDLEFLEN-DQGRRVAAFGFYAGFAGAAIGVLDWSFKQLNGNTK
(SDH)Ylipolyt GWKDVLSRFPAGNGTLYDLEFLED-DNGRRVAAFGFHAGFAGAAIGVETWAFQQTHPDSE
(SDH)Cneoform GWNDVLRRFAQGKGTLYDLEFLEDPVSHRRVAAFGFHAGFAGAAAGALAFAAQQTQNGQG
(SDH)Spombe   GWREVLSRFPAGNGLLYDLEFLQD-DNGRRVAAFGYHAGFAGSAISCLVWAHQLLHPNKQ
(SDH)Afumigat GWEKVLSRWPRGGGTLLDLEFLTD-ETGRRVAAFGYSAGYAGSALAIKNWAWQLTHPEGE
(ADH)Plapideu AARELTEQLMRVG--LTAIAYETVELPNRSLPLLTPMSIIAGRLSVQFGARFLERQQGGR
(ADH)Bsubtili AEPELAQALKDKG--VTAIAYETVSE-GRTLPLLTPMSEVAGRMAAQIGAQFLEKPKGGK
              .  .:          :  : :       * :. :   :  **
Prim.cons.    GW22VLSRFP3G2GTLYDLEFLED3D2GRRVAAFGFHAGFAGAAIGVL2WAFQQTHPGGE

                         190       200       210       220       230       240
                           |         |         |         |         |         |
(SDH)Scerevis ---------DLPAVSPYPNEKALVKDVTKDYKEALAT-GARKPTVLIIGALGRCGSGAID
(SDH)Calbican GTKGEGEGGELPGVTPYPNENELIKDVKIELEKALTKNGGQYPKCLVIGALGRCGSGAID
(SDH)Ylipolyt ---------NLPGVSAYPNETELVDKIKKDLAAAVEK-GSKLPTVLVIGALGRCGSGAID
(SDH)Cneoform ---------KLGELKPYPNEGEMVKEVSEALQGTKEG--NKGVKVLIIGALGRCGSGAVD
(SDH)Spombe   ----------FPAIRPFPNEKSLVRHVARQVRLALKKNNNQYPRILVIGALGRCGTGACD
(SDH)Afumigat ---------PLPGETPYANQDLLIESVKESLESGKKLS-GRPPKVLVIGALGRCGKGAVQ
(ADH)Plapideu G-------VLLGGVPGVKPGKVVILGGGVVGTEAAKMAVGLGAQVQIFDIN--VER----
```

```
(ADH)Bsubtili G-------ILLAGVPGVSRGKVTIIGGGVVGTNAAKMAVGLGADVTIIDLN--ADR----
                       :           :                        ::.
Prim.cons.    GTKGEGEG3LLPGV3PYPNEKEL2K2VK32L2EALKK2GG4GPKVL2IGALGRCGSGAID

                      250       260       270       280       290       300
                       |         |         |         |         |         |
(SDH)Scerevis LLHKVGIPDANILKWDIKETSRGGPFDEIPQ-ADIFINCIYLSKPIAPFTNMEKLNNP--
(SDH)Calbican LFKKIGIPDDNIAKWDMAETAKGGPFQEIVD-SDIFINCIYLSKPIPPFINKEILNNE--
(SDH)Ylipolyt LARKVGIPEENIIRWDMNETKKGGPFQEIAD-ADIFINCIYLSQPIPPFINYDLLNKE--
(SDH)Cneoform LFRKAGVAEENIIKWDMAETAKGGPFPEILD-VDIFVNCIYLSKPIPKFITSEFIAEAGA
(SDH)Spombe   LASKIGIPFDNILRWDINETKKGGPFTEITE-SDIFVNCIYLSMPIPKFCTVESLNVP--
(SDH)Afumigat LAKDVGIPESDIIQWDIEETKKGGPFREIVEDADIFINCIYLSAKIPPFVNTETLSSP--
(ADH)Plapideu -LSYLETLFGSRVELLYSNS-AE--IETAVAEADLLIGAVLVPGRRAPILVPASLVEQ--
(ADH)Bsubtili -LRQLDDIFGHQIKTLISNP-VN--IADAVAEADLLICAVLIPGAKAPTLVTEEMVKQ--
                      .    :.     :       *::: .: :.    .        :
Prim.cons.    L2RKVGIP23NIIKWDI3ETKKGGPFQEIVDEADIFINCIYLSKPIPPFINTESLN3PGA

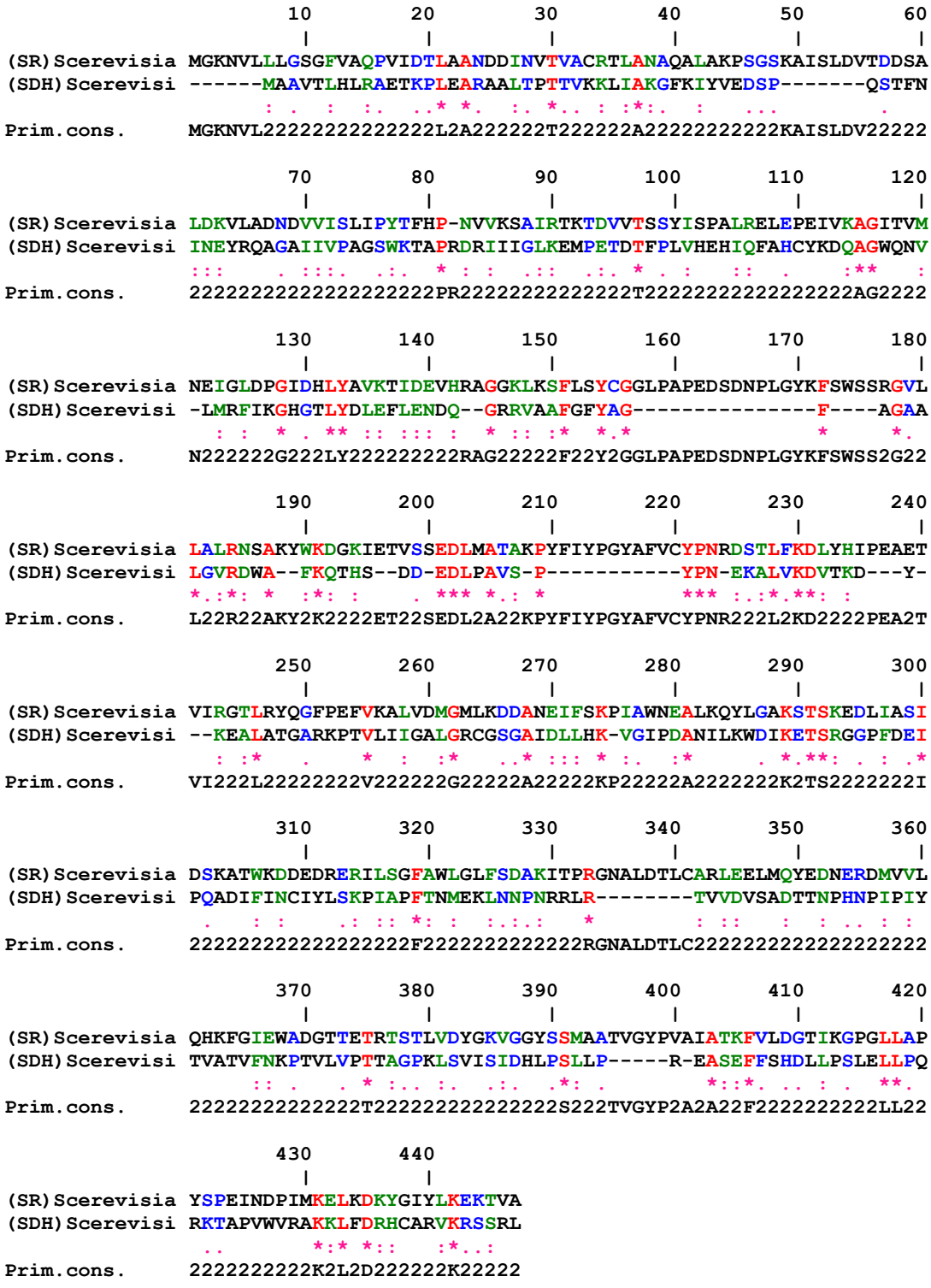
                      310       320       330       340       350       360
                       |         |         |         |         |         |
(SDH)Scerevis NRRLRTVVDVSADTTNPHNPIPIYTVATVFNKPTVLVPTT---AGPKLSVISIDHLPSLL
(SDH)Calbican NRKLTTIVDVSADTTNPHNPIPVYEIATVFNEPTVEVKLD---KGPKLSVCSIDHLPSLL
(SDH)Ylipolyt TRKLSVIVDVSADTTNPHNPVPVYTIATTFDHPTVPVETT---AGPKLSVCSIDHLPSLL
(SDH)Cneoform DRRLSVVVDVSCDTTNPHNPIPIYSINTTFPSPTVEVDTKG--VGKRCTVISIDHLPTLL
(SDH)Spombe   NRKLRVVCDVSCDTTNPNNPIPIYNVNTTFDHPTVEVKGVT--TPPPLEVISIDHLPTLL
(SDH)Afumigat NRRLSVICDVSADTTNPNNPIPVYSITTTFDKPTVTVPLPELAQGPPLSVISIDHLPSLL
(ADH)Plapideu MRTGSVIVDVAVDQ---GGCVETL-HPTSHTQPTYEVFGV--------VHYGVPNMPGAV
(ADH)Bsubtili MKPGSVIVDVAIDQ---GGIVETVDHITTHDQPTYEKHGV--------VHYAVANMPGAV
               :   .: **: *     . :      * .  **                .: ::*  :
Prim.cons.    NR2LSVIVDVSADTTNPHNPIP2Y2IATTFD3PTVEV22V3LAAGPKLSVISIDHLPSLL

                      370       380       390       400       410       420
                       |         |         |         |         |         |
(SDH)Scerevis PREASEFFSHDLLPSLELLPQRKTAPVWVRAKKLFDRHCARVKRSSRL------------
(SDH)Calbican PREASEFFAKDLMPSLLELPNRDTSPVWVRAKQLFDKHVARLDKE---------------
(SDH)Ylipolyt PREASEAFSEALLPSLLQLPQRDTAPVWTRAKALFDKHVLRIGE----------------
(SDH)Cneoform PREASEQFSTDLLPSLLQLPERQTAEVWVNAEKLFRTKLEEARKYDEEQGIKA-------
(SDH)Spombe   PRESSEAFSEALIPSLLALKDVDNAPVWVRAKKLYETMVQKL-----------------
(SDH)Afumigat PRESSEMFSEALLPSLLQLKDRKNARVWKQAEDLFNEKVATLPESMRA------------
(ADH)Plapideu PWTATQALNNSTLPYVVKLANQG-LKALETDDALAKGLNVQAHRLVHPAVQ---------
(ADH)Bsubtili PRTSTIALTNVTVPYALQIANKGAVKALADNTALRAGLNTANGHVTYEAVARDLGYEYVP
              *  ::  :    :*    : :     .     *
Prim.cons.    PREASEAFSE2LLPSLLQLPNRDTAPVWVRAK2LFD3HVARLG3S5REAV322LGYEYVP

                      430
                       |
(SDH)Scerevis --------------
(SDH)Calbican --------------
(SDH)Ylipolyt --------------
(SDH)Cneoform --------------
(SDH)Spombe   --------------
(SDH)Afumigat --------------
(ADH)Plapideu --QVFPDLA-----
(ADH)Bsubtili AEKALQDESSVAGA

Prim.cons.    AE2222D22SVAGA
```

Sequence alignment of saccharopine reductase (SR) and saccharopine dehydrogenase (SDH) (12 % identity and 20 % similarity)



Sequence alignment of α-aminoadipate semialdehyde synthetase (AASS) N-terminus from human and SDH from *S. cerevisiae* (19 % identity and 18 % similarity)

```
                    10        20        30        40        50        60
                     |         |         |         |         |         |
AASSHum      MLQVHRTGLGRLGVSLSKGLHHKAVLAVRREDVNAWERRAPLAPKHIKGITNLGYKVLIQ
SDHScer      --------------------MAAVTLHLRAETKPLEARAALTPTTVKKLIAKGFKIYVE
                                  **    * :.:. * **.*:*. :* :   *:*: ::
Prim.cons.   MLQVHRTGLGRLGVSLSKGLH22AV2222R222222E2RA2L2P222K22222G2K2222

                    70        80        90       100       110       120
                     |         |         |         |         |         |
AASSHum      PSNRRAIHDKDYVKAGGILQED-----ISEACLILGVKRPPE-EKLMSRKTYAFFSHTIK
SDHScer      DSPQSTFNINEYRQAGAIIVPAGSWKTAPRDRIIIGLKEMPETDTFPLVHEHIQFAHCYK
              * : ::: ::* :**.*:          ..  :*:*:*. ** :.:   : :  *:*  *
Prim.cons.   2S222222222Y22AG2I2222GSWKT222222I2G2K22PET22222222222F2H22K

                   130       140       150       160       170       180
                     |         |         |         |         |         |
AASSHum      AQEANMGLLDEILKQEIRLIDYEKMVDHRGVRVVAFGQWAGVAGMINILHGMGLRLLALG
SDHScer      DQAGWQNVLMRFIKGHGTLYDLEFLENDQGRRVAAFGFYAGFAGAA--LG---VRDWAFK
              * .  .:* .::* .  * * * : :.:* **.*** :**.**    *    :*  *:
Prim.cons.   2Q222222L2222K2222L2D2E222222G2RV2AFG22AG2AG22NIL2GMG2R22A22

                   190       200       210       220       230       240
                     |         |         |         |         |         |
AASSHum      -HHTPFMHIGMAHNYRNSSQAVQAVRDAGYEISLGLMPKSIGPLTFVFTGTGNVSKGAQA
SDHScer      QTHSDDEDLPAVSPYPNEK---ALVKDVTKDYKEALATGARKPTVLIIGALGRCGSGAID
               *:   .:  .  * *..     *:*.  : . .* . :  * .::: . *. ..**
Prim.cons.   Q2H22222222222Y2N22QAV22V2D22222222L222222P22222222G2222GA22

                   250       260       270       280       290       300
                     |         |         |         |         |         |
AASSHum      IFN--ELPCEYVEPHELKEVSQTGDLRKVYGTVLSRHHHLVRKTDAVYDPAEYDKHPERY
SDHScer      LLHKVGIPDANILKWDIKETSRGGPFDEIPQADIFINCIYLSKPIAPFTNMEKLNNPNRR
             :::   :*   :   ::**.*: * : ::  : :  :   : *. * :   *  ::*:*
Prim.cons.   222KV22P222222222KE2S22G22222222222222222K22A22222E2222P2R2

                   310       320       330       340       350       360
                     |         |         |         |         |         |
AASSHum      ISRFNTDIAPYTTCLINGIYWEQNTPRLLTRQDAQSLLAPGKFSPAGVEGCPALPHKLVA
SDHScer      LR-------------------------------------------------------TVVD
             :                                                        .:*
Prim.cons.   22RFNTDIAPYTTCLINGIYWEQNTPRLLTRQDAQSLLAPGKFSPAGVEGCPALPH22V2

                   370       380       390       400       410       420
                     |         |         |         |         |         |
AASSHum      ICDISADTGGSIEFMTECTTIEHPFCMYDADQHIIHDSVEGSGILMCSIDNLPAQLPIEA
SDHScer      VSADTTNPHNPIPIYTVATVFNKP-------TVLVPTTV-GPKLSVISIDHLPSLLPREA
             :.  :::. ..* : * .*.:::*         ::  :* *. : : ***:**: ** **
Prim.cons.   2222222222I222T22T2222PFCMYDAD2222222VEG222222SID2LP22LP2EA

                   430       440       450       460       470
                     |         |         |         |         |
AASSHum      TECFGDMLYPYVEEMILSDATQPLESQNFSPVVRDAVITSNGTLPDKYKYIQTLRESRE
SDHScer      SEFFSHDLLPSLELLPQRKTAP--------VWVR------AKKLFDR-HCARVKRSSRL
             :* *.. * * :* :   .::           **        .* *: :  :. *.**
Prim.cons.   2E2F222L2P22E222222222PLESQNFS22VRDAVITS222L2D2Y222222R2SR2
```

Sequence alignment of α-aminoadipate semialdehyde synthetase (AASS) C-terminus from human and SR from *S. cerevisiae* (39 % identity and 26 % similarity)

```
                    10        20        30        40        50        60
                     |         |         |         |         |         |
AASSHum       MGTRRKVLVLGSGYISEPVLEYLSRDGNIEITVGSDMKNQIEQLGKKYNINPVSMDICKQ
SRScere       MG--KNVLLLGSGFVAQPVIDTLAANDDINVTVACRTLANAQALAKPSGSKAISLDVT-D
              **  ::**:****:::::**:: *: :.:*::**..     : : *.*  . :.:*:*:  :
Prim.cons.    MGTR22VL2LGSG2222PV222L22222I22TV2222222222L2K2222222S2D22K2

                    70        80        90       100       110       120
                     |         |         |         |         |         |
AASSHum       EEKLGFLVAKQDLVISLLPYVLHPLVAKACITNKVNMVTASYITPALKELEKSVEDAGIT
SRScere       DSALDKVLADNDVVISLIPYTFHPNVVKSAIRTKTDVVTSSYISPALRELEPEIVKAGIT
              :. *. ::*.:*:****:**.:** *.*:.* .*.::**:***:***:*** .: .****
Prim.cons.    222L2222A22D2VISL2PY22HP2V2K22I22K222VT2SYI2PAL2ELE22222AGIT

                   130       140       150       160       170       180
                     |         |         |         |         |         |
AASSHum       IIGELGLDPGLDHMLAMETIDKAKEVGATIESYISYCGGLPAPEHSNNPLRYKFSWSPVG
SRScere       VMNEIGLDPGIDHLYAVKTIDEVHRAGGKLKSFLSYCGGLPAPEDSDNPLGYKFSWSSRG
              ::.*:*****:**: *:***:.:..*..::*::**********.*:*** ******. *
Prim.cons.    222E2GLDPG2DH22A22TID22222G2222S22SYCGGLPAPE2S2NPL2YKFSWS22G

                   190       200       210       220       230       240
                     |         |         |         |         |         |
AASSHum       VLMNVMQSATYLLDGKVVNVAGGISFLDAVTSMDFFPGLNLEGYPNRDSTKYAEIYGISS
SRScere       VLLALRNSAKYWKDGKIETVSS-EDLMATAKPYFIYPGYAFVCYPNRDSTLFKDLYHIPE
              **: : :**.*  ***: .*:.  .:: :...  ::**  :  ******* : ::* *..
Prim.cons.    VL22222SA2Y22DGK222V22G2222222222222PG22222YPNRDST22222Y2I22

                   250       260       270       280       290       300
                     |         |         |         |         |         |
AASSHum       AHTLLRGTLRYKGYMKALNGFVKLGLINREALPAFRPEANPLTWKQLLCDLVGISPSSEH
SRScere       AETVIRGTLRYQGFPEFVKALVDMGMLKDDANEIFS---KPIAWNEALKQYLGAKSTSKE
              *.*::******:*: : ::.:*.:*::: :*   *    :*::*:: * : :* ..:*:.
Prim.cons.    A2T22RGTLRY2G22222222V22G22222A222F2PEA2P22W222L2222G2222S22

                   310       320       330       340       350       360
                     |         |         |         |         |         |
AASSHum       DVLK----EAVLKKLGGDNTQLEAAEWLGLLGDEQVPQAESILDALSKHLVMKLSYGPEE
SRScere       DLIASIDSKATWKDDEDRERILSGFAWLGLFSDAKITPRGNALDTLCARLEELMQYEDNE
              *::     :*. *.  . :  *..  ****:.* ::.   . **:*. :*   :.*  :*
Prim.cons.    D222SIDS2A22K22222222L2222WLGL22D222222222LD2L222L22222Y222E

                   370       380       390       400       410       420
                     |         |         |         |         |         |
AASSHum       KDMIVMRDSFGIRHPSGHLEHKTIDLVAYGDINGFSAMAKTVGLPTAMAAKMLLDGEIGA
SRScere       RDMVVLQHKFGIEWADGTTETRTSTLVDYGKVGGYSSMAATVGYPVAIATKFVLDGTIKG
              :**:*::..***. ..*  * :*  ** **.:.*:*:** *** *.*:*:*::*** * .
Prim.cons.    2DM2V2222FGI2222G22E22T22LV2YG222G2S2MA2TVG2P2A2A2K22LDG2I22

                   430       440       450
                     |         |         |
AASSHum       KGLMGPFSKEIYGPILERIKAEGIIYTTQSTIKP
SRScere       PGLLAPYSPEINDPIMKELKDKYGIYLKEKTVA-
               **:.*:* ** .**::.:* :  ** .:.*:
Prim.cons.    2GL22P2S2EI22PI2222K2222IY2222T22P
```

ClustalW at NPS@ (**N**etwork **P**rotein **S**equence **A**nalysis) from Pole Bioinformatique Lyonnais, France was used to perform multiple sequence alignments of

SDH and Ala, SDH and SR, respectively. Results suggest that the residues involved in the substrate binding site and/or active site of ADH from *P. lapideum* (Lys10, Lys74, Glu13, Arg15, His95, Glu117, and Asp269) are all highly conserved in SDH among different organisms. However, SR shares very little sequence similarity with SDH at the amino acid level.

Family and Domain searches were carried out using the InterPro tool from EMBL-EBI (**E**uropean **M**olecular **B**iology **L**aboratories – **E**uropean **B**ioinformatic **I**nstitute) and Superfamily program (version 1.69) from HMM (**H**idden **M**arkov **M**odels) library and genome assignment server. SDH belongs to the Alanine Dehydrogenase and Pyridine Nucleotide Transhydrogenase family (IPR 008141). It contains Alanine dehydrogenase/PNT, C-terminal domain (IPR 007698) and Alanine dehydrogenase/PNT, N-terminal domain (IPR 007886). It also contain a NAD(P)-binding Rossmann-fold domain (SSF 51735), and a Formate/glycerate dehydrogenase catalytic domain-like (SSF 52283). By comparison, SR belongs to the Saccharopine Dehydrogenase family (IPR 005097), and this family is comprised of three structural domains that can not be separated in the linear sequence.

In aminals including humans, interestingly, the AASS, a bi-functional enzyme, catalyzes both SR and SDH reactions. The sequence alignment of the N-terminus of AASS and SDH, and the C-terminus of AASS and SR has been carried out, respectively. The residues involved in the substrate binding site and/or active site of SDH (Lys13, Glu16, Arg18, Lys77, His96, Glu122, Arg131, Asp319, and His320), and in the substrate binding sites of SR (Trp173, Pro126, Arg246, Arg223, and Ser98) are highly conserved in AASS N- and C- terminus, respectively.

APPENDIX II

Pre-steady-state Kinetic, Physical, and Spectral Properties of SDH

II.1 INTRODUCTION

In addition to the studies carried out on SDH and presented in the main body of this dissertation, studies included in this Appendix were also carried out. In all cases the studies are preliminary. However, each of the studies represents a viable line of research that can be followed up in the future. Methods are first presented followed by presentation of data and interpretation. It should be noted that none of the following individual projects in this Appendix is in the shape for publication.

II.2 MATERIALS AND METHODS

II.2.1 Pre-Steady-State Study of SDH by Stopped-Flow Kinetic Experiment

Pre-steady-state kinetic measurements were carried out using a temperature-controlled OLIS-RSM 1000 stopped-flow spectrophotometer. Sample solutions were prepared in two syringes at the same pH with a final buffer concentration of 100 mM Hepes at pH 7.0. The first syringe contained 2 mL of 45 μM SDH, while the second syringe contained a 2 mL mixture of NAD and saccharopine at concentrations of 10 mM and 100 mM, respectively. Thus, after mixing, final concentrations were half of those given above. Data were obtained in the rapid-scanning mode, over the wavelength range 300-540 nm. A spectrum obtained by mixing ddH_2O in the first syringe and the reactant mixture in the second syringe was used as a baseline for the plus enzyme experiments.

Data Processing. The time course of data at 340 nm from the rapid kinetic experiment was fitted using eq II.1 for a sequential process A-B-C, monitoring B and C, respectively.

$$y = 1 + \left[1/(k_1 - k_2) \right] \left[k_2 e^{-k_1 t} - k_1 e^{-k_2 t} \right] \qquad \text{(II.1)}$$

In eq II.1, k_1 and k_2 are fist-order rate constants, t is time, and e is 2.718. Fits to the data using an equation that describes two parallel first-order reactions were poor as judged by the residuals and a comparison of the theoretical time course derived from the fitted estimates and the experimental.

II.2.2 Determination of the Oligomerization State of SDH by HPLC

The Beckman analytical HPLC system was used to estimate the native M.W. of SDH by size exclusion chromatography. A TSK G3000SW column with a *M*r fractionation range of 10-50 kDa was used. The running buffer (mobile phase) contained 100 mM KH_2PO_4 and 100 mM K_2SO_4 at pH 7.5. The flow rate was set to 0.75 mL/min. A 10 μL (2 mg/mL) sample of His-tagged SDH (44 kDa per monomer) was loaded onto the column and collected over a chromatogram time of 1 hr. The standards for molecular mass determination were blue dextran (BD, 2000 kDa), alcohol dehydrogenase from yeast (AlcDH, 150 kDa), bovine serum albumin (BSA, 66 kDa), and carbonic anhydrase from bovine erythrocytes (CA, 29 kDa). Samples of 20 uL of each were loaded at the following concentrations: 1, 1, 1, and 2 mg/mL, respectively. The retention time for BD, AlcDH, BSA, CA, and SDH is 11. 7, 16.8, 18.4, 22.1, and 20.7 min, respectively. Elution

was monitored at 280 nm. And data were analyzed by plotting logM.W. against retention time using the Excel program.

II.2.3 Substrate Binding Study of SDH by Isothermal Titration Calorimetry

Titrations were carried out with a Micro Calorimetry System from MicroCal, Inc. The enzyme prepared for ITC was dialyzed overnight against 100 mM Tris at pH 7.5. In order to match the pH and buffer concentration between the solutions in the stirred cell and the injection syringe, the dialysis buffer was used to make up the substrate solutions for the injection syringe. The stirred cell contained SDH at a typical concentration of about 0.12 mM (enzyme monomer). The injection syringe contained substrates at a concentration greater than 10 times their respective K_m depending on the experiment. If necessary, in addition to the enzyme, the stirred cell also contained a substrate at a concentration greater than 10 K_m. The concentrations of substrates used in each experiment are given in the legends. For all experiments, a total 21 injections of a 4 μL injection volume were made at 240 s intervals at 15 ºC. Blank titrations were done in the absence of the enzyme to correct for heats of dilution and mixing. The control titrations were subtracted from the experimental titrations prior to data analysis. The data were analyzed by the Origin software provided by MicroCal, Inc, and data were fitted to a single-site model.

II.2.4 Substrate Binding by Fluorescence Titration

Fluorescence spectra were recorded on a Shimadzu RF-5301 PC spectrofluorometer. The reaction temperature was maintained at 25 ºC by a cuvette holder using a circular water bath. A quartz cuvette with a 1 mL volume and 1 cm path length

was used to record the spectrum for both sample and blank. Excitation and emission slit widths were set to 3.0 nm, and emission was scanned from 300-550 nm with the excitation monochromator fixed at 298 nm so that only Trps were excited. Blank spectra contained all sample components with the exception of enzyme (360 μg/mL), and were subtracted from sample spectra. The spectra of free enzyme were measured at pH 7.0 using a final concentration of 100 mM Tris. The concentrations of each substrate were either maintained at their reported K_m values or at saturation ($10K_m$).

II.2.5 Secondary Structure Determination of SDH by Circular Dichroism

Circular dichroic spectra were measured at room temperature using an upgraded AVIV-62DS-CD spectrometer equipped with a circulating bath to maintain temperature constant at 25 ºC. Spectra were obtained in a 0.2 cm quartz cuvette with a sample volume of 0.5 mL. The SDH concentration was 50 μg/mL in 20 mM KH_2PO_4 at pH 7.0. The blank contained all the components with the exception of enzyme and was subtracted to obtain the corrected spectrum. The time constant and the bandwidth were maintained at 100 ms and 1 nm, respectively. The averaging and dwell time were set at 1 s. The spectra were recorded in the far-UV range (250-198 nm), at intervals of 1 nm. The sample was scanned three times and the average is shown.

II.3 RESULTS AND DISCUSSIONS

II.3.1 Pre-Steady-State Study of SDH

The rapid-scanning-stopped-flow kinetic experiment was carried out by pushing a 45 μM SDH against a reaction mixture containing 10 mM NAD and 100 mM saccharopine. A prominent burst is the observed at the beginning of the progress curve,

Fig. II.1. The calculated burst rate is 8.8 ± 1.0 s^{-1}, the calculated steady-state rate is 0.8 ± 0.1 s^{-1}, and the calculated burst amplitude is about 30% maximum amplitude.

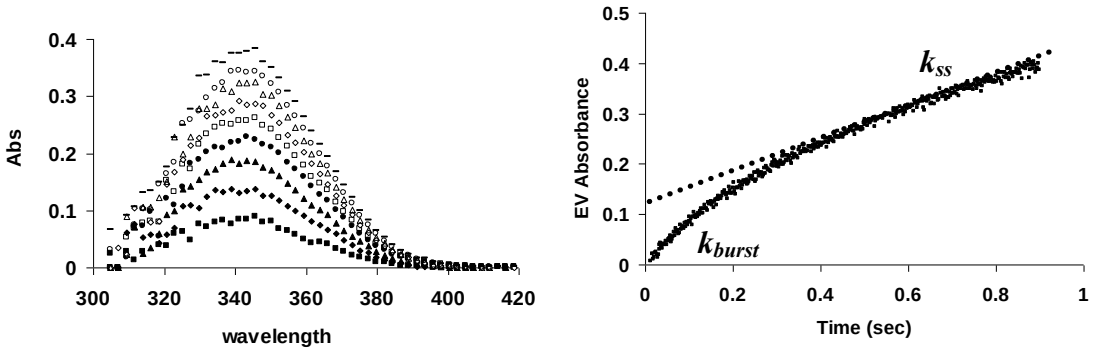


Figure II.1: Spectra from rapid-scanning-stopped-flow kinetic experiments. (A) Rapid scanning spectra of SDH. (B) Time course for the SDH reaction with NAD and saccharopine monitored at 340 nm. The final concentrations after dilution are as follows: enzyme, 22.5 μM; NAD, 5 mM; saccharopine, 50 mM. Solid curve is drawn through the experimental points generated from the fitted kinetic constants.

The burst observed in the stopped-flow experiment in the pre-steady-state time scale of SDH reaction indicates that a slow step occurs after the formation of NADH, the chromophoric substrate monitored. Results from the pH dependence of the primary isotope effect on $^{D}V_2$ and $^{D}(V_2/K_{Lys})$ suggest that a step other than hydride transfer becomes rate-limiting as the pH is increased, and this step is likely protonation/deprotonation of the carbinolamine nitrogen formed as an intermediate in imine hydrolysis (**Discussion 4.2.1.1.2**). Therefore, the pre-steady-state data are consistent with the isotope effect results. In addition, the calculated steady-state rate k_2 (k_{ss}, 0.8 s^{-1}) from pre-steady-state study is identical, within error, with the k_{cat} (1.1 s^{-1}) obtained from steady-state kinetic studies.

II.3.2 Size Exclusion Chromatography HPLC

On the basis of the elution profile of the standards, a standard curve was constructed and is shown in Fig. II.2. The equation for the standard curve is y = -5.3348x + 44.929. The retention time of the SDH is 20.7 min, allowing an estimation of a M.W. of 34,400 ± 4,800 Da. By comparison, the ProtParam tool from ExPASy (**E**xpert **P**rotein **A**nalysis **S**ystem) proteomics server of the Swiss Institute of Bioinformatics has been used to estimate the physical properties of SDH with and without His-tag, as shown in Table II.1. Data are consistent with the reported monomeric subunit estimation of SDH (*92*).

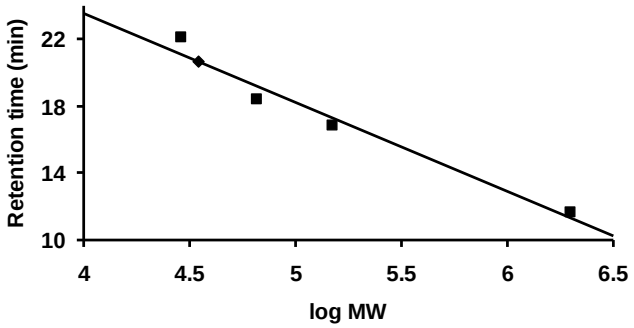


Figure II.2: HPLC elution profile. The position of standards for molecular mass determination is shown as ■, and from left to right, are carbonic anhydrase (29 kDa, 22.1 min), BSA (66 kDa, 18.4 min), alcohol dehydrogenase (150 kDa, 16.8 min), and blue dextran (2000 kDa, 11.7), respectively. SDH is shown as ♦.

Table II.1: Estimated Physical Properties of SDHs by ProtParam Tool.

	SDH	His-SDH
No. of amino acids	373	394
molecular weight	41464.8	43985.4
theoretical pI	9.18	9.18
extinction coefficient ($M^{-1}cm^{-1}$)	40210	40210

II.3.3 Substrate Binding by Isothermal Titration Calorimetry

The binding of substrates to SDH was examined by ITC, which allows an estimation of the equilibrium binding constant, enthalpy, and stoichiometry of binding if there is sufficient heat of binding. The ΔG of binding may be calculated using eq II.2, and the entropy of binding may be calculated using eq II.3.

$$\Delta G^{\circ} = -RT \ln K \qquad \text{(II.2)}$$

$$\Delta G^{\circ} = \Delta H^{\circ} - T\Delta S^{\circ} \qquad \text{(II.3)}$$

where *R* is the gas constant, *T* is the temperature, and *K* is the association constant.

Binding of NADH to SDH was detected by ITC, suggesting the existence of E:NADH complex. These data consistent with kinetic data, which indicate ordered binging of NADH prior to lysine and α-Kg (**Discussion 4.1.1**).The binding isotherm and the fitted data for binding of NADH to SDH is shown in Fig. II.3, A. The NADH titration was repeated twice with similar results. The data were fitted best to a model that specifies one set of sites, giving a stoichiometry (*N*) of 0.97, which refers to binding of one mole of ligand per mole of enzyme monomer. The obtained dissociation constant of NADH to SDH is 50 μM, in a good agreement with the kinetic value of 18 μM, determined from systematic initial velocity studies (**Discussion 4.1.4**). The fit also gave a ΔHº of -11.2 kcal/mol, and the free energy and entropy associated with the binding of NADH are -23.8 kcal/mol and 43 cal $mol^{-1}K^{-1}$, respectively. The errors on the fitted parameters mentioned above are all less than 10%.

Attempts to titrate SDH with α-Kg and NAD, respectively, gave no evidence of direct binding of these two substrates to SDH. A titration of enzyme with α-Kg in the

presence of saturating NADH, i.e. E:NADH gave no evidence of binding of α-Kg. The negative results may due to the high dissociation constants of substrate to enzyme. Additional experiments will be required as follow up.

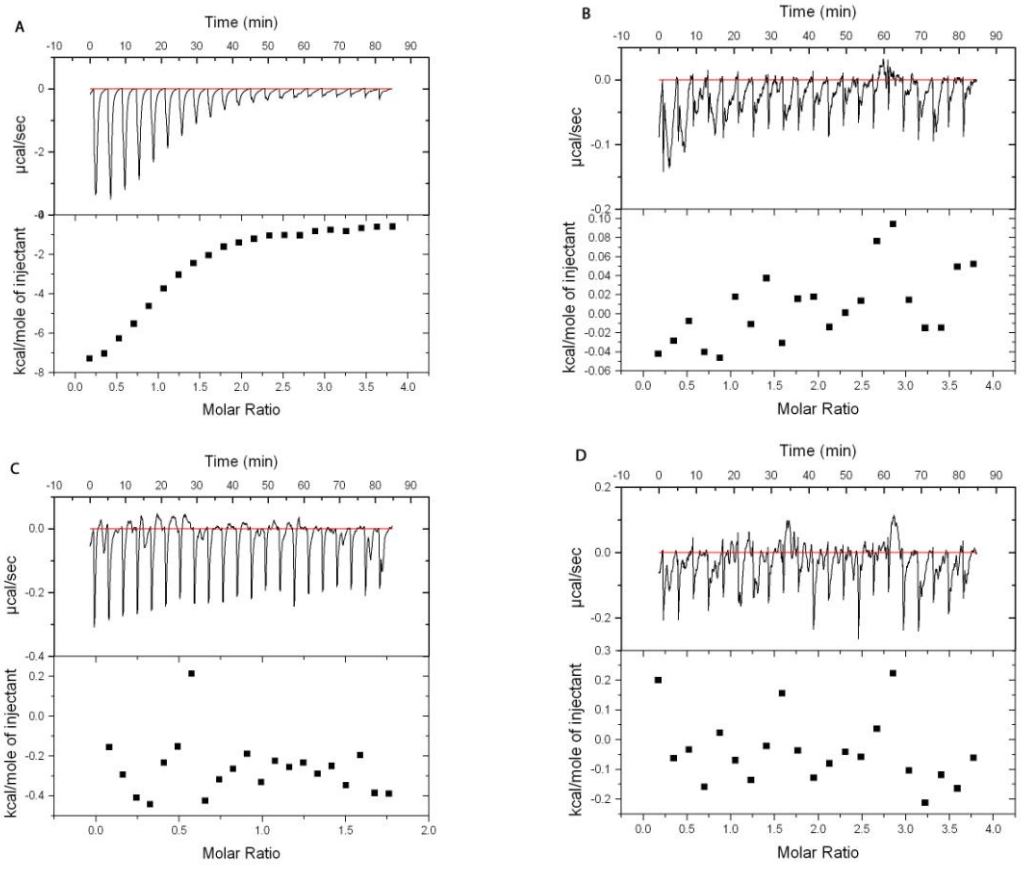


Figure II.3: Titrations of SDH with substrates. (A) Titration of SDH with NADH. The cell contained 0.12 mM SDH monomer in 100 mM Tris at pH 7.5. The syringe contained 7 mM NADH in the same buffer. (B) Titration of SDH with α-Kg. The cell contained 0.12 mM SDH monomer in 100 mM Tris at pH 7.5. The syringe contained 15 mM α-Kg in the same buffer. (C) Titration of SDH with NAD. The cell contained 0.12 mM SDH monomer in 100 mM Tris at pH 7.5. The syringe contained 7 mM NAD in the same buffer.(D) Titration of SDH:NADH complex with α-Kg. The cell contained 0.12 mM SDH monomer and 7 mM NADH in 100 mM Tris at pH 7.5. The syringe contained 7 mM NADH and 15 mM α-Kg in the same buffer. In all experiments, a total of 21 injections were made at 240 s intervals. Top panels are raw ITC data, while the bottom panels are data after the subtraction of the control titration and peak integration. The solid line is the fit to a one-site binding model.

II.3.4 Substrate Binding by Fluorescence Titration

The emission spectra of SDH did not change much, if at all, when either NADH, α-Kg, or NAD was added into SDH solution with a concentration of their respective reported K_m values (*1*), Fig. II.4 A-C. However, when concentration was increased about 10 times their respective K_m, a significant decrease in fluorescence signal at 335 nm was observed. In the case of lysine, signal did not change much at both limiting and saturating levels, Fig. II.4D. Since α-Kg and lysine do not absorb much at 298 nm, and the absorbance of 0.2 mM NADH and 2 mM NAD at 298 nm are 0.57 and 0.76, respectively, there is no significant interfilter effect in the fluorescence studies. Therefore, the decrease of fluorescence signal at 335 nm when the concentration of NADH, α-Kg, and NAD was increased, most likely due to a change on local environment around Trp residues as these substrates were added into enzyme solution. There are 5 Trps present in the primary amino acid sequence. Based on the apo-structure of SDH (unpublished data), Trp 104 is located on the top of the active site (a loop region) and solvent accessible. Trp 226 and Trp 353 are located on the surface of SDH and away from the active site, with the former in the nucleotide binding domain, and the latter in the catalytic domain. In addition, both Trp64 and Trp 151 are buried and away from the active site. Structural data suggest that Trp 104 might contribute the majority of the fluorescence signals, and Trp 226 and Trp 353 may also contribute due to the enzyme conformational change as substrate binds to the active site.

II.3.5 Secondary Structure Determination of SDH by Circular Dichroism

A sensitive physical method for estimating the secondary structural element of proteins is circular dichroism spectroscopy at wavelengths near the absorption band of the amide bond.

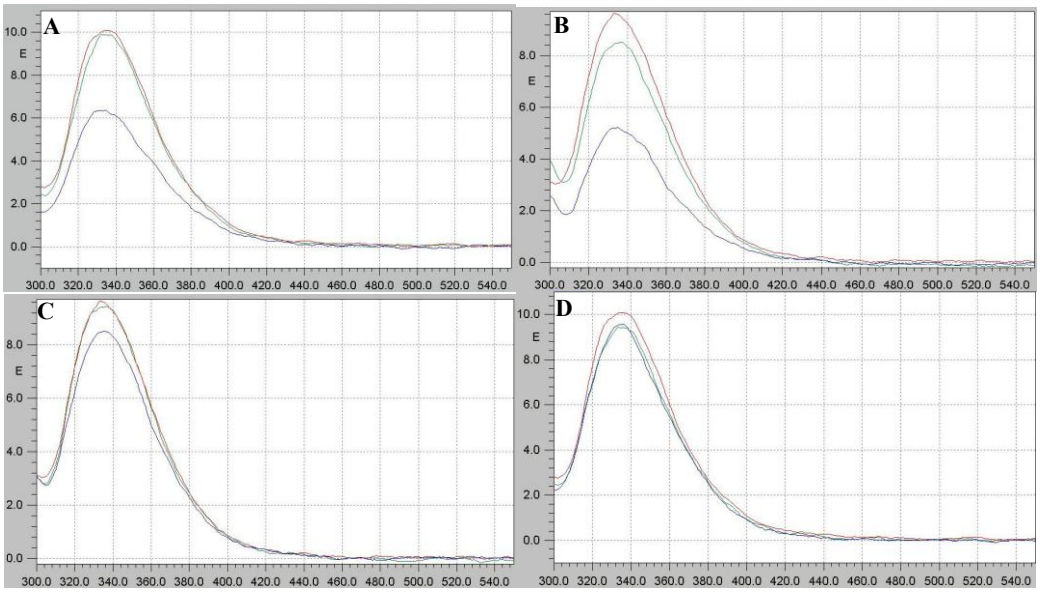


Figure II.4: Fluorescence emission spectra of SDH. Spectra were recorded with 360 μg/mL SDH in 100 mM Tris at pH 7.0, and corrected by subtracting blanks. (A) SDH only (red), SDH with 10 μM NADH (green), SDH with 0.2 mM NADH (blue) (B) SDH only (red), SDH with 50 μM NAD (green), SDH with 2 mM NAD (blue) (C) SDH only (red), SDH with 0.2 mM α-Kg (green), SDH with 5 mM α-Kg (blue) (D) SDH only (red), SDH with 1 mM lysine (green), SDH with 20 mM lysine (blue).

Because of the high dynode voltage at wavelengths below 210 nm, Hepes buffer was not used for CD studies. The CD spectrum of the His-tagged SDH was recorded in 20 mM KH_2PO_4 at pH 7.0 (Fig. II.5). As shown, the spectrum shows a strong negative ellipticity at 208 and 222 nm, suggesting both α-helical and β-sheet secondary structural components are present. The protein type seems to be α/β because the intensity of 208 nm

band is lower than that of 222 nm (*127*). The mean residue ellipticity [θ] was calculated from eq II.4 (*128*):

$$[\theta] = \frac{\theta^{\circ} MRW}{10lc} \qquad \text{(II.4)}$$

where [θ] is the molar ellipticity in degrees centimeter squared per decimole, θ° is the measured ellipticity angle recorded by the instrument in milidegrees at wavelength λ, the mean residue weight (*MRW*) is 111 from amino acid analysis, l is the optical path length of the cell in cm, c is the concentration of protein in mg/mL. The calculated $[\theta]_{208nm}$ and $[\theta]_{222nm}$ are -39600 and -41200 deg·cm^2/dmole, respectively.

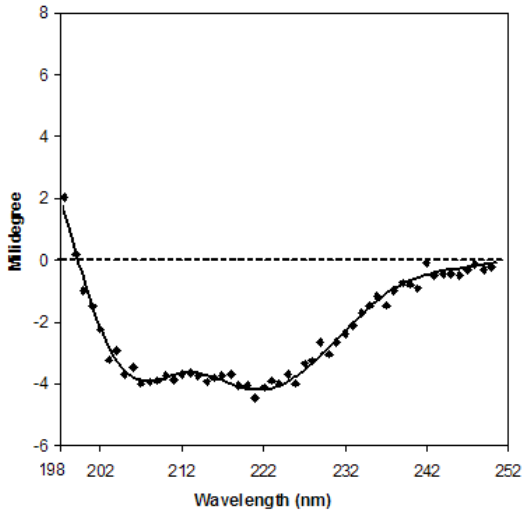


Figure II.5: Far-UV circular dichroism spectrum of SDH. Spectrum was recorded with 50 μg/mL SDH in 20 mM KH_2PO_4 at pH 7.0, and corrected by subtracting blank.

Based on $[\theta]_{222nm}$, percentage of α-helix of SDH has been estimated to be 19% using eq II.5 (*128*):

$$fraction\,\alpha - helix = \left(-[\theta]_{222nm} + 3000\right)/39000 \qquad \text{(II.5)}$$

However, results of secondary structure prediction using the PhD program from PredictProtein Server of EMBL-Heidelberg, Germany, suggests that SDH contains 36% α-helix, 17% β-sheet, and 47% coil structure, while the His-tagged SDH contains 37% α-helix, 16% β-sheet, and 47% coil structure. The precise information on secondary structure awaits the structural analysis of three dimensional structure of SDH.

APPENDIX III

Crystallization of SDH

III.1 INTRODUCTION

Structure is a powerful tool to study the mechanisms of enzymes. With a detailed three-dimensional structure in hand, SDH can be studied at a deeper level. Functions of different domains can be defined through the domain or motif search from the Protein Data Bank once SDH structure is obtained. It is also possible that a conformational change of SDH may occur upon substrate binding. Therefore, by comparing the crystal structures of apo and ligand-bound SDH, the substrate binding site(s) and/or enzyme active site can be defined. Furthermore, the structure will give a clue to which amino acid residues may be selected to perform site-directed mutagenesis to test the proposed chemical mechanism.

The first step and the first bottle-neck to solve SDH structures by X-ray crystallography is to obtain SDH crystals. The hanging drop vapor diffusion technique and the commercial sparse matrix screen from Hampton Research are commonly used to initiate protein crystallization trials. Once conditions are optimized and cryo-conditions are worked out, X-ray diffraction data can be collected and processed via either an in-house source or at the synchrotron. This chapter describes the crystallization of SDH, and preliminary X-ray diffraction analysis.

III.2 MATERIALS AND METHODS

III.2.1 Protein Sample Preparation

The purified SDH in 100 mM Hepes at pH 7.0 and 300 mM imidazole was dialyzed against 100 mM Tris at pH 7.0, and then concentrated to about 10 mg/mL using an Amicon ultrafiltration device with a YM 10 membrane. Purified SDH was judged to be monomeric in solution based on HPLC. The protein concentration was determined by the Bradford assay and UV absorbance at 280 nm using an ε of 40.2 $mM^{-1}cm^{-1}$. The sample was filter sterilized before crystallization trials.

III.2.2 Protein Crystallization

All crystallization experiments were performed at 4 ºC and 25 ºC using the hanging drop vapor diffusion method (*129*). Equal volumes (2 μL) of the reservoir and protein solution were mixed to form drops on the cover slides. The Hampton Research Crystal Screens I & II, designed using the sparse-matrix screening technique (*130*), were used to identify initial crystallization conditions. In order to obtain more preliminary crystallization conditions of SDH, the purified protein sample was shipped to the Hauptman-Woodward Institute (HWI) for screening of their 1536 conditions using the microbatch method under paraffin oil.

III.2.3 Characterization of Crystals

Crystals were soaked in a cryoprotectant solution containing mother liquor with 15 % glycerol for 5-10 min prior to mounting in a 100 K (Oxford Series 700 cryosystem) nitrogen stream. Diffraction data were collected at the Cu *Kα* wavelength (1.5418 Å) using a Rigaku/MSC RU-H3R rotating-anode X-ray generator operated at 50 kV/100 mA

with a R-Axis IV^{++} image-plate detector. The crystal to detector distances were set at 100 or 120 mm, and data were collected using an oscillation angle of 0.5° or 1°. The exposure times were set to 4 min per image. Diffraction data were indexed, integrated and scaled using the d*TREK® data processing package (version 9.2D) (*131*).

III.2.4 Ellman (DTNB) Assay

In order to estimate the number of accessible thiols in SDH, the enzyme was treated with 5,5'-dithiobis (2-nitrobenzoate) (DTNB). The product of TNB was monitored at 412 nm. Purified SDH was dialyzed against a solution containing 100 mM K_2HPO_4 at pH 7.3 and 1 mM EDTA. The DTNB stock solution (3 mM) was made up in 100 mM K_2HPO_4 buffer at pH 7.3. Spectra were recorded on a Beckman DU 640 UV/vis spectrophotometer, and blanked with the dialysis buffer. Temperature was maintained at 25 ºC using a Beckman temperature controller. Reactions were carried out in cuvettes with a path length of 1 cm in a final volume of 1 mL containing SDH with a concentration greater than 2 μM. The increase of the absorbance at 412 nm was monitored immediately after 50 μL of 3 mM DTNB was added into the 1 mL protein sample, followed by through mixing. From the increase in absorbance, the number of moles of thiol accessible per mole of protein was estimated using an ε of 13.6 $mM^{-1}cm^{-1}$.

III.3 RESULTS AND DISCUSSION

III.3.1 Ellman (DTNB) Assay

The concentration of SDH used for DTNB assay was determined to be 13 μM by both the Bradford assay and UV absorbance at 280 nm. The absorbance was increased about 0.2386 once DTNB was added into the SDH protein sample, resulting in a

calculation of 16.9 μM thiol accessible. The ratio of the thiol and enzyme concentrations gave a value of 1.35, suggesting that one cysteine of SDH out of total four is accessible to solvent, which is most likely Cys 364. Based on the apo-structure of SDH (unpublished data), Cys 364 is sitting on the surface of SDH, located on an α-helix of the catalytic domain, away from the central cavity. In addition, structural data suggest that Cys 205 forms a disulfide bond with Cys 249 in the nucleotide binding domain, inconsistent with previously reported result (*93*).

III.3.2 Protein Crystallization

Several conditions from Hampton Research Crystal Screen I and II resulted in crystals of various size, morphology, and quantity (Hampton Screen I Formulations 6, 9, 15, 17, 28, 31, and 39, and Hampton Screen II Formulations 13, 14, 23, 26, and 42). Polyethylene glycol (PEG) or PEG monomethyl ether (PEGMME) in the molecular weight range 2000-8000, and ammonium sulfate were used as precipitant for the positive conditions. Crystals were observed over a wide pH range (4.6-8.5), at both 4 °C and 25 °C. In the case of the HWI screening, about 30 promising conditions were found. PEG in the M.W. range 4000-20000 was common to all of the positive conditions. Crystals were also observed over a wide pH range (4.0-10.0). A number of different salts, e.g., KCl, NH_4Br, NH_4Cl, $(NH_4)_2SO_4$, KH_2PO_4, NH_4SCN, LiBr, KNO_3, and RbCl, can be used as a additive at a concentration of 100 mM.

Optimization studies using PEG of different molecular weights and ammonium sulfate at different concentrations, variation of the protein concentration, and inclusion of different salt additives at different concentrations in the crystallization setup, resulted in

the growth of four crystal forms of SDH, Table III.1. Data collection and processing statistics for the different crystal forms are summarized in Table III.2.

Table III.1: Summary of Crystallization Conditions.

	Form I	Form II	Form III	Form IV
Precipitant	26% (w/v) PEGMME 2000	24% (w/v) PEG 4000	22% (w/v) PEG 8000	2.4 M ammonium sulfate
Protein Conc. (mg/mL)	4.5	4.0	3.8	5.0
Additive	0.2 M ammonium sulfate	--	0.2 M ammonium sulfate	2% (w/v) PEG 400
pH	0.1 M Tris pH 7.0	0.1 M Tris pH 7.0	0.1 M Tris pH 7.0	0.1 M Tris pH 7.0
Average Size	(0.29*0.35*0.05) mm	(0.13*0.13*0.13) mm	(0.08*0.08*0.04) mm	(0.2*0.1*0.02) mm

Table III.2: Data-collection and Processing Statistics for SDH Crystals.

	Form I	Form II	Form III	Form IV
Bravais Lattice or Space Group	C2 Monoclinic	C2 Monoclinic	$P2_12_12_1$ Orthorhombic	C2 Monoclinic
Unit-cell dimensions (Å)	a=112.4, b=55.1, c=74.8 α=90º, β=116.5º, γ=90º	a=112.6, b=55.0,c=75.0 α=90º, β=116.3º, γ=90º	a=65.0, b=75.0, c=74.5 α=90º, β=90º, γ=90º	a=112.6, b=55.0, =74.9 α=90º, β=116.5º, γ=90º
Resolution (Å)	1.7	1.8	1.9	2.0
Mean I/σ (I)	27.6 (4.0)	11.0 (2.4)	12.7 (2.5)	5.0 (2.1)
No. of observations	372012	226400	248475	136510
Unique reflections	53040	41240	60660	27436
Completeness (%)	98.6 (98.2)	99.1 (100.0)	99.0 (98.0)	99.2 (97.9)
R_{merge}	0.05 (0.36)	0.10 (0.45)	0.07 (0.32)	0.11 (0.27)
Mosaicity (degree)	0.96	0.825	0.93	1.08
Molecules in asymmetric unit	1	--	1	--
Mat. coef V_M (Å^3/Da)	2.4	--	2.1	--
Solvent content (%)	48.3	--	40.4	--

Values for the outer resolution shell of data are given in parentheses.

Crystal Form I was grown with a 4.5 mg/mL protein stock solution and reservoir consisting of 0.2 M ammonium sulfate, 0.1 M Tris pH 7.0, 26% (w/v) PEGMME 2000. These crystals displayed a diamond-like morphology, Fig. III.1 (a), and diffracted to 1.7 Å resolution when data were collected using a Cu rotating anode X-ray diffraction system. Autoindexing calculations performed with d*TREK (*131*) indicated a centered monoclinic lattice with unit cell dimensions *a* =112.4, *b* =55.1, *c* =74.8. Analysis of the solvent content using the method of Matthews (*132*) suggested the presence of only one SDH molecule per asymmetric unit and a solvent content of 48.3%. Clearly, form I is optimal for high-resolution structure determination due to its high diffraction quality.

Crystal Form II was obtained using a protein stock solution of 4.6 mg/mL. The optimal reservoir condition was 26% (w/v) PEG 4000, 0.1 M ammonium sulfate, and 0.1 M Tris at pH 7.0. These crystals grew within a week after setup and took the cubic form with an average size of (0.13*0.13*0.13) mm, Fig. III.1 (b). Diffraction to 1.8 resolution was observed, and autoindexing suggested a centered monoclinic lattice with unit cell dimensions *a* =112.6, *b* =55.0, *c* =75.0.

Crystal Form III grew in the presence of 3.8 mg/mL SDH, 22% (w/v) PEG 8000, and 0.1 M Tris at pH 7.0. Form III crystals have space group $P2_12_12_1$ with unit cell dimensions *a* =112.6, *b* =55.0, *c* =75.0. The asymmetric unit contains two SDH molecules, with a Matthews coefficient of 2.1 and a solvent content of 40.4%. These crystals are relatively small compared to the other form crystals, but, diffracted to 1.9 Å.

Crystal Form IV was obtained when ammonium sulfate was used as precipitant, instead of PEG. The optimal reservoir condition was 2.4 M ammonium sulfate, 2% (w/v) PEG 400, and 0.1 M Tris at pH 7.0. Crystals exhibited a triangular plate-like morphology,

Fig. III.1 (d), and grew very slow. They originally grew as thin plates with very poor diffraction quality, but eventually reached an average size of (0.2*0.1*0.02) mm in about 1 month. Although they had a thin edge, these crystals still diffracted to 2.0 Å.

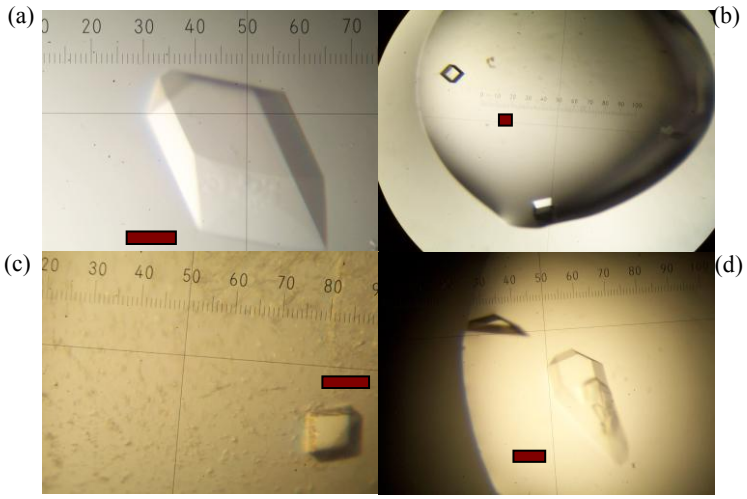


Figure III.1: Four crystal forms of SDH. Forms I, II, III, and IV are shown in panels (a), (b), (c), and (d), respectively. The bar in each figure represents approximately 100 μm.

With these native diffraction datasets, we reached a good starting point to elucidate the 3D structure of SDH. However, there is still a second bottle neck, the phase problem, which needs to be solved in order to determine the structure of SDH. Molecular replacement is often employed to solve the phase problem by borrowing the phase angles from a homologous model. However, if a suitable candidate is not available, two alternative methods, multiple isomorphous replacement (MIR) and multiple anomalous dispersion (MAD), can be considered. Once the intensity, position, and phase information of all reflections have been obtained, an initial electron density map can be calculated. A model can then be built by fitting the primary amino acid sequence into the electron density map. After model refinement and structure validation, the three dimensional structure will be obtained. All these future studies need to be followed up.

APPENDIX IV

Cloning and Expression of PIPOX

IV. 1 INTRODUCTION

The substrate for SDH in the direction of lysine formation is saccharopine. Because the cost of commercial saccharopine is very high, it can be synthesized enzymatically from L-pipecolic acid according to Fig. IV.1. The pathway for L-pipecolic acid oxidation is found in *Rhodotorula glutinis* (*133*), and also as part of the lysine degradative pathway in monkeys and humans (*134*). L-pipecolic acid is first oxidized by L-pipecolic acid oxidase (PIPOX), an H_2O_2-forming peroxisomal oxidase containing covalently bound FAD, to Δ^1–piperidine-6-carboxylic acid, a cyclic imine that spontaneously hydrolyzes to form α-aminoadipic acid semialdehyde (AAS) at physiologic pH. The semialdehyde can then be converted to saccharopine by saccharopine reductase (SR), the penultimate enzyme of the α-aminoadipate pathway.

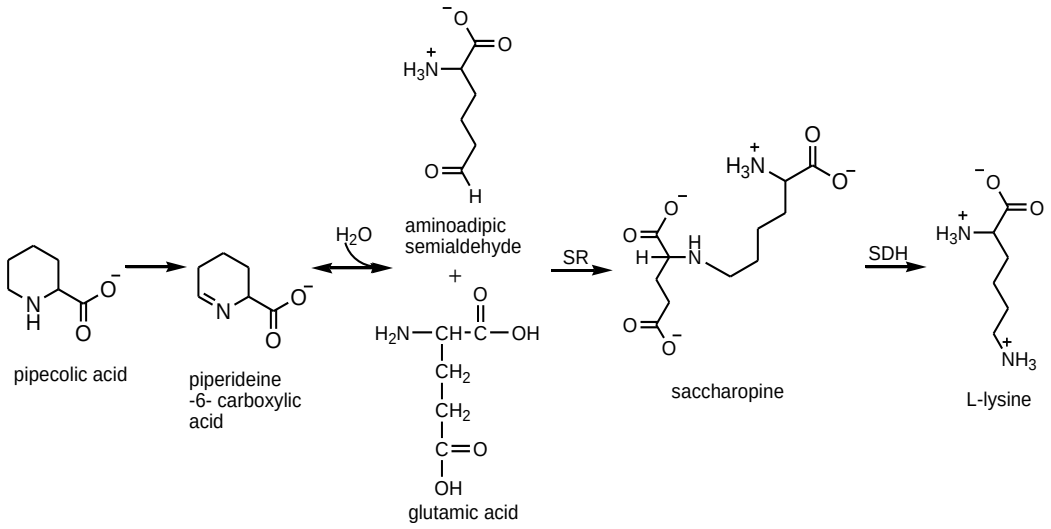


Figure IV.1: Enzymatic synthesis of saccharopine

IV. 2 MATERIALS AND METHODS

IV.2.1 Molecular Cloning of PIPOX

A 1187 bp DNA fragment encoding PIPOX was successfully amplified by PCR reaction with a human cDNA ligated into a pOTB7 plasmid as the template using the following protocol: one cycle of initial denaturation at 94 °C for 2 min, followed by 35 cycles of denaturation at 94 °C for 30 s, annealing at 45 °C for 45 s, and extension at 72 °C for 1.5 min. The enzyme used was Platinum Pfx polymerase, which produces blunt-end PCR products. The forward primer was designed as AAACATATGGCGGCTCAGAAAGATCTCTGG, while the reverse primer was designed as TTTCTCGAGTCAAAGGTGGGCTTTGCCCAGG. The purified PCR product (PIPOX DNA) was then ligated into linearized pUC12 vector which was digested with *Sma*I to create blunt-end and was gel-purified. *E. coli* DH5α cells were transformed with the recombinant plasmid, and positive colonies were verified by the X-gal and IPTG colony screening protocol.

For subcloning into an expression vector, a procedure similar to that for the *Lys1* (SDH gene) was used (**Materials and Methods 2.2**). The PIPOX gene was excised from the recombinant plasmid described above with two *Nde*I/*Xho*I restriction endonucleases. The purified fragment containing the PIPOX gene was subcloned using T4 ligase into the pET16b expression vector, which was previously treated by *Nde*I/*Xho*I. *E. coli* BL21(DE3) RIL cells were then transformed, single colonies were grown on LB/Amp medium. The new plasmid was designated pipoxHX2, and restriction endonuclease mapping was performed to confirm the presence of the PIPOX gene.

The pipoxHX2 plasmid-containing strain was grown at 37 °C in LB supplemented with 100 μg/mL amplicillin and 25 μg/mL chloramphenicol. Induction with 2 mM IPTG (final concentration) was accomplished once the OD_{600} reached 0.8. Cell growth was then continued at 30 ºC overnight. After centrifugation, the harvested cells were suspended in 100 mM KCl and 50 mM Hepes at pH 8.0, containing the following protease inhibitors: 1mM EDTA, 0.1 mM benzamidine, 0.4 μg/mL leupeptin, and 0.7 μg/mL pepstain. Cells were sonicated on ice for 1.5 minutes with a 15 s pulse followed by a 30 s rest, using a MISONIX Sonicator XL. After the cell debris was removed by centrifugation at 12000*g* for 15 min, the collected supernatant was mixed with the Ni-NTA resin at 4 ºC, washed with 5 mM imidazole at pH 7.5, and then eluted with buffer containing 30 mM imidazole at pH 7.5. The PIPOX-containing sample, identified by SDS-PAGE, was concentrated and dialyzed against 100 mM K_2HPO_4 in D_2O using an Amicon ultrafiltration device with a YM 10 membrane.

IV.2.2 PIPOX Reaction Monitored by NMR

Since L-pipecolic acid, Δ^1–piperidein-6-carboxylic acid (the cyclic form), and AAS (the linear form) have different structures, ^{1}H NMR spectra were used to follow the PIPOX reaction. The chemical shifts for protons were predicted using the ChemDraw program, Fig. IV.2 A.

Solution in D_2O of 30 mM L-pipecolic acid and 100 mM K_2HPO_4 buffer was prepared, and adjusted to pD 8.4 using either DCl or NaOD. Experiments were performed on a Varian Mercury VX-300 MHz spectrometer with a Varian four-nucleus autoswitchable PFG probe, and spectra were collected using the PRESAT pulse sequence

supplied by Varian, Inc. The spectra were collected with a sweep width of 4803.1 Hz, 152 repetitions, and an acquisition time of 1.998 s.

IV. 3 RESULTS AND DISCUSSION

A chemical shift at 9.95 ppm was observed after PIPOX was added into L-pipecolic acid solution, Fig. IV.2 B. This peak corresponded to the C(6)-H of the semialdehyde, indicating the production of aldehyde. However, the same peak disappeared after the reaction mixture was allowed to sit overnight, suggesting the production of 2-amino-6,6-dihydroxy-hexanoic acid and the unstability of AAS. The production of AAS was recorded according to the chemical shift of aldehyde at 9.95 ppm over a time period of 20 min in the presence of PIPOX, Fig. IV.2 C. The area of the peak reached a maximum in 5 min after PIPOX was added. In order to examine whether the AAS produced can serve as a substrate for SR, 100 μL of freshly made L-pipecolic acid and PIPOX mixture was added into a reaction mixture containing 100 mM Hepes at pH 6.8, 0.2 mM NADPH, 10 mM L-glutamate, and 0.27 μM SR. The observed disappearance of absorbance at 340 nm (NADPH) suggested that AAS produced by PIPOX was converted to saccharopine.

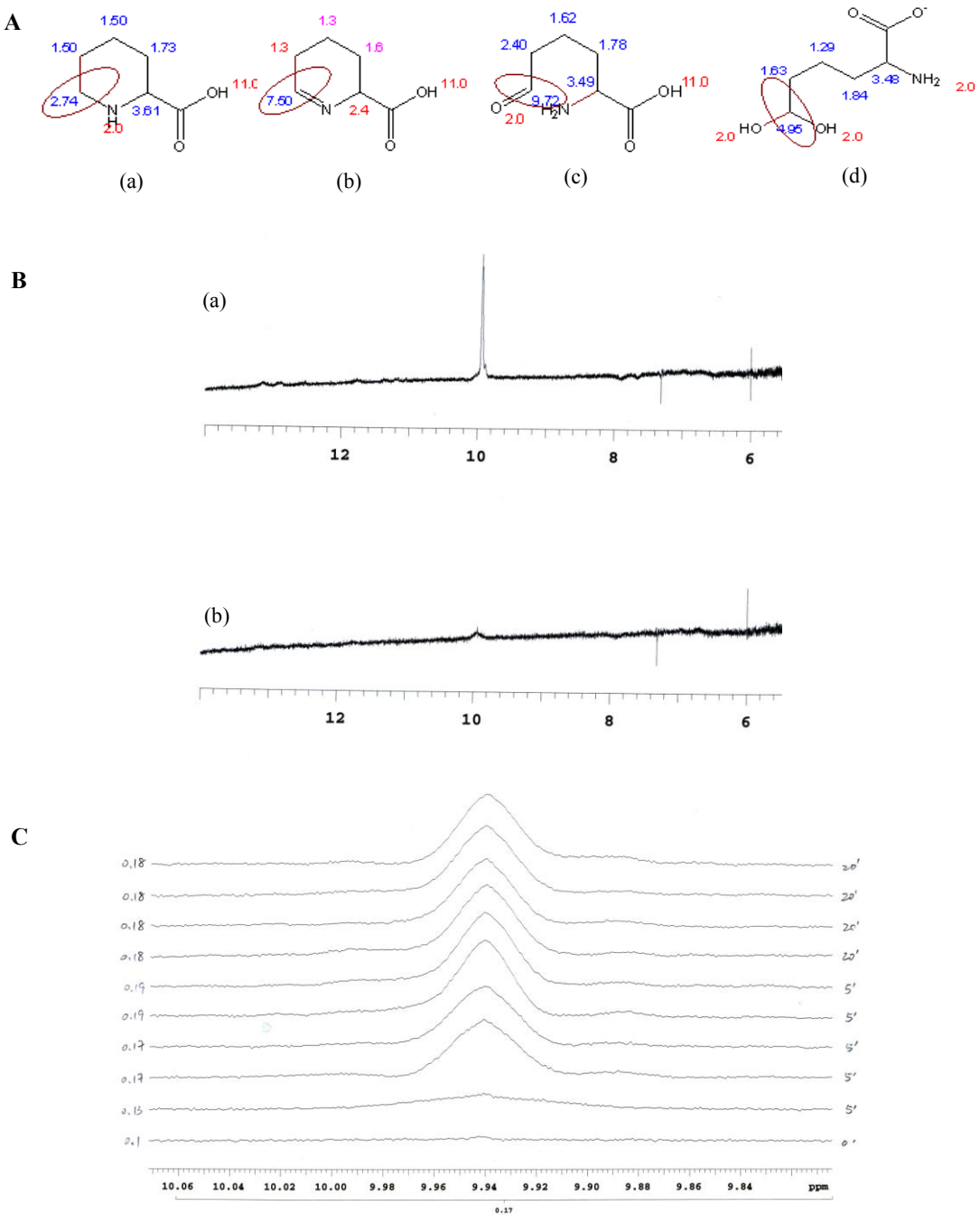


Figure IV.2: ^{1}H NMR spectra of PIPOX reaction. (A) Predicted NMR chemical shifts for L-pipecolic acid (a), Δ^{1}–piperidein-6-carboxylic acid (b), α-aminoadipic acid semialdehyde (c), and 2-amino-6,6-dihydroxy-hexanoic acid (d), respectively. Estimation quality: blue = good, magenta = medium, and red = rough. (B) Appearance of the chemical shift at 9.95 ppm after PIPOX was added into L-pipecolic acid solution. (a) is the spectrum one hour after PIPOX was added., while (b) is the spectrum obtained after adding PIPOX at time zero. (C) the time course of PIPOX reaction by monitoring the area of the chemical shift of aldehyde at 9.95 ppm. Numbers at the right side are time in minutes, while at left side are values of area.

References

1. Zabriskie, T. M. and Jackson, M. D. (2000) Lysine biosynthesis and metabolism in fungi. *Nat. Prod. Rep. 17*, 85-97.

2. Umbargar, H. E. (1978) Amino acid biosynthesis and its regulation. *Annu. Rev. Biochem. 47*, 533-606.

3. Bhattacharjee, J. K. (1985) α-Aminoadipate pathway for the biosynthesis of lysine in lower eukaryotes. *Crit. Rev. Microbiol. 12*, 131-151.

4. Vogel, H. J. (1960) Two modes lysine synthesis among lower fungi: evolutionary significance. *Biochim. Biophys. Acta 41*, 172-174.

5. Berges, D. A., DeWolf, W. E., Jr., Dunn, G. L., et al. (1986) Peptides of 2-aminopimelic acid: antibacterial agents that inhibit diaminopimelic acid biosynthesis. *J. Med. Chem. 29*, 89-95.

6. Bhattacharjee, J. K. (1992) Evolution of α-aminoadipate pathway for the synthesis of lysine in fungi, in *Handbook of Evolution of Metabolic Function* (Mortlock, R. P., Ed.), CRC Press, Boca Raton, FL, pp. 47-80.

7. Bhattacharjee, J. K. and Strassman, M. (1967) Accumulation of tricarboxylic acids related to lysine biosynthesis in a yeast mutant. *J. Biol. Chem. 242*, 2542-2546.

8. Gaillardin, C. M., Ribert, A. M., and Heslot, H. (1982) Wild type and mutant forms of homoisocitric dehydrogenase in the yeast *Saccharomycopsis lipolytica*. *Eur. J. Biochem. 128*, 489-494.

9. Ye, Z. H. and Bhattacharjee, J. K. (1988) Lysine biosynthesis pathway and biochemical blocks of lysine auxotrophs of *Schizosaccharomyces pombe*. *J. Bacteriol. 170*, 5968-5970.

10. Glass, J. and Bhattacharjee, J. K. (1971) Biosynthesis of lysine in *R. glutinis*: accumulation of homocitric, homoaconitic, and homoisocitric acids in a leaky mutant. *Genetics 67*, 365-376.

11. Kunze, G., Bode, R., Schmidt, H., Samsonova, I. A., and Birnbaum D. (1987) Identification of a *lys2* mutant of *C. maltosa* by means of transformation. *Curr. Genet. 11*, 385-391.

12. Broquist, H. P. (1971) Lysine biosynthesis (yeast). *Methods Enzymol. 17*, 112-129.

13. Jaklitsch, W. M. and Kubicek, C. P. (1990) Homocitrate synthase from *Penicillium chrysogenum*. Localization, purification of the cytosolic isoenzyme, and sensitivity to lysine. *Biochem. J. 269*, 247-253.

14. Garrad, R. C. and Bhattacharjee, J. K. (1992) Lysine biosynthesis in selected pathogenic fungi: characterization of lysine auxotrophs and the cloned *LYS1* gene of *Candida albicans*. *J. Bacteriol. 174*, 7379-7384.

15. Andi, B., West, A. H., and Cook, P. F. (2004) Stabilization and characterization of histidine-tagged homocitrate synthase from *Saccharomyces cerevisiae*. *Arch. Biochem. Biophys. 421*, 243-254.

16. Strassman, M. and Weinhouse, S. (1953) Biosynthetic pathways. III. The biosynthesis of lysine *Torulopsis utilis*. *J. Am. Chem. Soc. 75*, 1680-1684.

17. Vogel, H. J. (1965) Lysine biosynthesis and evolution, in *Handbook of Evolving Genes and Proteins* (Bryson, V., Ed.), Academic Press, New York, pp. 25-40.

18. Nishida, H., Nishiyama, M., Kobashi, N., Kosuge, T., Hoshino, T., and Yamane, H. (1999) A prokaryotic gene cluster involved in synthesis of lysine through the aminoadipate pathway: a key to the evolution of amino acid biosynthesis. *Genome Res. 9*, 1175-1183.

19. Cunin, R., Glandsorff, N., Pierard, A., and Stalon, V. (1986) Biosynthesis and metabolism of arginine in bacteria. *Microbiol. Rev. 50*, 314-352.

20. Nishida, H. and Nishiyama, M. (2000) What is characteristic of fungal lysine synthesis through the α-aminoadipate pathway? *J. Mol. Evol. 51*, 299-302.

21. Hammer, T., Bode, R., Schmidt, H. and Birnbaum, D. (1991) Distribution of three lysine-catabolizing enzymes in various yeast species. *J. Basic. Microbiol. 31*, 43-49.

22. Jacq, C., Alt-Morbe, J., Andre, B., et al. (1997) The nucleotide sequence of *Saccharomyces cerevisiae* chromosome IV. *Nature 387*, 75-78.

23. Philippsen, P., Kleine, K., Pohlmann, R., et al. (1997) The nucleotide sequence of *Saccharomyces cerevisiae* chromosome XIV and its evolutionary implications. *Nature 387*, 93-98.

24. Tettelin, H., Agostoni Carbone, M. L., Albermann, K., et al. (1997) The nucleotide sequence of *Saccharomyces cerevisiae* chromosome VII. *Nature 387*, 81-84.

25. Borell, C. W., Urrestarazu, L.A., and Bhattacharjee, J. K. (1984) Two unlinked lysine genes (*LYS9* and *LYS14*) are required for the synthesis of saccharopine reductase in *Saccharomyces cerevisiae*. *J. Bacteriol. 159*, 429-432.

26. Wang, L., Okamoto, S., and Bhattacharjee, J. K. (1989) Cloning and physical characterization of linked lysine genes (*LYS4*, *LYS15*) of *S. cerevisiae*. *Curr. Genet. 16*, 7-12.

27. Urrestarazu, L. A., Borell, C. W., and Bhattacharjee, J. K. (1985) General and specific controls of lysine biosynthesis in *Saccharomyces cerevisiae. Curr. Genet. 9*, 341-344.

28. Irvin, S. D. and Bhattacharjee, J. K. (1998) A unique fungal lysine biosynthesis enzyme shares a common ancestor with tricarboxylic acid cycle and leucine biosynthetic enzymes found in diverse organisms. *J. Mol. Evol. 46*, 401-408.

29. Karsten, W. E. and Cook, P. F. (2000) Pyridine nucleotide-dependent β-hydroxyacid oxidative decarboxylases: an overview. *Protein Pept. Lett. 7*, 281-286.

30. Ye, Z. H., Garrad, R. C., Winston, M. K, and Bhattacharjee, J. K. (1991) Use of alpha-aminoadipate and lysine as sole nitrogen source by *Schizosaccharomyces pombe* and selected pathogenic fungi. *J Basic Microbiol. 31*, 149-56.

31. Kosuge, T. and Hoshino T. (1998) Lysine is synthesized through the α-aminoadipate pathway in *Thermus thermophilus*. *FEMS Microbiol. Lett. 169*, 361-367.

32. Kobashi, N., Nishiyama, M., and Tanokura, M. (1999) Aspartate kinase-independent lysine synthesis in an extremely thermophilic bacterium, *Thermus thermophilus*: lysine is synthesized via α-aminoadipic acid not via diaminopimelic acid. *J. Bacteriol. 181*, 1713-1718.

33. Baldwin, J. E., Shiau, C., Byford, M., and Schofield, C. J. (1994) Substrate specificity of L-delta-(alpha-aminoadipoyl)-L-cysteinyl-D-valine synthetase from *Cephalosporium acremonium*: demonstration of the structure of several unnatural tripeptide products. *Biochem. J. 301*, 367-372.

34. Palmer D. R., Balogh, H, Ma, G., Zhou, X., Marko, M., and Kaminskyj, S. G. (2004) Synthesis and antifungal properties of compounds which target the alpha-aminoadipate pathway. *Pharmazie. 59*, 93-98.

35. Ramos, F., Dubois, E., and Piérard, A. (1988) Control of enzyme synthesis in the lysine biosynthetic pathway of *Saccharomyces cerevisiae.* Evidence for a regulatory role of gene *LYS14*. *Eur. J. Biochem. 171*, 171-176.

36. Wolfner, M., Yep, D., Messenguy, F., and Fink, G. R. (1975) Integration of amino acid biosynthesis into the cell cycle of *Saccharomyces cerevisiae*. *J. Mol. Biol. 96*, 273-290.

37. Becker, B., Feller, A., El Alami, M., Dubois, E., and Pierard, A. (1998) A nonameric core sequence is required upstream of the *LYS* genes of *Saccharomyces cerevisiae* for Lys14p- mediated activation and apparent repression by lysine. *Mol. Microbiol. 29*, 151-163.

38. Ramos, F., Verhasselt, P., Feller, A., et al. (1996) Identification of a gene encoding a homocitrate synthase isoenzyme of *Saccharomyces cerevisiae*. *Yeast 12*, 1315-1320.

39. Tucci, A. F. and Ceci, L. N., (1972) Homocitrate synthase from yeast. *Arch. Biochem. Biophys. 153*, 742-750.

40. Ramos, F., and Wiame, J. M. (1985) Mutation affecting the specific regulatory control of lysine biosynthetic enzymes in *Saccharomyces cerevisiae*. *Mol. Gen. Genet. 200*, 291-294.

41. Feller, A., Ramos, F., Piérard, A., and Bubois, E. (1999) In *Saccharomyces cerevisiae,* feedback inhibition of homocitrate synthase isoenzymes by lysine modulates the activation of *LYS* gene expression by Lys14p. *Eur. J. Biochem. 261*, 163-170.

42. Harrison, S. C. (1991) A structural taxonomy of DNA-binding domains. *Nature 353*, 715-719.

43. Vallee, B. L., Coleman, J. E., and Auld, D. S. (1991) Zinc fingers, zinc clusters, and zinc twists in DNA-binding protein domains. *Proc. Natl. Acad. Sci.* USA *88*, 999-1003.

44. Marmorstein, R., Carey, M., Ptashne, M., and Harrison, S. C. (1992) DNA recognition by *GAL4*: structure of a protein-DNA complex. *Nature 356*, 408-414.

45. Marmorstein, R. and Harrison, S. C. (1994) Crystal structure of a PPR1-DNA complex: DNA recognition by proteins containing a Zn_2Cys_6 binuclear cluster. *Genes Dev. 8*, 2504-2512.

46. Schjerling, P. and Holmberg, S. (1996) Comparative amino acid sequence analysis of the C_6 zinc cluster family of transcriptional regulators. *Nucleic Acids Res. 24*, 4599-4607.

47. Bañuelos, O., Casqueiro, J., Gutiérrez, S., and Martín, J. F. (2000) Overexpression of the *lys1* gene in *Penicillium chrysogenum*: homocitrate synthase levels, α-aminoadipic acid pool and penicillin production. *Appl. Microbiol. Biotechnol. 54*, 69-77.

48. Wulandari, A. P., Miyazaki, J., Kobashi, N., Nishiyama, M., Hoshino, T., and Yamane, H. (2002) Characterization of bacterial homocitrate synthase involved in lysine biosynthesis. *FEBS Lett. 522*, 35-40.

49. Andi, B., West. A. H., and Cook P. F. (2005) Regulatory mechanism of histidine-tagged homocitrate synthase from *Saccharomyces cerevisiae*: I. Kinetic studies. *J. Biol. Chem. 280*, 31,624-31,632.

50. Friedrich, C. G. and Demain, A. L. (1977) Homocitrate synthase as the crucial site of the lysine effect on penicillin biosynthesis. *J. Antibiot. 30*, 760-761.

51. Somerson, N. L., Demain, A. L., and Nunheimer, T. D. (1961) Reversal of lysine inhibition of penicillin production by α-aminoadipic acid. *Arch. Biochem. Biophys. 93*, 238-241.

52. Luengo, J. M., Revilla. G., López, M. J., Villanueva, J. R., and Martín, J. F. (1980) Inhibition and repression of homocitrate synthase by lysine in *Penicillium chrysogenum. J. Bacteriol. 144*, 869-976.

53. Tracy, J. W. and Kohlhaw, G. B. (1975) Reversible, Coenzyme-A-mediated inactivation of biosynthetic condensing enzymes in yeast: a possible regulatory mechanism. *Proc. Nat. Acad. Sci.* USA *72*, 1802-1806.

54. Hampsey, D. M. and Kohlaw, G. B. (1981) Inactivation of yeast α-isopropyl malate synthase by CoA. *J. Biol. Chem. 256*, 3791-3796.

55. Tracy, J. W. and Kohlhaw, G. B. (1977) Evidence for two distinct CoA binding sites on yeast α-isopropylmalate synthase. *J. Biol. Chem. 252*, 4085-4091.

56. Kohlhaw, G. B. (2003) Leucine biosynthesis in fungi: entering metabolism through the back door. *Microbiol. Mol. Biol. Rev. 67*, 1-15.

57. Qian, J., West, A. H., and Cook, P. F. (2006) Acid-base chemical mechanism of homocitrate synthase from *Saccharomyces cerevisiae*. *Biochemistry 45*, 12136-12143.

58. Andi, B., West, A. H., and Cook, P. F. (2004) Kinetic mechanism of histidine-tagged homocitrate synthase from *Saccharomyces cerevisiae*. *Biochemistry 43*, 11790-11795.

59. Perez-campo, F.-M., Nicaud, J.-M., Gaillardin, C., and Dominguez, A. (1996) Cloning and sequencing of the *LYS1* gene encoding homocitrate synthase in the yeast *Yarrowia lipolytica*. *Yeast 12*, 1459-1469.

60. Copley, R. R. and Bork, P. (2000) Homology among (betaalpha) (8) barrels: implications for the evolution of metabolic pathways. *J. Mol. Biol. 303*, 627-640.

61. Beinert, H., Kennedy, M. C., and Stout, C. D. (1996) Aconitase as iron-sulfur protein, enzyme, and iron-regulatory protein. *Chem. Rev. 96*, 2335-2373.

62. Grodsky, N. B., Soundar, S., and Colman, R. F. (2000) Evaluation by site-directed mutagenesis of aspartic acid residues in the metal site of pig heart NADP-dependent isocitrate dehydrogenase. *Biochemistry 39*, 2193-2200.

63. Matsuda, M. and Ogur, M. (1969) Separation and specificity of the yeast glutamate-α-ketoadipate transaminase. *J. Biol. Chem. 244*, 3352-3358.

64. Matsuda, M. and Ogur, M. (1969) Enzymatic and physiological properties of the yeast glutamate-α-ketoadipate transaminase. *J. Biol. Chem. 244*, 5153-5158.

65. Sagisaka, S. and Shimura, K. (1962) Studies in lysine biosynthesis. IV. Mechanism of activation and reduction of α–aminoadipic acid. *J. Biochem. 52*, 155-161.

66. Larson, R. L., Sandine, W. D., and Broquist, H. P. (1963) Enzymatic reduction of α-aminoadipic acid: relation to lysine biosynthesis. *J. Biol. Chem. 238*, 275-282.

67. Sinha, A. K. and Bhattacharjee, J. K. (1971) Lysine biosynthesis in *Saccharomyces*, conversion of α-aminoadipate into α-aminoadipic δ-semialdehyde. *Biochem. J. 125*, 743-749.

68. Suyarna, K., Seah, L., Bhattacharjee, V., and Bhattacharjee, J. K. (1998) Molecular analysis of the *LYS2* gene of *Candida albicans*: homology to peptide antibiotic synthetases and the regulation of the α-aminoadipate reductase. *Curr. Genet. 33*, 268-275.

69. Lambalot, R. H., Gehring, A. M., Flugel, R. S., et al. (1996) A new enzyme superfamily--the phosphopantetheinyl transferases. *Chem. Biol. 3*, 932-936.

70. Ehmann, D. E., Gehring, A. M, and Walsh, C. T. (1999) Lysine biosynthesis in *Saccharomyces cerevisiae*: mechanism of α–aminoadipate reductase (*LYS2*) involves posttranslational phosphopantetheinylation by *LYS5*. *Biochemistry 38*, 6171-6177.

71. Praphanphoj, V., Sacksteder, K. A., Gould, S. J., Thomas, G. H., and Geraghty, M. T. (2001) Identification of the α-aminoadipic semialdehyde dehydrogenase-phosphopantetheinyl transferase gene, the human ortholog of the yeast *LYS5* gene. *Mol. Genet. Metab. 72*, 336-342.

72. Guo, S., Evans, S. A., Wilkes, M. B., and Bhattacharjee, J. K. (2001) Novel posttranslational activation of the *LYS2*-encoded α–aminoadipate reductase for biosynthesis of lysine and site-directed mutational analysis of conserved amino acid residues in the activation domain of *Candida albicans*. *J. Bacteriol. 183*, 7120-7125.

73. Jones, E. W. and Fink, G. R. (1982) Regulation of amino acid and nucleotide synthesis in yeast, in *Molecular Biology of the Yeast Saccharomyces*, *Metabolism and Gene Regulation* (Strathern, J. N., Jones, E. W. and Broach, J. R., Eds.), Cold Spring Harbor Laboratory, Cold Spring Harbor, NY, pp. 181-299.

74. Andi, B., Cook, P. F., and West, A. H. (2006) Crystal structure of the histidine-tagged saccharopine reductase from *Saccharomyces cerevisiae* at 1.7Å resolution. *Cell Biochem. Biophys. 46*, 17-26.

75. Rossmann, M. G., Liljas, A., Branden, C. I., and Banaszak, L. J. (1975) Evolutionary and structural relationship among dehydrogenases. *Enzymes 11*, 51-102.

76. Johansson, E., Steffens, J. J., Lindqvist, Y., and Schneider, G. (2000) Crystal structure of saccharopine reductase from *Magnaporthe grisea*, an enzyme of the α-aminoadipate pathway of lysine biosynthesis. *Struct. Fold. Des. 8*, 1037-1047.

77. Brunhuber, N. M. and Blanchard, J. S. (1994) The biochemistry and enzymology of amino acid dehydrogenases. *Crit. Rev. Biochem. Mol. Biol. 29*, 415-467.

78. Weiss, P. M., Chen, C. -Y., Cleland, W. W., and Cook, P. F. (1988) Primary deuterium and ^{15}N isotope effects as a mechanistic probe of alanine and glutamate dehydrogenases, *Biochemistry 27*, 4814-4822.

79. Rife, J. E. and Cleland, W. W. (1980a) Kinetic mechanism of glutamate dehydrogenase. *Biochemistry*, *19*, 2321-2328.

80. Schroder, I., Vadas, A., Johnson, E., Lim, S., and Monbouquette, H. G. (2004) A novel archaeal alanine dehydrogenase homologous to ornithine cyclodeaminase and μ-crystallin. *J. Bacteriol. 186*, 7680-7689.

81. Ohshima, T. and Soda, K. (1979) Purification and characterization of alanine dehydrogenase from *Bacillus sphaericus. Eur. J. Biochem. 100*, 29-39.

82. Alizade, M. A., Bressler, R., and Brendel, K. (1975) Stereochemistry of the hydrogen transfer to NAD catalyzed by (S)alanine dehydrogenase from *Bacillus subtilis. Biochim. Biophys. Acta 397*, 5-8.

83. Hashimoto, H., Misono, H., Nagata, S., and Nagasaki, S. (1989) Activation of L-lysine ε-dehydrogenase from *Agrobacterium tumefaciens* by several amino acids and monocarboxylates. *J. Biochem. 106*, 76-80.

84. Scapin, G., Reddy, S. G., and Blanchard, J. S. (1996) Three-dimensional structure of *meso*-diaminopimelic acid dehydrogenase from *Corynebacterium glutamicum*. *Biochemistry 35*, 13,540-13,551.

85. Fujioka, M. and Takata, Y. (1979) Stereospecificity of hydrogen transfer in the saccharopine dehydrogenase reaction. *Biochim. Biophys. Acta 570*, 210-212.

86. Sugimoto, K. and Fujioka, M. (1984) Chemical mechanism of saccharopine dehydrogenase (NAD^+, L-lysine-forming) as deduced form initial rate pH studies. *Arch. Biochem. Biophys. 230*, 553-559.

87. Stillman, T. J., Baker, P. J., Britton, K. L., and Rice, D. W. (1993) Conformational flexibility in glutamate dehydrogenase. Role of water in substrate recognition and catalysis. *J. Mol. Biol. 234*, 1131-1139.

88. Baker, P. J., Turnbull, A. P., Sedelnikova, S. E., Stillman, T. J., and Rice, D. W. (1995) A role for quaternary structure in the substrate specificity of leucine dehydrogenase. *Structure 3*, 693-705.

89. Baker, P. J., Sawa, Y., Shibata, H., Sedelnikova, S. E., and Rice, D. W. (1998) Analysis of the structure and substrate binding of *Phormidium lapideum* alanine dehydrogenase. *Nat. Struct. Biol. 5*, 561-567.

90. Vanhooke, J. L., Thoden, J. B., Brunhuber, N. M. W., Blanchard, J. S., and Holden, H. M. (1999) Phenylalanine dehydrogenase from Rhodococcus sp. M4: High-resolution X-ray analyses of inhibitory ternary complexes reveal key features in the oxidative deamination mechanism. *Biochemistry 38*, 2326-2339.

91. Baker, P. J., Waugh, M. L., Wang, X-G, et al. (1997) Determinants of the substrate specificity in the superfamily of amino acid dehydrogenases. *Biochemistry 36*, 16,109-16,115.

92. Ogawa, H. and Fujioka, M. (1978) Purification and characterization of saccharopine dehydrogenase from baker's yeast. *J. Biol. Chem. 253*, 3666-3670.

93. Ogawa, H., Okamoto, M. and Fujioka, M. (1979) Chemical modification of the active site sulfhydryl group of saccharopine dehydrogenase (L-lysine-forming). *J. Biol. Chem*. *254*, 7030-7035.

94. Ford, R. A. and Bhattacharjee, J. K. (1995) Molecular properties of the *lys1+* gene and the regulation of α-aminoadipate reductase in *Schizosaccharomyces pombe*. *Curr. Genet. 28*, 131-137.

95. Fujioka, M. and Nakatani, Y. (1974) Saccharopine dehydrogenase, a kinetic study of coenzyme binding. *J. Biol. Chem. 249*, 6886-6891.

96. Fujioka, M. and Nakatani, Y. (1972) Saccharopine dehydrogenase, interaction with substrate analogues. *Eur. J. Biochem. 25*, 301-307.

97. Fujioka, M. and Nakatani, Y. (1970) A kinetic study of saccharopine dehydrogenase reaction. *Eur. J. Biochem. 16*, 180-186.

98. Sugimoto, K. and Fujioka, M. (1978) The reaction of pyruvate with saccharopine dehydrogenase. *Eur. J. Biochem. 90*, 301-307.

99. Fujioka, M., Takata, Y., Ogawa, H., and Okamoto, M. (1979) The inactivation of saccharopine dehydrogenase (L-lysine-forming) by diethyl pyrocarbonate. *J. Biol. Chem. 255*, 937-942.

100. Ogawa, H. and Fujioka, M. (1980) The reaction of pyridoxal-5'-phosphate with an essential lysine residue of saccharopine dehydrogenase (L-lysine-forming). *J. Biol. Chem. 255*, 7420-7425.

101. Fujioka, M. and Takata, Y. (1981) Role of arginine residue in saccharopine dehydrogenase (L-lysine-forming) from baker's yeast. *Biochemistry 20*, 468-472.

102. Saunders, P. P. and Broquist, H. P. (1966) Saccharopine, an intermediate of the aminoadipic acid pathway of lysine biosynthesis, saccharopine dehydrogenase. *J. Biol. Chem. 241*, 3435-3440.

103. Fujioka, M. and Tanaka, M. (1978) Enzymic and chemical synthesis of ε–N-(L-propionyl-2)-L-lysine. *Eur. J. Biochem. 90*, 297-300.

104. Cleland, W. W. (1963) The kinetics of enzyme-catalyzed reactions with two or more substrates. *Biochim. Biophys. Acta 67*, 173-187.

105. Fujioka, M. (1975) Saccharopine dehydrogenase, substrate inhibition studies. *J. Biol. Chem. 250*, 8986-8989.

106. Ogawa, H., Hase, T., and Fujioka, M. (1980) Amino acid sequence of a peptide containing an essential cysteine residue of yeast saccharopine dehydrogenase (L-lysine-forming). *Biochim. Biophys. Acta 623*, 225-228.

107. Viola, R. E., Cook, P. F., and Cleland, W. W. (1979) Stereoselective preparation of deuterated reduced nicotinamide adenine nucleotides and substrates by enzymatic synthesis, *Anal. Biochem. 96*, 334-340.

108. Northrop, D. B. and Duggleby R. G. (1987) Preparation and storage of isotopically labeled reduced nicotinamide adenine dinucleotide, *Anal. Biochem. 165*, 362-364.

109. Schowen, K. B. and Schowen, R. L. (1982) Solvent isotope effects on enzyme systems, *Methods Enzymol. 87*, 551.

110. Quinn, D. M. and Sutton, L. D. (1991) Theoretical basis and mechanistic utility of solvent isotope effects in *Enzyme Mechanism for Isotope Effects* (Cook, P. F., Ed.), CRC Press, Inc., Boca Raton, FL, pp 73-126.

111. Northrop, D. B. (1977) in *Isotope Effects on Enzyme-Catalyzed Reactions* (Cleland, W. W., O'Leary, M. H. & Northrop, D. B., Eds.), University Park Press, Baltimore, MD. p 122.

112. Cook, P. F. and Cleland, W. W. (1981a) Mechanistic deductions from isotope effects in multireactant enzyme mechanisms, *Biochemistry 20*, 1790-1796.

113. Marquardt, D. W. (1963) An algorithm for least square estimation of nonlinear parameters. *J. Soc. Ind. Appl. Math. 11*, 431-441.

114. Cleland, W.W. (1979) Statistical analysis of enzyme kinetic data, *Methods Enzymol. 63*, 103-108.

115. Viola, R. E. and Cleland, W. W. (1982) Initial velocity analysis for terreactant mechanisms, *Methods in Enzymology 87*, 353-366.

116. Brown, H. C., McDaniel, D. H., and Haflinger, O. (1955) Determination of organic structures by physical methods, Vol. 1 (Braude, E. A. and Nachod F. C. Ed.), Academic Press, Inc, NY, p 567-662.

117. Cleland, W. W. (1970) Steady-state enzyme kinetics. In The Enzymes (Boyer, P. D., ed.) vol. 2, Academic Press, New York, pp. 1-65.

118. Northrop, D. B., and Cleland, W. W. (1974) The kinetics of pig heart triphosphopyridine nucleotide-isocitrate dehydrogenase. II. Dead-end and multiple inhibition studies. *J. Biol. Chem. 249*, 2928-2931

119. Yonetani, T. and Theorell, H. (1964) Studies on liver alcohol dehydrogenase complexes. III. Multiple inhibition kinetics in the presence of two competitive inhibitors. Arch. Biochem.Biophys. *106*, 243-251.

120. Cleland, W. W. (1977) Determining the chemical mechanisms of enzyme-catalyzed reactions by kinetic studies. *Adv. Enzymol. Relat. Areas Mol. Biol. 45*, 273-387.

121. Blanchard, J. S., and Cleland, W. W. (1980) Kinetic and chemical mechanisms of yeast formate dehydrogenase, *Biochemistry 19*, 3543-3550.

122. Cook, P. F. and Cleland, W. W. (1981b) pH variation of isotope effects in enzyme-catalyzed reactions. 1. Isotope- and pH-dependent steps the same. Kinetic mechanism of alcohol dehydrogenase, *Biochemistry 20*, 1797-1805.

123. Karsten, W. E. and Cook, P. F. (2006) Isotope effects in chemistry and biology (Kohen, A. and Limbach, H. H. Ed.), CRC Press, Inc., Boca Raton, FL, pp. 793-809.

124. Xu, H., West, A. H., and Cook, P. F. (2006) Overall kinetic mechanism of saccharopine dehydrogenase from *Saccharomyces cerevisiae, Biochemistry 45*, 12156-12166.

125. Cook, P. F. and Cleland, W. W. (1981b) pH variation of isotope effects in enzyme-catalyzed reactions. 2. Isotope-dependent step not pH-dependent. Kinetic mechanism of alcohol dehydrogenase, *Biochemistry 20*, 1805-1816.

126. Hermes, J. D., Roeske, C. A., O'Leary, M. H., and Cleland, W. W. (1982) Use of multiple isotope effects to determine enzyme mechanisms and intrinsic isotope effects. Malic enzyme and glucose-6-phosphate dehydrogenase. *Biochemistry 21***,** 5106-5114.

127. Pelton, J. T. and McLean, L. R. (2000) Spectroscopic methods for analysis of protein secondary structure. *Anal. Biochem. 277*, 167-176.

128. Morrisett, J. D., David, J. S. K., Pownall, H. J., and Gotto, A. M., Jr. (1973) Interaction of an apolipoprotein (ApoLP-Alanine) with phosphatidylcholine, *Biochemistry 12*, 1290-1299.

129. McPherson, A. (1998) Crystallization of Biological Macromolecules. Cold Spring Harbor Laboratory Press.

130. Jancarik, J. and Kim, S.-H. (1991) Sparse matrix sampling, a screening method for crystallization of proteins. *J. Appl. Cryst. 24*, 409-411.

131. Pflugrath, J. W. (1999) The finer things in X-ray diffraction data collection. *Acta Cryst. D55*, 1718-1725.

132. Matthews, B. W. (1968) Solvent content of protein crystals. *J. Mol. Biol. 33*, 491-497.

133. Kinzel, J. J. and Bhattacharjee, J. K. (1982) Lysine biosynthesis in *Rhodotorula glutinis*: properties of pipecolic acid oxidase. *J. Bacteriol. 151,* 1073-1077.

134. Mihalik, S. J., McGuinness, M., and Watkins, P. A. (1991) Purification and characterization of peroxisomal L-pipecolic acid oxidase from monkey liver. *J. Biol. Chem. 266*, 4822-4830.

135. Jia, Y., Tomita, T., Yamauchi, K., Nishiyama, M., and Palmer, D. R.J. (2006) Kinetics and product analysis of the reaction catalyzed by recombinant homoaconitase form Thermus thermophilus. *Biochem. J. 396*, 479-485.

136. Weiss, P. M., Gavva, S. R., Harris, B. G., Urbauer, J. L., Cleland, W. W., and Cook, P. F. (1991) Multiple isotope effects with alternative dinucleotide substrates as a probe of the malic enzyme reaction. *Biochemistry 30*, 5755-5763.

137. Gruen, L. C. and McTigue, P. T. (1963) Hydration equilibria of aliphatic aldehydes in H_2O and D_2O, *J. Chem. Soc. 166*, 5217-5223.

138. Xu, H, West, A. H., and Cook, P. F. (2007) A proposed proton shuttle mechanism of saccharopine dehydrogenase from *Saccharomyces cerevisiae, Biochemistry 46*, 871-882.

139. Klinman, J. P. and Matthews R. G. (1985) Calculation of substrate dissociation constants from steady-state isotope effects in enzyme-catalyzed reactions, *J. Am. Chem. Soc. 107*, 1058-1060.